2004

Inverted Echo Sounder Data Report Ulleung Basin of Japan/East Sea June 1991 to July 2001

Douglas A. Mitchell

Yongsheng Xu

See next page for additional authors

Authors
Douglas A. Mitchell, Yongsheng Xu, Karen L. Tracey, D. Randolph Watts, Mark Wimbush, and William Teague

GRADUATE SCHOOL OF OCEANOGRAPHY
UNIVERSITY OF RHODE ISLAND
NARRAGANSETT, RHODE ISLAND

Inverted Echo Sounder Data Report

Ulleung Basin of Japan/East Sea

June 1999 to July 2001

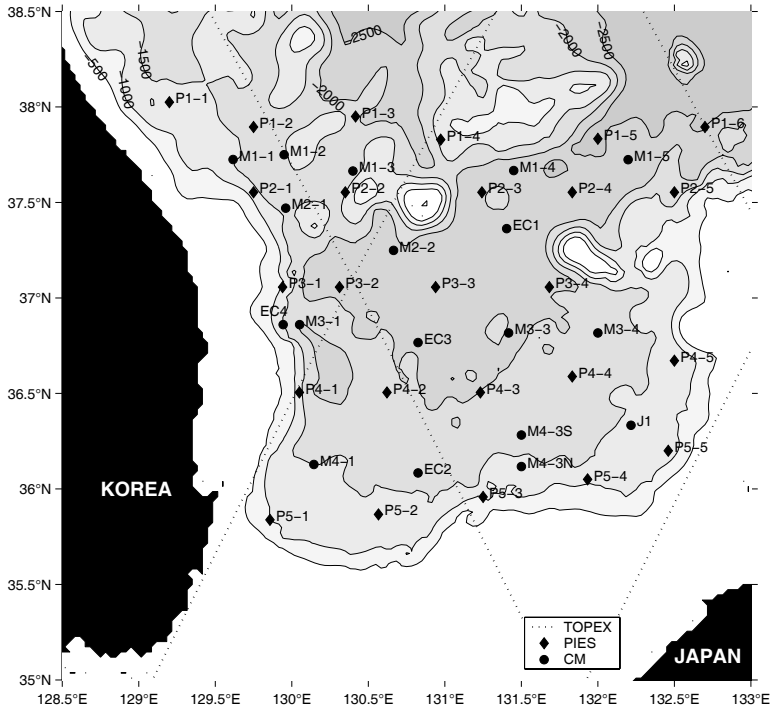

by
Douglas A. Mitchell
Yongsheng Xu
Karen L. Tracey
D.Randolph Watts
Mark Wimbush
William Teague

GSO Technical Report 2004-02
October 2004

ABSTRACT

Observations were conducted from June 1999 to July 2001 to study the shallow and deep current variability in the southwest Japan/East Sea. Data were collected during the field experiment with a two-dimensional array of pressure-gauge equipped inverted echo sounders (PIES) and deep recording current meters (RCM). The collection, processing and calibration of the PIES are documented in this report. Descriptions of the processes used to identify and remove jumps (offsets) in the pressure and travel time records, that resulted when the instruments were jostled or moved by deep crab-fishing activities in the Japan/East Sea, are given. Time series plots of travel time, bottom pressure, and temperature are presented for the 24 recovered instruments. Basic statistics of the hourly data are tabulated.

Contents

List of Tables

List of Figures

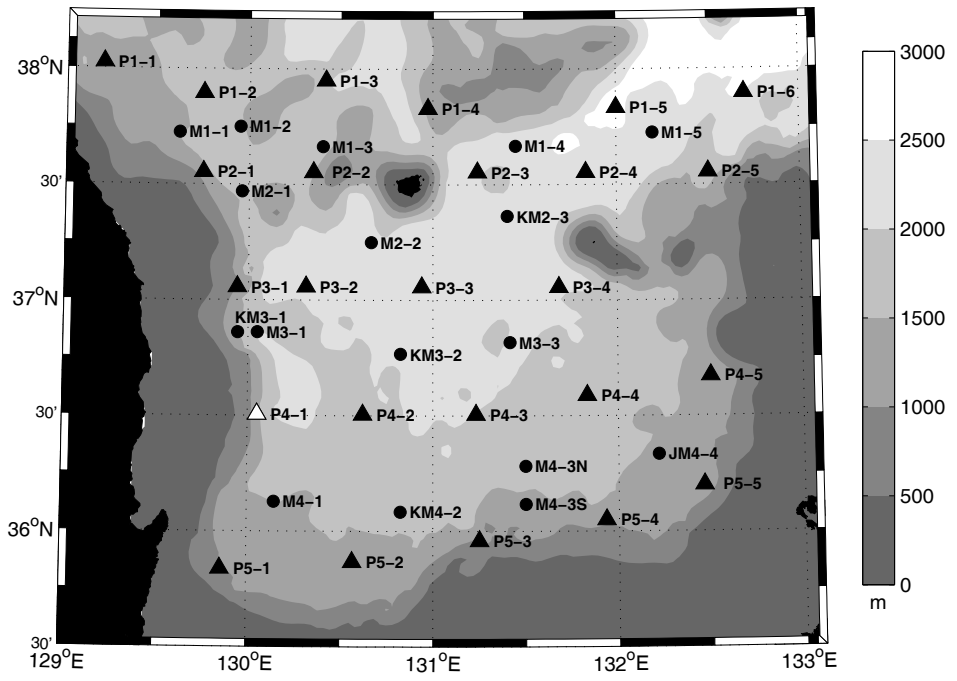

Figure 1: **Bathymetry and locations of long-term instrument deployments. Solid black triangles indicate the 24 recovered PIES locations and solid white triangle denotes the lost PIES at site P4-1. Solid circles show current-meter mooring locations. All instruments are labeled to the right except KM3-1, which is labeled directly above.**

1 Setting and Experiment Design

1.1 Introduction

This report focuses on data collected from an array of 25 pressure-gauge-equipped inverted echo sounders (PIES) deployed in the Ulleung Basin of the southwestern Japan/East Sea (JES) during June 1999 to July 2001. In this report the collection, processing, and calibration of the PIES data are documented. The measurements were made under the support of the Office of Naval Research. Other data collected as part of the experiment included expendable bathythermograph (XBT) surveys, conductivity-temperature-depth (CTD) surveys, and velocity measurements obtained with moored current meters.

The locations of all the moored instruments is shown in Figure 1. The PIES were deployed in an approximately 5 by 5 two-dimensional array with instruments separated by about 55 km in both the North/South and East/West directions. Interspersed within the PIES array were 18 current meter moorings, each consisting of one current meter approximately 23 m above the bottom. The current meter records are documented in Xu *et al.* [2003].

1.2 PIES Description

The PIES array during the JES experiment was a collaborative effort between the University of Rhode island (URI) and the Naval Research Laboratory (NRL). Three different models of inverted echo sounders were used in this experiment. The type designated SD-NRL in Table 1 was Sea Data Model 1665 with standard options built for NRL. Type SD-URI was also Sea Data Model 1665, but the components were assembled at URI. Type WHISL in Table 1 was built by Woods Hole Instrument Systems Ltd. for NRL. All three instrument types ping at a frequency of 10.24 kHz. The Model 1665 instruments record the data to internal

cassette tapes and the WHISL models record to solid state memory.

In addition to the travel time detector, these instruments were also equipped to measure pressure and temperature. Chaplin and Watts (1984) provide a description of the IES circuitry and mooring configuration and Watts and Kontoyiannis (1990) describe instruments with pressure and temperature sensors included.

The Paros Digiquartz pressure sensors (Table 1) had one of two full-scale ranges, either 6000 psi (approximately 4000 dbar) or 10000 psi (approximately 6800 dbar). The 6000 psi sensors were owned by URI (Paros serial numbers primarily ranging between 20000 and 40000) and had been previously deployed for many months. Because of this pre-pressurization, they performed with minimal drift, typically < 0.2 dbar during the two year deployment. The WHISL instruments (owned by NRL) had never been deployed, and their new 10000 psi sensors (Paros serial numbers $>$50000) exhibited slightly larger drifts (0.1–0.7 dbar). The internal reference oscillators in these WHISL instruments may also have drifted, but this could not be confirmed. Five 10000 psi sensors (Paros serial numbers 18860–19934) owned by NRL were installed in non-WHISL model instruments. Although these gauges had been previously deployed, they exhibited very large ($>$2 dbar), atypical drifts.

The PIES instruments were moored one meter above the ocean floor and sampled at hourly intervals throughout the deployment. At the designated sampling time, a burst of 24 acoustic pulses (10.24 KHz) were transmitted at 10 second intervals, and the time each ping took to travel the round trip distance to the sea surface was measured.

Typical deployment depths of 1000-3000 m produce full travel times between 1-4 seconds; thus with a resolution of 0.05 ms, each measurement would require a storage space of 18 bits. However, the variability of the travel time signal in the JES region is about 0.01 seconds making it unnecessary to record the full travel time measurement. By recording just the 13 least significant bits, variability of up to 0.4 seconds can be resolved, with only a constant integer multiple of 0.4 seconds excluded. The constant can be determined *a priori* by knowing the bottom depth at the instrument site to within 300 m; it may be added back into the recorded travel times after the instrument is recovered.

1.3 Data Recovery

The deployment locations of the PIES are listed in Table 1 and plotted in Figure 1. The instruments were deployed on a cruise aboard the R/V Revelle (HAHNARO-06) during June 6 – June 15, 1999. They were recovered during June 21 – July 4, 2001 aboard the R/V Melville ("Cook" Leg 09). Initially, 23 PIES were recovered and two instruments were not. Acoustic communication was established with P3-2, but it would not release from the bottom. Acoustic communication was not established with P4-1, and it is believed to have been lost to crab fishing activity. Nearly three years after the recovery cruise, in March 2004, the P3-2 instrument was found by a Korean fisherman near Ulleung Island and its data tape was returned to URI.

Complete travel time, pressure, and temperature records were obtained for 22 of the 24 recovered instruments. For the two remaining instruments, the travel time record for P1-5 failed after three months and the temperature record for P5-4 failed completely (Figure 2).

1.4 Time Base

The PIES instruments sampled and recorded nominally at one-hour intervals. However, the instruments exhibited varying amounts of clock drift during the two-year deployment. If the clock drifted less than 2 minutes between launch and recovery, the timing associated with each sample was shifted by half the total drift and the one-hour sampling interval was maintained. If the clock drift exceeded 2 minutes, the sampling

Table 1: PIES Positions, Serial Numbers, Instrument type, Pressure Sensor Serial Number and Rating, and Deployment Depth. P4-1 was not recovered. P3-2 was found later (see text).

Site	PIES S/N	instr. type	Paros S/N	Paros rating–psi	Latitude (N)	Longitude (E)	depth (m)
P1-1	88	SD-URI	31162	6000	$38°01.50'$	$129°12.00'$	1175
P1-2	121	WHISL	51911	10000	$37°53.70'$	$129°45.00'$	1682
P1-3	118	WHISL	50496	10000	$37°57.02'$	$130°25.00'$	1881
P1-4	119	WHISL	50526	10000	$37°49.72'$	$130°58.38'$	1386
P1-5	117	WHISL	50532	10000	$37°50.00'$	$132°00.02'$	2644
P1-6	66	SD-URI	33822	6000	$37°53.69'$	$132°42.02'$	2536
P2-1	23	SD-NRL	18862	10000	$37°33.20'$	$129°45.00'$	1047
P2-2	120	WHISL	50543	10000	$37°33.20'$	$130°21.00'$	1650
P2-3	71	SD-URI	31724	6000	$37°33.20'$	$131°14.57'$	2207
P2-4	68	SD-URI	40275	6000	$37°33.20'$	$131°49.97'$	2382
P2-5	116	WHISL	50530	10000	$37°33.20'$	$132°30.00'$	1696
P3-1	17	SD-NRL	36873	6000	$37°04.00'$	$129°56.40'$	1023
P3-2	70	SD-URI	17849	6000	$37°03.40'$	$130°18.72'$	2214
P3-3	69	SD-URI	33816	6000	$37°03.40'$	$130°56.40'$	2221
P3-4	72	SD-URI	19539	10000	$37°03.40'$	$131°40.98'$	2165
P4-1	107	WHISL	47151	10000	$36°30.30'$	$130°03.03'$	1375
P4-2	77	SD-URI	28197	6000	$36°30.30'$	$130°37.32'$	2038
P4-3	74	SD-URI	19552	10000	$36°30.30'$	$131°13.98'$	2058
P4-4	112	WHISL	53566	10000	$36°35.32'$	$131°49.97'$	1809
P4-5	106	WHISL	50525	10000	$36°40.30'$	$132°30.00'$	1194
P5-1	24	SD-NRL	18860	10000	$35°50.27'$	$129°51.51'$	1036
P5-2	111	WHISL	53565	10000	$35°52.00'$	$130°34.02'$	1402
P5-3	15	SD-NRL	19934	10000	$35°57.50'$	$131°15.00'$	1257
P5-4	86	SD-URI	36884	6000	$36°03.00'$	$131°55.98'$	1165
P5-5	87	SD-URI	36883	6000	$36°12.00'$	$132°27.60'$	1055

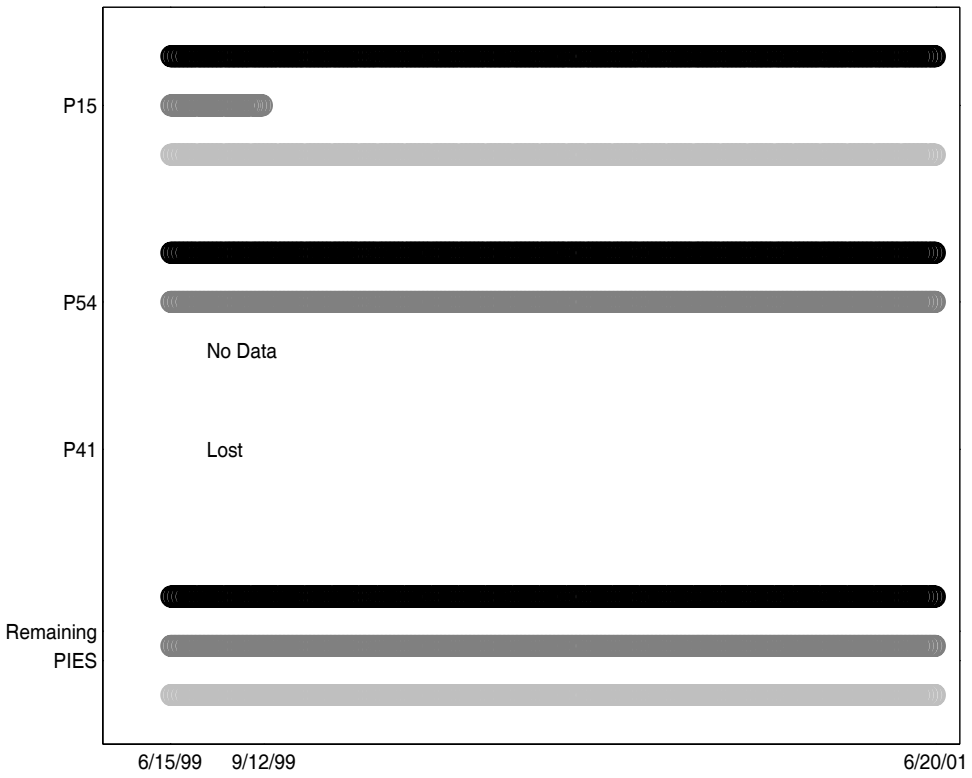

Figure 2: **Time line of collected data for the 23 recovered PIES. Pressure is noted with the dark shaded line, τ with the medium shaded line, and temperature with the lightly shaded line.**

interval was adjusted to be slightly longer or shorter than one hour, so that the observed times at launch and recovery were assigned to the first and last data records, respectively. All times are reported as decimal day since January 1, 1999 0000 UTC. Thus, January 1, 1999 at 1200 UTC would be given as 0.5.

2 Data Processing and Calibration

2.1 Data Processing

The basic steps in the PIES data processing included recovery of the data from the cassette tapes and conversion of the recorded counts into scientific units. The data processing and low-pass filtering was accomplished by a series of MATLAB routines specifically developed for the PIES. The steps are described below and schematically illustrated in Figures 3 and 6. Sections 2.2–2.7 provide a complete description of the processing schemes applied to the PIES data.

New difficulties were encountered during the processing of the PIES data, specifically, pressure (P) and travel time (τ) jumps (offsets) at 11 sites, and complicated sensor drifts at 10 sites (Figures 12–14). The temperature records were not affected. The jumps apparently resulted from the instruments being displaced to different depths by the deep crab fishing activity in the region. The P and τ jumps always occurred simultaneously at an individual site and had relative displacements consistent with vertical movement of the instrument ranging from tens of meters to centimeters, either upward or downward.

The most complicated drifts all occurred on pressure sensors with similar serial numbers, suggesting the possibility of a bad batch. These sensors have since been retired. Four of the records had the added complication of a very strong drift at the beginning of the record that trended in opposition to the remainder

of the record. In order to produce coherent maps of P and τ, these jumps and drifts needed to be estimated and removed from the records.

The dynamically important pressure signal was on the order of 1–3 cm, nearly an order of magnitude smaller than either the dominant basin average signal ($\sim$50 cm) or the tidal signal ($\sim$15 cm). This dynamic pressure signal was also considerably less than many of the jumps and drifts, which ranged up to 34 dbar and 3–4 dbar, respectively. The smallness of the dynamic pressure signal relative to the basin average, tides, jumps, and drifts required that these other signals be calculated with a high order of accuracy.

2.2 Temperature

Temperature is measured by the PIES in order to account for the temperature sensitivity of pressure sensors. It is measured inside the glass sphere and therefore does not provide an accurate measurement of the instantaneous *in situ* water temperature. The measurement is taken during a 50–60 sec time window at the end of the hourly sampling period. The time assigned to each temperature measurement is the midpoint of this sampling window. The temperature records from 23 of the 24 PIES required minimal processing to remove spikes (large outliers). The PIES at P5-4 required special processing because the temperature measurement failed.

Although the temperature counter of P5-4 functioned normally while the instrument was in the laboratory, after the instrument was deployed only zero values were recorded. In order to accurately determine pressure from the recorded frequencies, it was necessary to generate a temperature record for this instrument.

We decided to combine the temperature records from neighboring sites P5-3 and P5-5 to produce the temperature record for site P5-4. We synthesized temperatures by averaging time-shifted and low-pass filtered temperatures from these adjacent sites. We shifted the temperatures from P5-3 and P5-5 in opposite directions, to account for signal propagation, for time lags ranging between 0 and 50 days. We also low-pass filtered the records using a suite of cutoff periods ranging from 0 to 75 days. Since the dynamically-important pressure signals were small, it was important to minimize the noise introduced by the choice of temperature signal. Initially we attempted to minimize the RMS of the temperature record because it did not require us to recalculate the pressures. However, we decided it was best to minimize the RMS of the pressure record itself, because the pressure record was the data we were interested in studying. Thus, a pressure record was generated for each temperature record synthesized. The smallest RMS (0.008782 dbar) was obtained using the temperatures synthesized by averaging the records from P5-3 and P5-5 that were time shifted by 24 days and low-pass filtered using a cutoff period of 65 days (Figure 83).

The hourly temperature records are shown in Figures 78–83 and basic statistics are given in Table 7.

2.3 Bottom Pressure

All pressure measurements were corrected for the temperature sensitivity of the sensor using calibration coefficients supplied by the manufacturer. Since the temperature record failed at site P5-4, the pressure record was corrected using a proxy temperature record, which is described in the above section. The raw pressure records are shown in Figures 12–14.

2.4 Processing the "Jump-Free" Pressure Records

A simple scheme designed to increase the signal-to-noise ratio for each step, shown schematically in Figure 3, was used to process the pressure records that had no jumps (P1-3, P1-6, P2-2, P2-3, P2-5, P3-2, P3-3,

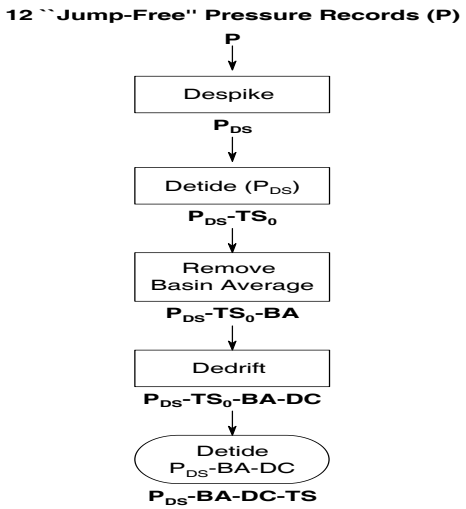

Figure 3: **12 "Jump-Free" Pressure Records Data Processing Flowchart.**

P3-4, P4-3, P4-5, P5-3, P5-4, and P5-5). The scheme was broken into five steps:

1. Remove "large" spikes from the raw data, where "large" was defined as spikes greater in magnitude than 10 dbar. These isolated large spikes were present in most of the records and occurred from internal electronic sources or tape reading errors. These records were referred to as P_{DS}.
2. Calculate and remove the tidal signal (Detide) from P_{DS} using Tidal Response Analysis (TRA, described below), where this preliminary tidal signal is called TS_0.
3. Remove the Basin Average (described below), referred to as BA.
4. Calculate and remove the drift curve (Dedrift) from $P_{DS} - TS_0 - BA$, where the drift curve is referred to as DC.
5. Detide the original despiked record with TRA after removal of the BA and the drift curve, i.e. detide $P_{DS} - BA - DC$. This generates the greatest signal-to-noise ratio of the tidal signals possible. The improved tidal signal is called simply TS.

2.4.1 Detiding

Tidal response analysis (TRA) (Munk and Cartwright, 1966) was used to determine the tidal constituents from the pressure records of each instrument. In order to enhance the signal-to-noise ratio of the tidal signal, which was less than a millimeter for some constituents, the BA and drift curves (DC) were removed from the pressures prior to running the TRA for the final time. The amplitude and phase of the constituents for each instrument are given in Table 2. To illustrate the tidal variation between sites, a 65-day segment of the tidal signals for all 24 sites are plotted in Figure 15.

Table 2: Amplitudes (H) and phases(G) of the eight major tidal constituents. Amplitudes are given in millibars and Greenwich Epoch phases are given in degrees.

Site		O1	K1	Q1	P1	M2	K2	N2	S2
P1-1	H (mbar)	4.670	4.895	1.013	1.675	6.537	0.455	1.511	1.796
	G (deg)	193.514	226.517	173.788	224.712	183.798	201.626	166.643	202.079
P1-2	H (mbar)	4.629	4.801	1.009	1.644	5.986	0.384	1.406	1.535
	G (deg)	192.174	224.452	172.831	222.724	182.390	198.889	164.323	199.893
P1-3	H (mbar)	4.707	4.851	1.039	1.661	5.692	0.359	1.368	1.431
	G (deg)	189.925	221.175	170.961	219.626	178.634	192.540	160.745	194.168
P1-4	H (mbar)	4.754	4.847	1.020	1.665	5.248	0.316	1.298	1.257
	G (deg)	188.003	218.600	169.541	216.899	172.992	181.783	156.237	184.374
P1-5	H (mbar)	4.927	5.042	1.085	1.724	5.444	0.346	1.348	1.368
	G (deg)	186.499	215.765	169.064	214.309	169.841	180.094	152.359	182.477
P1-6	H (mbar)	5.008	5.140	1.095	1.758	5.655	0.381	1.405	1.488
	G (deg)	185.714	214.501	168.687	213.029	167.786	180.245	150.855	182.073
P2-1	H (mbar)	4.524	4.590	0.991	1.576	5.567	0.329	1.329	1.334
	G (deg)	191.779	224.252	172.487	222.493	182.946	199.009	163.882	200.491
P2-2	H (mbar)	4.590	4.683	1.015	1.606	5.182	0.289	1.279	1.173
	G (deg)	189.405	220.512	170.017	219.021	177.795	187.292	158.563	190.465
P2-3	H (mbar)	4.750	4.831	1.051	1.654	5.000	0.282	1.255	1.131
	G (deg)	186.827	216.787	168.781	215.326	172.517	178.607	154.437	182.262
P2-4	H (mbar)	4.883	4.974	1.077	1.702	5.057	0.308	1.285	1.214
	G (deg)	185.722	214.903	168.206	213.473	167.940	172.859	150.611	176.395
P2-5	H (mbar)	4.950	5.077	1.094	1.733	5.415	0.353	1.375	1.377
	G (deg)	185.721	214.132	169.169	212.723	165.584	173.207	148.670	176.019
P3-1	H (mbar)	4.362	4.336	0.954	1.495	4.474	0.176	1.099	0.778
	G (deg)	190.042	221.911	170.215	220.252	182.882	190.361	161.588	195.573
P3-2	H (mbar)	4.217	4.144	0.930	1.430	3.928	0.144	0.997	0.628
	G (deg)	186.835	216.692	167.433	215.320	174.741	176.605	157.792	182.537
P3-3	H (mbar)	4.499	4.514	1.004	1.548	4.199	0.194	1.106	0.780
	G (deg)	184.684	214.623	166.347	213.229	171.010	159.821	151.461	168.493
P3-4	H (mbar)	4.876	4.894	1.085	1.677	4.481	0.256	1.196	0.987
	G (deg)	182.925	211.819	165.246	210.484	162.997	153.267	145.541	159.788
P4-2	H (mbar)	3.948	3.804	0.900	1.309	3.021	0.116	0.865	0.366
	G (deg)	184.764	213.270	166.609	212.162	172.648	104.588	149.919	124.359
P4-3	H (mbar)	4.362	4.435	0.971	1.516	3.454	0.209	0.992	0.729
	G (deg)	176.322	205.066	159.054	203.726	158.483	117.823	141.051	127.624
P4-4	H (mbar)	5.159	5.083	1.163	1.745	4.092	0.270	1.137	0.986
	G (deg)	178.134	207.705	159.948	206.392	153.752	131.099	137.969	138.100
P4-5	H (mbar)	5.408	5.213	1.251	1.787	4.636	0.317	1.248	1.181
	G (deg)	188.803	212.758	172.295	212.191	152.884	140.691	138.641	145.824
P5-1	H (mbar)	3.654	3.062	0.848	1.078	1.529	0.431	0.213	1.434
	G (deg)	199.824	237.624	178.765	235.352	268.839	12.257	195.783	6.611
P5-2	H (mbar)	2.708	2.177	0.695	0.756	1.246	0.369	0.605	1.185
	G (deg)	184.540	199.715	166.280	201.486	127.720	56.874	121.421	56.051
P5-3	H (mbar)	3.282	4.065	0.727	1.347	2.703	0.331	0.868	1.093
	G (deg)	162.584	180.406	152.212	179.775	135.899	86.002	124.749	89.663
P5-4	H (mbar)	6.639	6.086	1.479	2.124	3.964	0.357	1.164	1.242
	G (deg)	165.870	202.897	144.187	200.634	139.404	111.060	127.365	115.861
P5-5	H (mbar)	6.426	5.635	1.468	1.973	4.502	0.358	1.253	1.290
	G (deg)	180.493	210.394	160.714	209.186	143.917	125.136	131.393	129.925

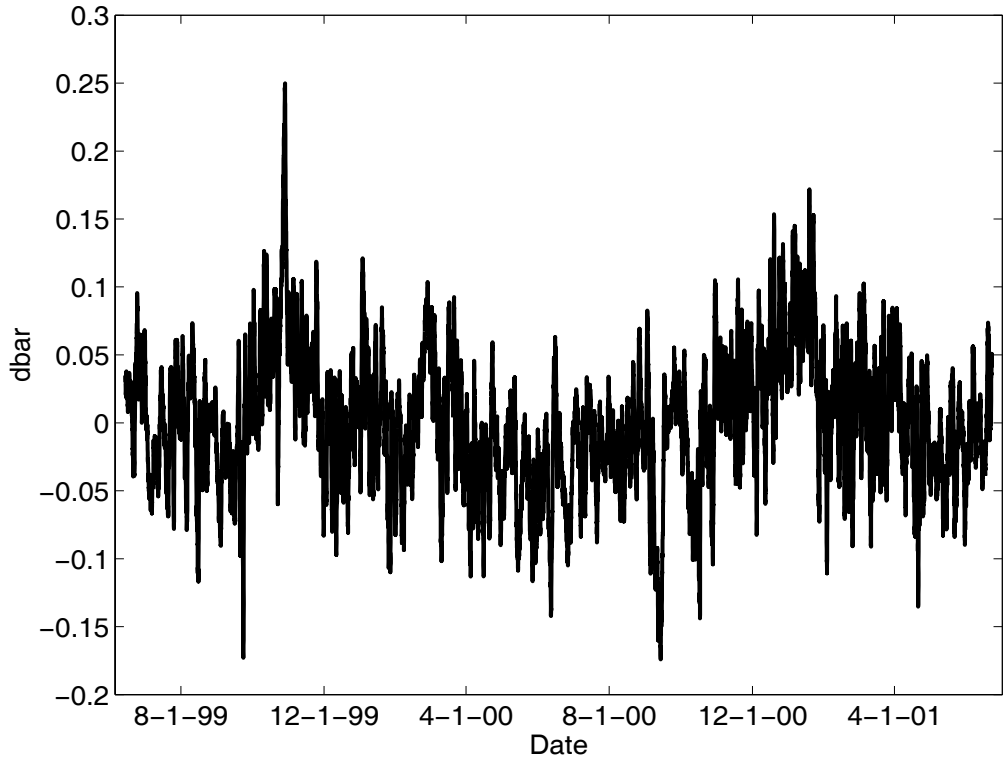

Figure 4: **The Basin Average constructed from the demeaned/detided/dedrifted records from sites P2-3, P3-3, and P5-5.**

2.4.2 Basin Average

The bottom pressure records of all 24 PIES in the Ulleung Basin exhibited a remarkably similar, coherent signal. This coherent signal was determined to be in response to atmospheric forcing (Park and Watts, 2003). The basin-wide average signal was constructed from three pressure records (P2-3, P3-3, P5-5) that displayed little sensor drift, good signal-to-noise ratio, and no jumps. Prior to averaging, the three records were demeaned, detided with TRA, and dedrifted with an exponential/linear scheme described in Watts and Kontoyiannis (1990). The mean of the three resultant records was calculated to determine the basin-wide signal (BA) plotted in Figure 4.

2.4.3 Dedrifting

The determination of "best-fit" drift curves followed a hierarchal order of complexity from a single linear function to double exponential linear functions. In each case, drift curves were calculated in an ascending order of complexity until a suitable fit was found. By doing this we ensured that the simplest function of time was used to calculate the drift curves. Three of the "jump-free" records (P1-6, P3-4, P4-3) and seven of the records with jumps (P1-1, P1-2, P1-4, P2-1, P4-2, P4-4, and P5-1) required the drift curves be calculated piece-meal due to the complexity of the drifts involved.

In all cases, the rate of drift decayed as a function time and was approximated by the following functions,

$$Drift = Et + F \tag{1}$$

$$Drift = Ce^{-Dt} + Et + F \tag{2}$$

$$Drift = Ae^{-Bt} + Ce^{-Dt} + Et + F, \tag{3}$$

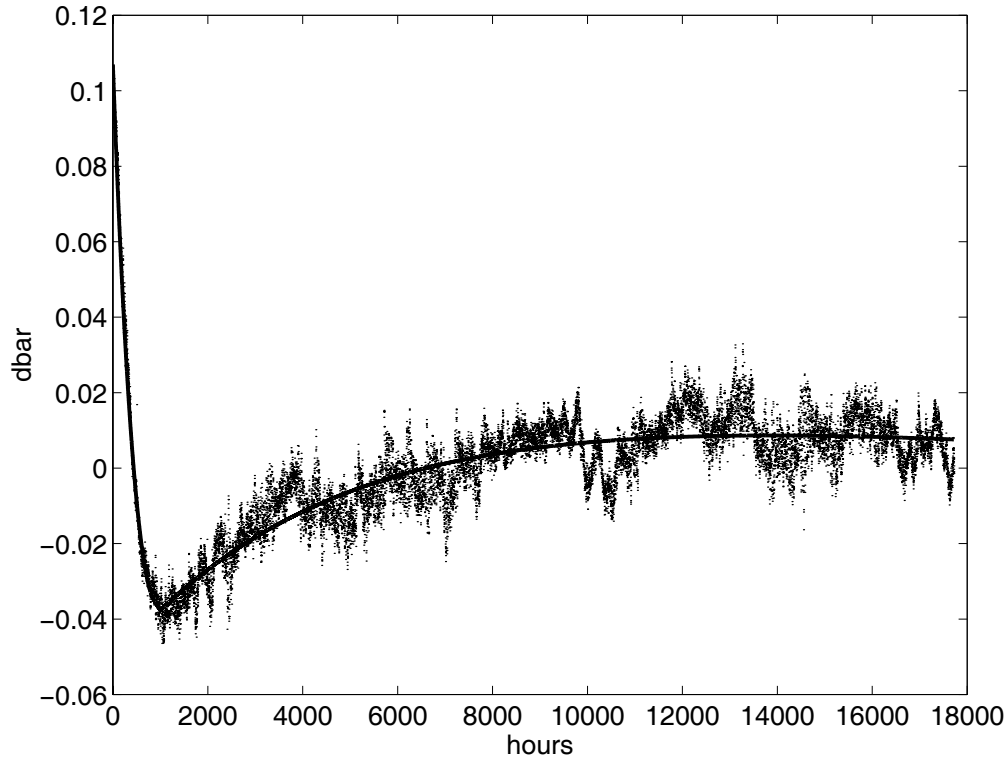

Figure 5: **The drift curve and the data it was fit to for site P1-6, showing the change in character near hour 1000.**

depending on the complexity of the drift.

The overdetermined sets of equations were solved for A, B, C, D, E, and F with the MATLAB function *fmincon*, which uses a constrained nonlinear optimization method. Drifts were fitted to residual pressure records that had the record mean, basin average, and tidal signals removed ($P_{DS} - TS_0 - BA$). The fitted drift curves for each instrument are shown in Figures 16–18 superimposed on the $P_{DS} - TS_0 - BA$ data.

P1-1, P1-2, P1-4, P1-6, P2-1, P3-4, P4-2, P4-3, P4-4, and P5-1 required fitting distinct drift curves to different portions of the records. We did this because the nature of the drifts, for undetermined reasons, changed character and could not be fitted with a single function. Figure 5 shows the drift curve calculated for site P1-6. The drift changes character near hour 1000. A double exponential/linear function was used prior to hour 1000, and a single exponential/linear was used after hour 1000. To be sure that the drift curves matched at hour 1000, a linear function between hours 850 to 1000 was used to ensure continuity between the two fits. Similar techniques were used on the remaining sites.

2.5 Processing the Pressure Records with Jumps

The pressure records from the remaining 11 sites (P1-1, P1-2, P1-4, P1-5, P2-1, P2-2, P3-1, P4-2, P4-4, P5-1, P5-2) contained jumps (Figures 12–14). A combined total of 32 jumps ranging up to 34 dbar in magnitude (tabulated in Table 3) were identified in these records. Special care was required during the processing to identify and remove these jumps correctly.

The processing scheme of the records with jumps, outlined in Figure 6, was very similar to the processing described above for records without jumps. The processing sequence was as follows:

1. Remove “large” spikes from the raw data, where “large” is defined as outliers greater in magnitude

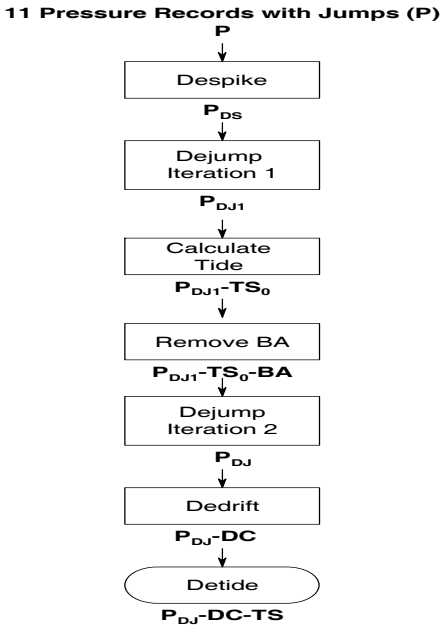

Figure 6: **11 Pressure Records with Jumps Data Processing Flowchart.**

than any jumps present. These spikes were not identified and removed by the standard despiking routine, instead new code was written. This made certain that the jumps and their adjacent data points would not be mistakenly identified as spikes. Records with the large spikes removed are referred to as P_{DS}.

2. Perform Iteration 1 of the dejump routine, referred to as P_{DJ1}, described below.
3. Calculate the preliminary tidal signal, TS_0, using TRA.
4. Remove BA and TS_0 from the first iteration dejumped record, $P_{DJ1} - TS_0 - BA$.
5. Perform Iteration 2 of the dejump routine, called P_{DJ}, described below.
6. Calculate the drift curve DC detailed above and remove it, as $P_{DJ} - BA - DC$.
7. After adding TS_0 back in, detide again with TRA to find the improved tidal signal, TS.

2.5.1 Jump Identification and Removal

Each jump occurred within a relatively short time period of four hours or less. Over this time interval, the tidal signals dominated, allowing us to use the periodicity of the tides as a means of identifying the timing and size of the jumps. Once the initial jump estimates were removed, the preliminary tidal signal (TS_0) was calculated and removed from the pressure records. Additionally, the BA was removed to further reduce true ocean signal variability. The resulting residual pressure records were expected to vary negligibly over the short jump time interval, allowing us to set all points within the jump equal to the sample just prior to the jump and adjust the remainder of the record accordingly. The process used to remove the jumps will be described next using the pressure record from site P3-1. The jump used in this illustration had a magnitude

of 2.1844 dbar (Figure 7, top panel). All other jumps in this record as well as at the other sites were removed with this same scheme.

Iteration 1. The purpose of this step is to eliminate jumps from the pressure records reasonably well, so that the tidal signals can be determined with the response analysis program.

The hourly measurements affected by the jumps are identified in the P_{DS} data record. These are depicted by two open circles in the top two panels of Figure 7 and will be referred to here as J1 and J2, respectively. Measurements that occurred 24 hours prior to J1 and J2 are also found. These points,referred to as P1 and P2, are marked by two open diamonds in the middle panel of Figure 7. Because the tides are periodic, P1 and P2 should be in approximately at the same phase of the tide as J1 and J2. Thus, P1 and P2 can be used to estimate the amount of variability due to the tides that would be expected at J1 and J2.

The size of the tidal signal at measurement J1 is estimated as follows. The pressure difference between P1 and the measurement immediately prior to it (P0) is calculated as $\Delta p_1 = P1 - P0$. This difference is assumed to be caused solely by the tides. The expected value at J1 is estimated as $DJ1 = J0 + \Delta p_1$, where J0 is the measurement taken just before J1. The same procedure is applied to J2: estimate $\Delta p_2 = P2 - P1$ and apply it to give $DJ2 = DJ1 + \Delta p_2$. The final step is to calculate $\Delta_{jump} = J2 - DJ2$ and remove from all points in the record after point DJ2. This procedure is followed each jump identified in the record. The resulting jump-free record is referred to as P_{DJ1}.

This tidal signal TS_0 was determined with TRA from the P_{DJ1} records.

Iteration 2. The purpose of this step is to produce pressure records with the largest ocean signals removed so that jumps would be eliminated with more confidence.

The TS_0 and BA signals were removed from the despiked record P_{DS} to produce a record with small residuals, $P_{DS} - TS_0 - BA$. This residual record contains jumps, the drift, and dynamically important pressures, as well as the errors from the tidal and basin average calculations. We make the assumption that the dynamic signals were static over the course of a jump (1–4 hours). This permitted us to set the measurements during the jump ($J1$ and $J2$) to be equal to the last value prior to the jump ($J0$). The magnitude of the jump was then calculated as the value of the last measurement involved in the jump prior to correction minus its corrected value ($\Delta = J2 - J0$). All subsequent measurements in the record were then adjusted by the value of Δ. This process is depicted by asterisks in the bottom panel of Figure 7.

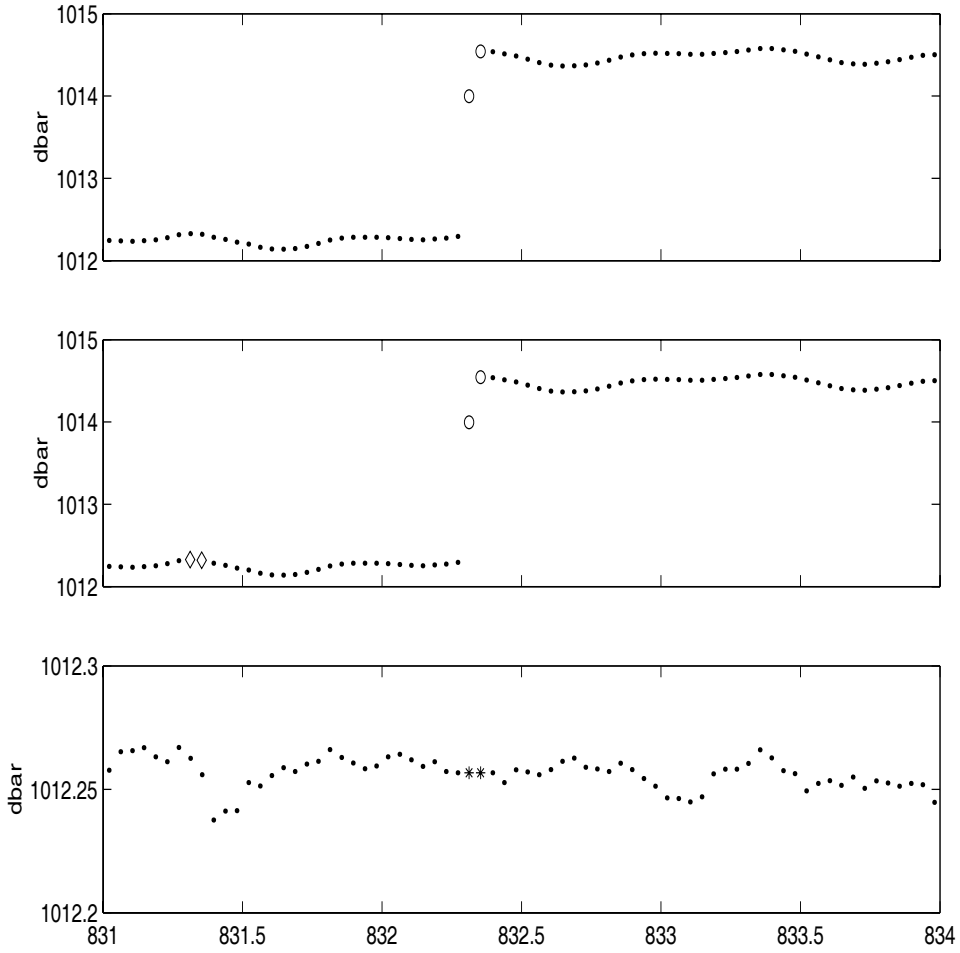

Figure 7: **Dejumping process illustrated for the first jump at site P3-1. Top panel: Open circles represent the measurements involved in the jump. Second panel: Iteration 1 of the dejumping method. Open diamonds depict the measurements that were used to predict the tidal values during the jump. Bottom panel: Iteration 2 of the dejumping method (p). The asterisks show the measurements involved in the jump are set equal to the value just prior to the jump, and all subsequent values were adjusted accordingly.**

Table 3: Pressure Jumps: Magnitude in dbar and time in decimal day since Jan 1, 1999.

Site	# of Jumps	Δp	Time
P1-1	2	0.0063	233.94
		0.0130	234.77
P1-2	4	0.0177	379.85
		2.6553	516.69
		0.0140	517.02
		0.0035	672.90
P1-4	6	-0.0162	177.19
		-0.0567	221.19
		0.0267	223.65
		0.0261	225.15
		0.0346	248.40
		0.0062	525.73
P1-5	1	-1.8646	246.52
P2-1	3	33.8994	198.10
		0.0398	274.27
		-16.9416	494.65
P2-4	1	0.0133	178.40
P3-1	3	2.1844	832.27
		-4.1219	873.65
		-0.0272	880.44
P4-2	3	-0.8577	176.81
		0.0145	184.65
		-0.0037	880.44
P4-4	2	-1.0605	247.77
		-0.1836	359.94
P5-1	4	0.0126	360.52
		0.0749	598.48
		0.1946	621.56
		0.0343	622.14
P5-2	3	-0.7292	220.85
		-0.2646	335.06
		-1.1492	861.77

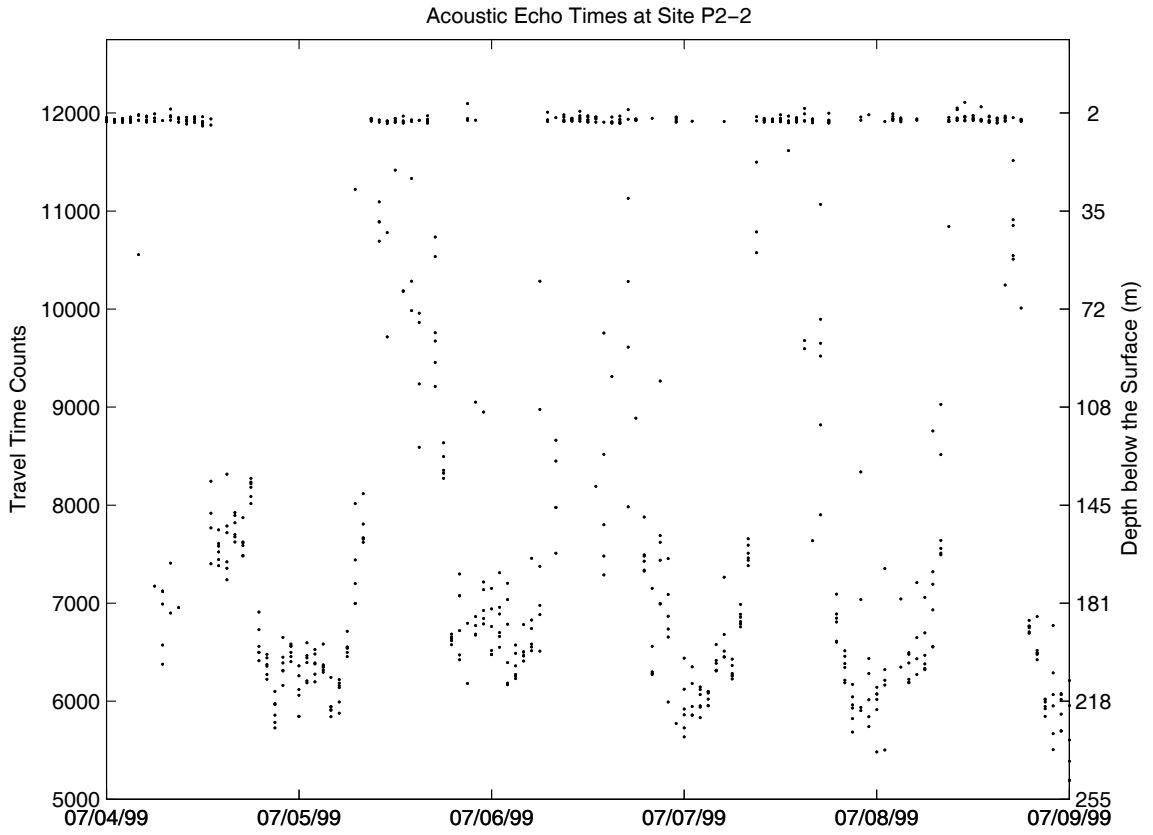

Figure 8: **Biological activity is shown by the vertical movement of early echo returns. The echo reflections off the sea surface correspond to counts of nearly 12000. Counts near 6000 are early echoes that reflected off some organisms located about 220 m below the surface.**

2.6 Travel Time Processing and Calibration

2.6.1 Raw Time Series and Biological Interference

During each hourly sample burst, the PIES emitted a set of 24 pings and the times of the returning echoes were recorded internally. Figures 46–48 display all the echo returns (τ) as individual dots. The desired surface reflections appear as a continuous line in each panel. Jumps, caused when the instruments were jostled by fishing activity, are clearly visible as abrupt offsets in these traces.

In addition to the surface returns, many of the records exhibited a large amount of scatter. Most of the scatter was attributable to echoes that returned early. An enlargement of the scatter at site P2-2 (Figure 8) shows a diurnal pattern to the echo returns. The earliest echo returns consistently occurred during the daytime hours (note that local time leads UT by 9 hours). The echoes became progressively longer (closer to the sea surface) during the evening hours. This pattern is consistent with vertical migration of zooplankton. It is conjectured that the pings emitted from the PIES reflected off the high concentrations of fish or squid which followed the food source. The records in Figures 46–48 show more activity at sites nearer the coasts than in the center of the basin. They also show more activity during the first year of the deployment period.

The 24 travel times taken each sampling period are first windowed to remove the largest scatter. From the remaining values, a single representative τ was chosen by using an average of several points near the first-quartile value of a Rayleigh distribution. After jump removal and low-pass filtering, the final calibration step was to project the measured travel times onto a common pressure level.

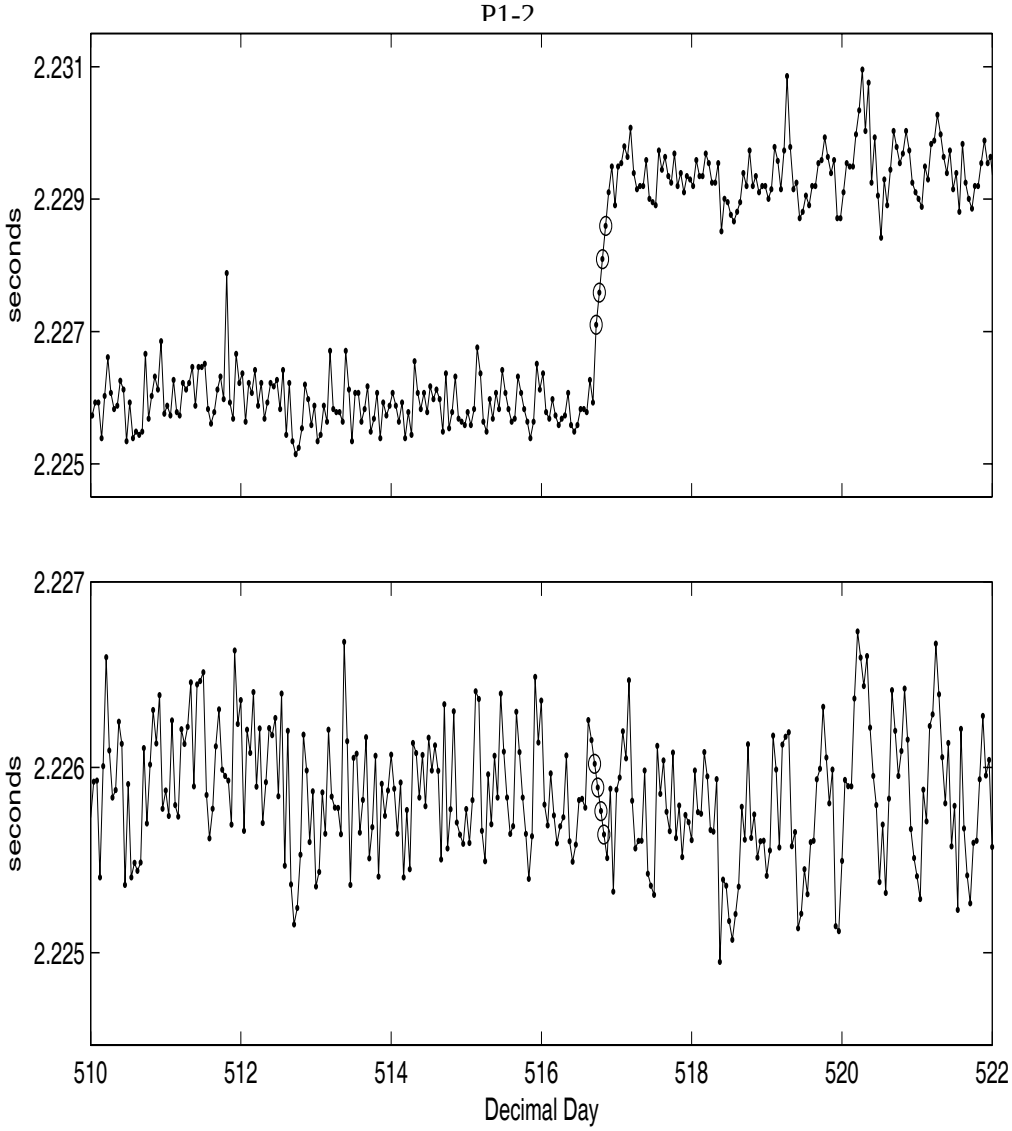

Figure 9: **The top panel shows the travel time jump and the bottom panel shows the same section of the record dejumped. The circles highlight the points involved in the jump. The time axis is hours from instrument deployment, and the jump occurs at decimal day 516.69.**

2.6.2 Removal of Travel Time Jumps

The 11 sites with pressure record jumps described above also have corresponding travel time jumps that must be removed. The travel time jump is directly proportional to the pressure jump and calculated as $\Delta\tau = 2(\Delta p/1.01)c^{-1}$, where c is the speed of sound at the bottom and $\Delta p/1.01$ expresses the identified pressure jump as a depth change. We use the sound speed at the bottom, because this is where the extra distance traveled by the sound pulse occurs.

The process is illustrated in Figure 9 for site P1-2. The four circled points represent a τ jump, and are referred to as J1 through J4. First, $\Delta\tau$ is subtracted from J4 and all subsequent measurements. Points J1–J3 are replaced with values linearly interpolated between J0 and DJ4, where DJ4 is the corrected J4 value and J0 is the measurement just prior to J1. This procedure is repeated for all jumps.

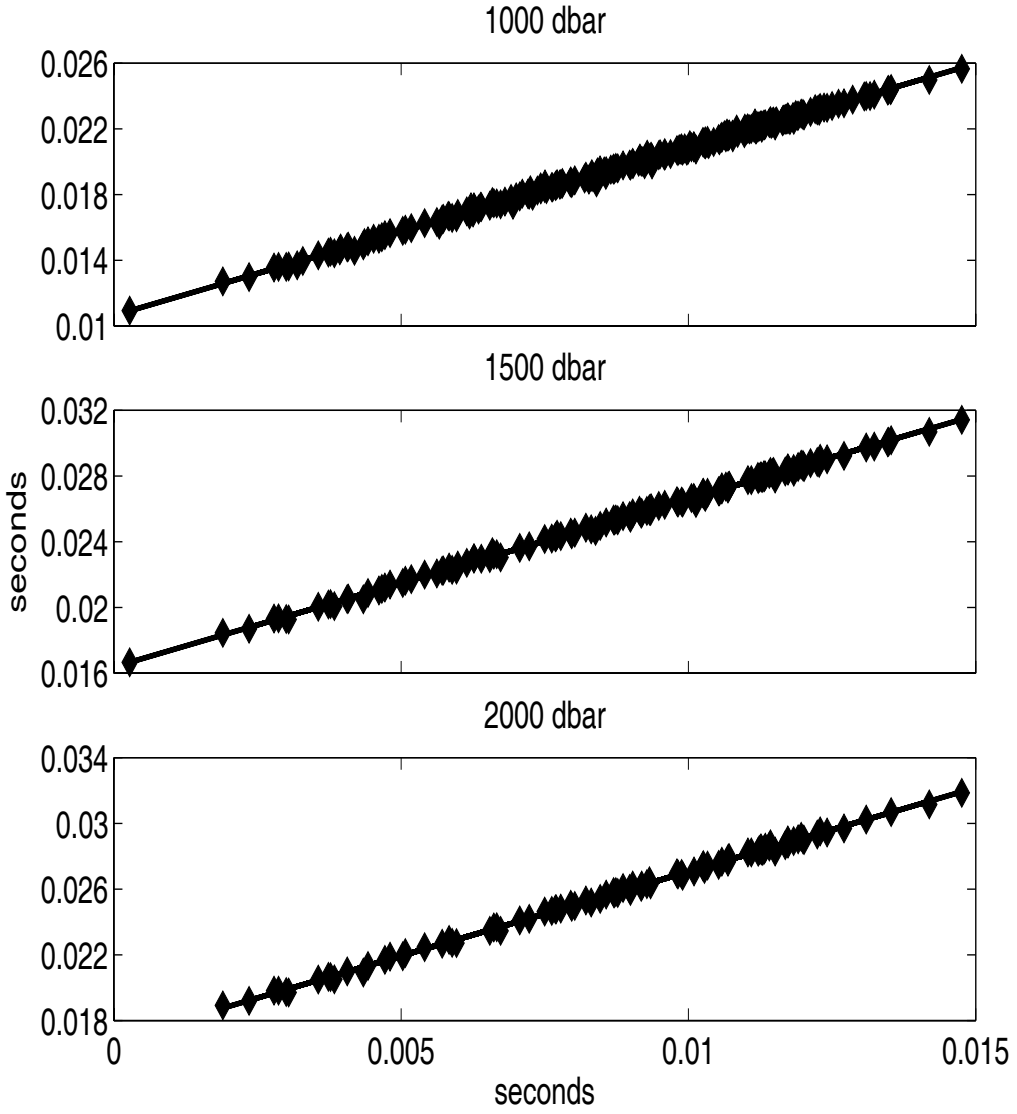

Figure 10: **Comparison of the round trip travel time for a bottom pressure of 500 dbar with the travel times for bottom pressures of 1000 dbar (top), 1500 dbar (middle), and 2000 dbar (bottom).**

2.6.3 Calibration to τ_{500}

It is convenient to have all the travel time data referenced to a common pressure level for subsequent scientific analyses. The calibration steps employed here primarily follow the methods developed by Meinen and Watts (1998). Because baroclinicity in the JES below 500 dbar is weak, and because most CTD casts extend only that deep, 500 dbar was selected as the common pressure level. To determine the projections, we used hydrographic data from several sources: Japan Oceanographic Data Center, Korea Oceanographic Data Center, Northwestern Pacific Hydrobase (MacDonald *et al.*, 2001), Lynne Talley's hydrographic surveys (http://sam.ucsd.edu/onr_jes/) and casts collected on our recovery cruise.

Each hydrocast was interpolated to a common pressure vector with 10 dbar spacing. The casts were then integrated from a suite of deep pressure levels to the surface to simulate the round trip travel times (τ_p) that would be attained from instruments deployed at those depths. For this study, τ_p was simulated for bottom pressures between 600–2700 dbar. Linear relationships were found for the τ_p versus τ_{500} comparisons for all depths (Figure 10). The slopes **A** and intercepts **B** of these relationships were determined. However, since the variations in τ_p are on the orders of milliseconds while the magnitudes are on the order of several seconds, large computational errors can occur when determining these parameters. To minimize the errors,

A and **B** were obtained after removal of a large constant from the travel times. This constant, τ_{con}, was defined as the round trip travel time that would be measured if the sound speed were fixed at 1500 ms^{-1}:

$$\tau_{con}(p) = \frac{2(\frac{p}{1.01})}{1500}$$

where the factor 1.01 dbar m^{-1} converts bottom pressure in decibars to depth in meters.

Different slopes and intercepts were obtained for the relationships between τ_{500} and τ_p for $600 \leq p \leq 2700$ dbar. Figure 11 shows the values obtained for **A**, **b**, and **B** versus pressure. The parameter **b** is the intercept value with the large constant removed, while **B** is the full intercept value. No physical justification could be determined for the observed structure in **A** for $p > 2300$ dbar. Instead this structure was attributed to the limited number of hydrocasts extending to deeper levels (i.e. sampling error). Superimposed on the top two panels are the best fit curves:

$$\mathbf{A}(p) = \begin{cases} a_1 p^4 + a_2 p^3 + a_3 p^2 + a_4 p + a_5 & for\ p \leq 2300\ dbar \\ 9.7547 \times 10^{-1} & for\ p > 2300\ dbar \end{cases}$$
$$\mathbf{b} = b_1 p + b_2$$

where $a_1 = 1.6944 \times 10^{-14},\ a_2 = -1.1256 \times 10^{-10},\ a_3 = 2.6970 \times 10^{-07},\ a_4 = -2.7879 \times 10^{-04},\ a_5 = 1.08353,\ b_1 = -3.8869 \times 10^{-6},\ b_2 = -6.5050 \times 10^{-03}$. The value of **A** for pressures below 2300 db are forced to equal that obtained for p=2300 dbar to avoid introducing nondynamical variability. The intercept **B** is defined as

$$\mathbf{B(p)} = \quad -\mathbf{A(p)}\frac{\mathbf{p}}{\mathbf{750}} + \frac{\mathbf{500}}{\mathbf{750}} + \mathbf{b}$$

where $\frac{500}{750}$ is $\tau_{con}(p)$ for $p = 500$ m (removed from τ_{500}).

All the PIES deployed in the JES were equipped with pressure sensors, and the mean pressure measured at each site was used in the above formulas. The mean values were calculated from the records that had been dejumped, detided and dedrifted. Before applying the formulas, additional adjustments to the pressure and travel time records were required. First, the mean regional atmospheric pressure of 10.14 dbar was removed, since the pressure sensors measured absolute (not gauge) pressure. Second, 0.6 dbar was subtracted to account for the physical separation of the pressure sensor and transducer on the PIES. Third, 3.0 msec were subtracted from the measured travel times to account for an internal response delay of the echo detector. The travel time measured by each instrument (τ_{PIES}) was projected onto τ_{500} using

$$\tau_{500} = \mathbf{A}(p) \times \tau_{PIES} + \mathbf{B}(p)$$

where p is the mean measured pressure, as determined above.

Due to the pressure jumps and sensor drifts, the accuracy of the mean pressures is questionable and may introduce errors into τ_{500}. So further calibration of τ_{500} was necessary. This was accomplished through the use of CTD casts taken at each PIES site approximately 24 hours prior to their recovery and from CTD casts taken at some sites by the National Fisheries and Research Development Institute (NFRDI) and the Japanese Oceanographic Data Center (JODC). There were a total of nine CTD casts taken in August, November, and December 1999, February, April, June, August, October, and December 2000 over 10 sites (P1-2, P1-3, P1-4, P2-2, P2-3, P3-1, P3-2, P3-3, P4-2, and P4-3) by NFRDI. There were two CTD casts taken in June 2000 and June 2001 over two sites (P4-4, P5-5) by JODC. For each CTD cast, τ_{500} was calculated from the temperature and salinity profiles. The calibration coefficient was then calculated as $C_{CTD} = \overline{\tau_{500_{PIES}} - \tau_{500_{CTD}}}$, where the overbar means the average of all available CTD measurements at the site (except for P1-5 which required special calibration, described below). The calibration coefficients are shown in Table 4. The best estimate of τ_{500} is then,

$$\tau_{500} = \mathbf{A}(p) \times \tau_{PIES} + \mathbf{B}(p) + C_{CTD}.$$

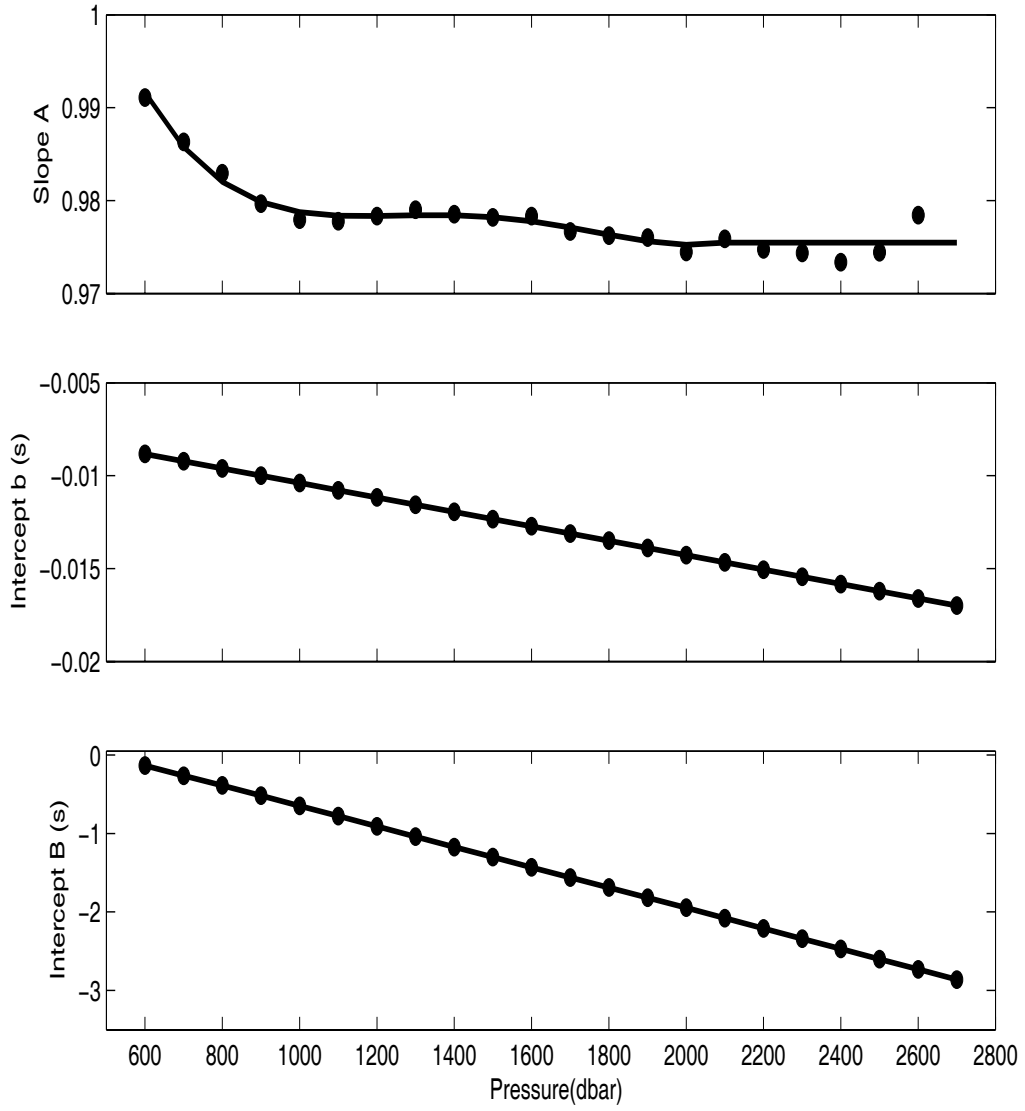

Figure 11: Top panel: Slope **A**. Middle panel: intercept **b** determined with the constant $\tau_{con}(p)$ removed. Bottom panel: full intercept value **b**. All parameters are plotted as a function of pressure.

Table 4: τ_{500} calibration coefficient C_{CTD} calculated from CTDs taken at the PIES sites.

Site	C_{CTD}	Site	C_{CTD}
P1-1	2.1815 ms	P3-2	-0.0028 ms
P1-2	1.5096 ms	P3-3	-0.3165 ms
P1-3	2.9111 ms	P3-4	10.3334 ms
P1-4	1.6807 ms	P4-2	9.8386 ms
P1-5	2.2495 ms	P4-3	6.6115 ms
P1-6	-0.6929 ms	P4-4	6.4957 ms
P2-1	16.4823 ms	P4-5	0.6740 ms
P2-2	3.6025 ms	P5-1	5.4287 ms
P2-3	-1.2967 ms	P5-2	2.9832 ms
P2-4	1.3002 ms	P5-3	12.9066 ms
P2-5	3.8464 ms	P5-4	2.7802 ms
P3-1	-1.2226 ms	P5-5	2.2836 ms

Site P1-5 required a different method of calibration because the τ measurement failed after three months. This rendered the CTD collected 24 hours prior to its recovery useless for calibration. We chose to calculate C_{CTD} for P1-5 by using the calibrated data from the adjacent sites. First we calculated the mean τ_{500} at P1-5 over the 90-day period it operated. We also calculated the mean τ_{500} (calibrated using C_{CTD}) of sites P1-4 and P1-6 over the same time period. The calibration coefficient C_{CTD} for P1-5 was calculated by linearly interpolating these means as:

$$C_{CTD,P1-5} = \overline{\tau_{500}(P1-4, 90\ d)}\frac{\Delta x_{P1-5}}{\Delta x_{P1-6}} + \overline{\tau_{500}(P1-6, 90\ d)}\frac{\Delta x_{P1-6} - \Delta x_{P1-5}}{\Delta x_{P1-6}} - \tau_{500}(P1-5, 90\ d)$$

where Δx is the distance of sites P1-5 and P1-6 from P1-4.

Expected errors in τ_{500} arise from uncertainties in the τ and pressure measurements and the processing methods. The accuracy of the travel time measurement, which is 1 ms (Chaplin and Watts, 1984), contributes an uncertainty in τ_{500} after 120 hour low-pass filtering, of $\epsilon_\tau = 1\ \text{ms}/\sqrt{120} = 0.09$ ms. An additional error arises from the projection to 500 dbar from the actual bottom pressure. This error is due to the scatter about the **A** and **B** versus pressure curves shown in Figure 11. The combined error ϵ_{AB} was determined by quantifying the scatter of the τ_{500} versus τ_p relationships shown in Figure 10. The scatter ranged from 0.1 to 0.4 ms, thus, we set ϵ_{AB}=0.4 ms. The accuracy of the pressure sensor is given as $\pm 0.01\%$ of the sensor's full scale. Sensors with two different full scales were used for this experiment: 6000 psi ($\sim$4000 dbar) and 10000 psi ($\sim$6800 dbar), giving pressure sensor accuracies of 0.40 and 0.68 dbar. Assuming the average sound speed is 1500 m s^{-1}, these yield travel time uncertainties ϵ_{ps} of $2(0.4)/1500$ and $2(0.68)/1500$, or about .5 ms and 1 ms. Additional sources of error in the pressure records due to the removal of pressure jumps and drifts must also be determined. The minimum accuracy of the method used to remove the pressure jumps is determined by the scatter in the pressure record immediately before and after the jumps, which is typically 0.01 dbar. This gives a travel time uncertainty due to pressure jumps $\epsilon_{pj} = 0.013$ ms. The uncertainty arising from removing the drift is difficult to quantify, however, a reasonable estimate is possible due to the dominance of the basin average signal (BA). The final pressure records, which have been detided, dejumped (if necessary), dedrifted, and low pass filtered to remove the error associated with ϵ_{ps}, should only contain the basin average and the remaining ocean signal. Since we do not know the ocean signal *a priori*, we assume its long term mean is zero and take the mean of the final pressure record minus the basin average as the uncertainty of the drift removal, that is $\overline{p_{fin} - BA}$. This yields a typical uncertainty for the drift removals of 0.0012 dbar or $\epsilon_{pd} = 10^{-6}$ ms. Thus, the total uncertainty of τ_{500} is $\epsilon_{total} = (\epsilon_\tau^2 + \epsilon_{AB}^2 + \epsilon_{ps}^2 + \epsilon_{pj}^2 + \epsilon_{pd}^2)^{\frac{1}{2}} = 0.65$ ms for the 6000 psi sensor and 1.1 ms for the 10000 psi sensor. Bias errors may exceed these random errors: Echo detector times may have varied between these old model instruments by 2 ms. Pressure sensors may have drifted in calibration by a few decibars, equivalent to a few milliseconds. Some instruments changed depth. These latter errors account for much of the C_{CTD} offsets in Table 4.

2.7 Leveling and Low-Pass Filtering

The hourly pressure records were also leveled to a common geopotential using the mean currents measured by the current meter moorings following the procedures described in Watts *et al.* (2001). Leveled records are obtained by subtracting the mean pressure and adding the leveling constants listed in Table 5.

The leveled pressure and τ_{500} records were low-pass filtered using a fourth-order Butterworth filter with a cutoff period of 120 hours. The filter was passed forward and backward in time to avoid introducing phase shifts. Approximately 40 hours of data at each end of the filtered records were discarded to avoid startup transients. After filtering, the time series were sampled at 12-hour intervals centered at 0000 and 1200 UT. The low-pass filtered pressures are shown in Figures 22–45 together with the hourly leveled pressures. The low-pass filtered τ_{500} records are in Figures 72–77.

3 Pressure Records for Each Instrument

This section illustrates the hourly pressure records from the least to highest degree of processing.

The raw records are shown in Figures 12–14. These records include the tides, jumps and drifts. The site designation and Paros serial number are labeled in each panel. The type of inverted echo sounder are indicated as URI for SD-URI models, SD for SD-NRL models, and WHI for WHISL models. Time in days since January 1, 1999 0000 UT is plotted along the x-axis and selected dates are indicated.

Figure 15 shows a 65-day portion of the tidal signal for each instrument to illustrate the site-to-site variation.

Hourly residual pressure records which have the jumps, means, basin average, and tides removed are shown in Figures 16–18 with the fitted drift curves superimposed.

The best quality hourly pressure data, containing all ocean signals, are plotted in Figures 19–21. These pressures have had jumps, drifts and spikes removed, but still include the basin average and the tidal signals. These records are provided on the accompanying CD-ROM. Table 5 lists the mean and standard deviation for each site. The minimum and maximum were calculated after removing the mean from the records since the ranges are small relative to the bottom depth.

The leveled pressure records (jumps, basin average, tides, means, and drifts removed and leveling constant added) are plotted using an expanded time axis. Each instrument is shown on a separate page (Figures 22–45). The hourly pressures are plotted in gray with the 120-hour low-pass filtered records superimposed in black. The leveling constants are listed in Table 5. The low-pass filtered records are provided on the accompanying CD-ROM.

Table 5: Statistics on the hourly pressure records shown in Figures 19–21. The minimum (min) and maximum (max) were calculated after removing the mean. The standard deviations (STD) and leveling constants (LC) are listed.

Site	Start Time (UT)	End Time (UT)	Time Interval (hours)	Mean (dbar)	LC (dbar)	Min (mbar)	Max (mbar)	STD (mbar)
11	15 June 1999 21:30:12	23 June 2001 03:30:12	1.0	1164.073	0.00081	-2.088	2.485	0.608
12	15 June 1999 21:29:54	23 June 2001 03:29:54	1.0	1657.201	0.00297	-3.870	3.905	1.093
13	15 June 1999 21:29:60	23 June 2001 03:29:60	1.0	1868.961	0.00383	-2.988	2.916	0.855
14	15 June 1999 21:29:38	23 June 2001 03:29:38	1.0	1370.603	0.00012	-11.825	6.670	1.739
15	15 June 1999 21:29:10	23 June 2001 03:29:10	1.0	2631.094	0.00003	-3.459	3.955	1.051
16	15 June 1999 21:29:51	23 June 2001 03:24:51	9.9999530E-001	2520.794	-0.00016	-2.608	2.422	0.631
21	15 June 1999 21:30:08	23 June 2001 03:30:08	1.0	1018.049	-0.00263	-4.150	4.416	1.220
22	15 June 1999 21:30:03	23 June 2001 03:30:03	1.0	1627.430	0.00075	-3.558	4.482	1.128
23	15 June 1999 21:30:35	23 June 2001 03:30:35	1.0	2197.038	0.00238	-1.827	1.717	0.492
24	15 June 1999 21:29:53	23 June 2001 03:29:53	1.0	2364.553	-0.00018	-2.497	2.197	0.765
25	15 June 1999 21:30:01	23 June 2001 03:30:01	1.0	1680.302	0.00036	-4.637	4.685	1.370
31	15 June 1999 21:29:25	23 June 2001 03:29:25	1.0	1012.167	-0.00514	-4.981	3.150	0.876
32	15 June 1999 21:29:45	23 June 2001 03:20:44	1.0	2197.042	-0.00523	-3.870	3.311	0.872
33	15 June 1999 21:30:25	23 June 2001 03:30:25	1.0	2203.019	0.00027	-2.373	2.148	0.666
34	15 June 1999 21:29:35	23 June 2001 03:29:35	1.0	2148.495	-0.00235	-2.149	2.140	0.627
42	15 June 1999 21:29:37	23 June 2001 03:29:37	1.0	2016.719	-0.00173	-2.810	2.600	0.770
43	15 June 1999 21:29:46	23 June 2001 03:21:48	9.9999250E-001	2036.741	-0.00157	-2.436	2.662	0.659
44	15 June 1999 21:29:46	23 June 2001 03:29:46	1.0	1817.409	0.00047	-3.923	5.192	0.995
45	15 June 1999 21:31:15	23 June 2001 03:31:15	1.0	1214.067	0.00098	-4.997	5.137	1.342
51	15 June 1999 21:29:37	23 June 2001 03:20:09	9.9999110E-001	1013.643	-0.00041	-4.917	4.371	1.096
52	15 June 1999 21:29:02	23 June 2001 03:29:02	1.0	1384.450	-0.00248	-4.299	5.066	1.139
53	15 June 1999 21:29:43	23 June 2001 03:20:54	9.9999170E-001	1235.822	0.00036	-5.743	3.715	1.024
54	15 June 1999 21:29:02	23 June 2001 03:29:02	1.0	1144.312	0.00036	-3.857	3.687	0.860
55	15 June 1999 21:29:60	23 June 2001 03:29:60	1.0	1065.882	0.00035	-2.469	2.157	0.605

Figure 12: **P1-1–P2-2 Raw Pressure Records.**

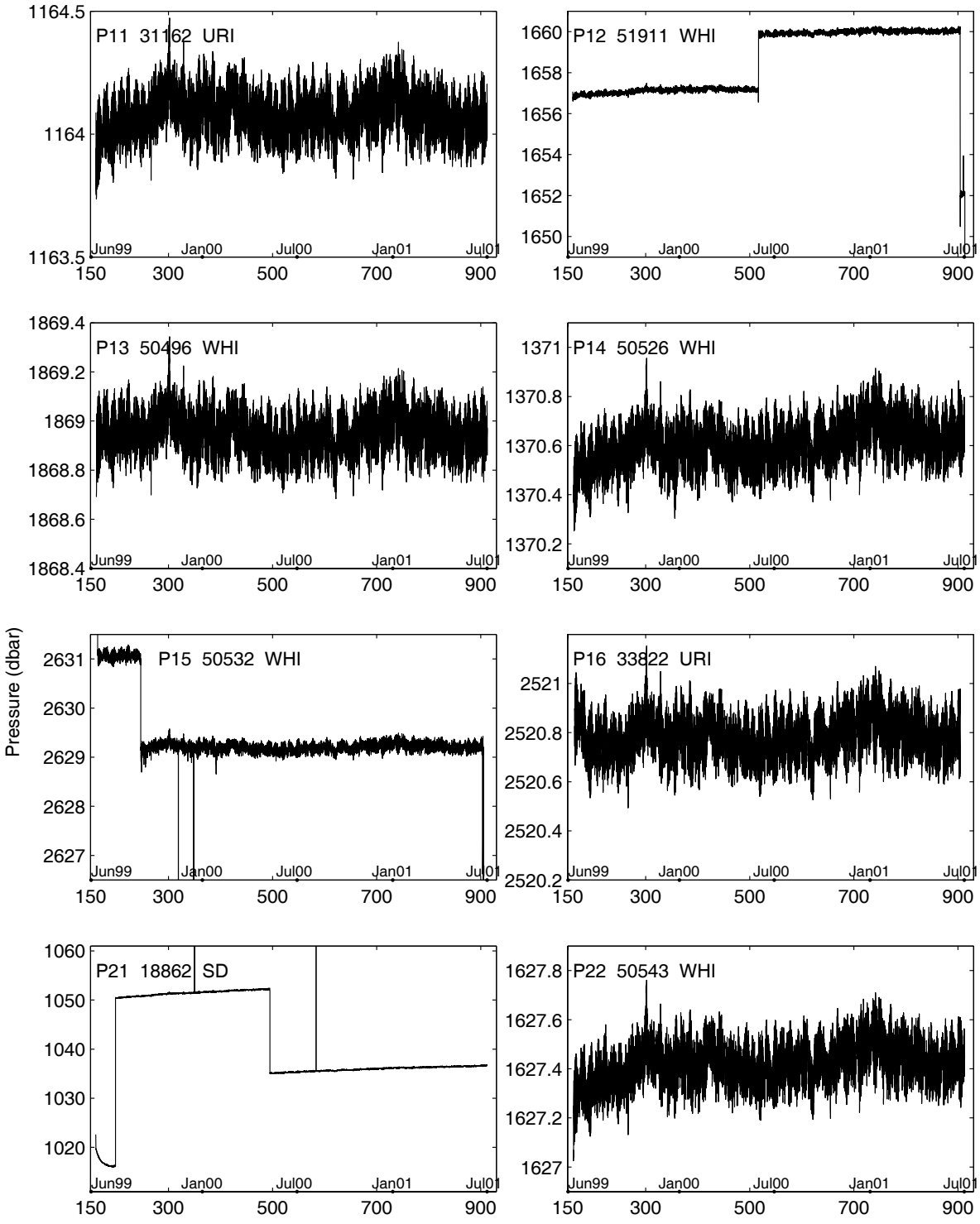

Figure 13: **P2-3–P4-2 Raw Pressure Records.**

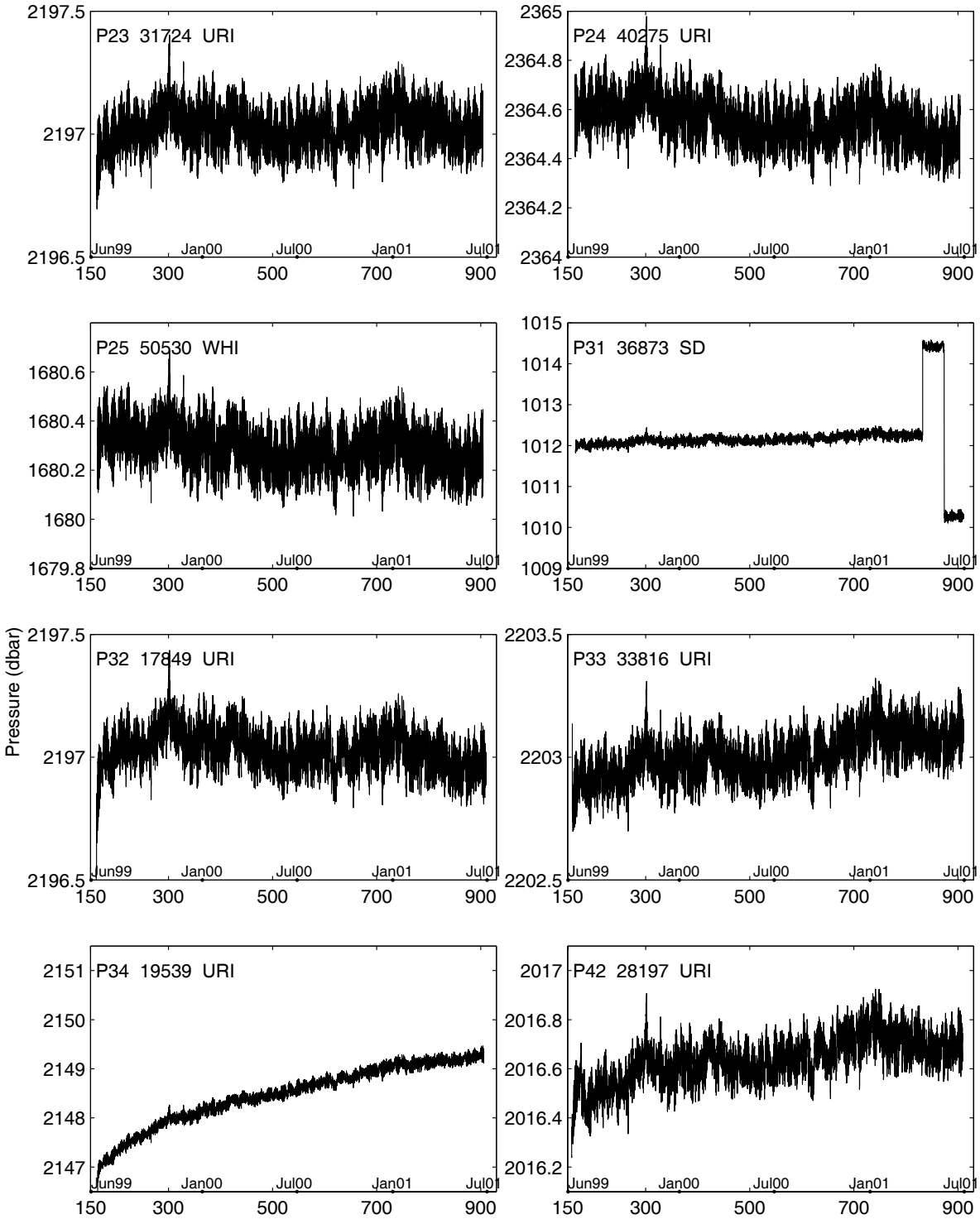

Figure 14: **P4-3–P5-5 Raw Pressure Records.**

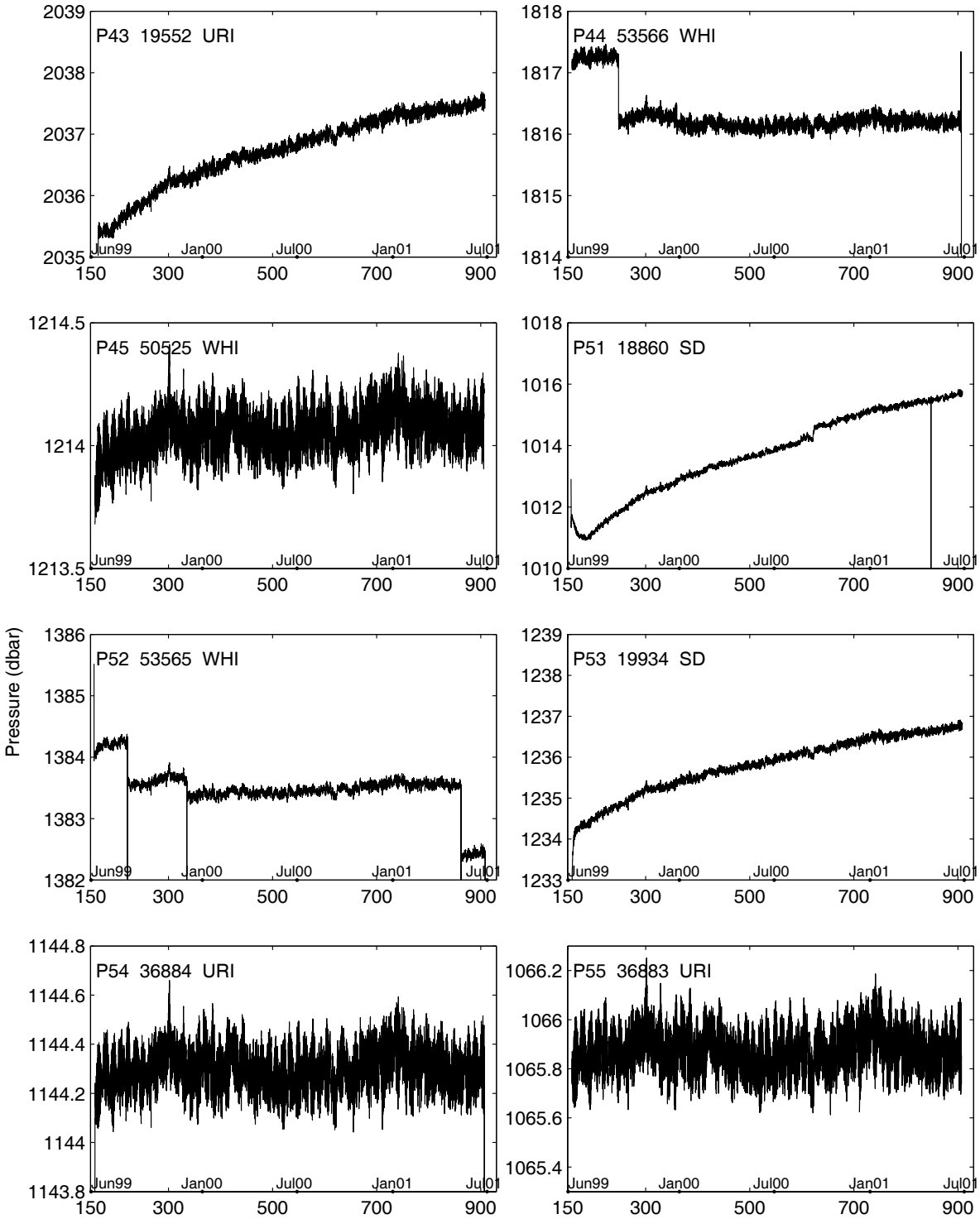

Figure 15: **65-day Portion of the P1-1–P5-5 Tidal Records**

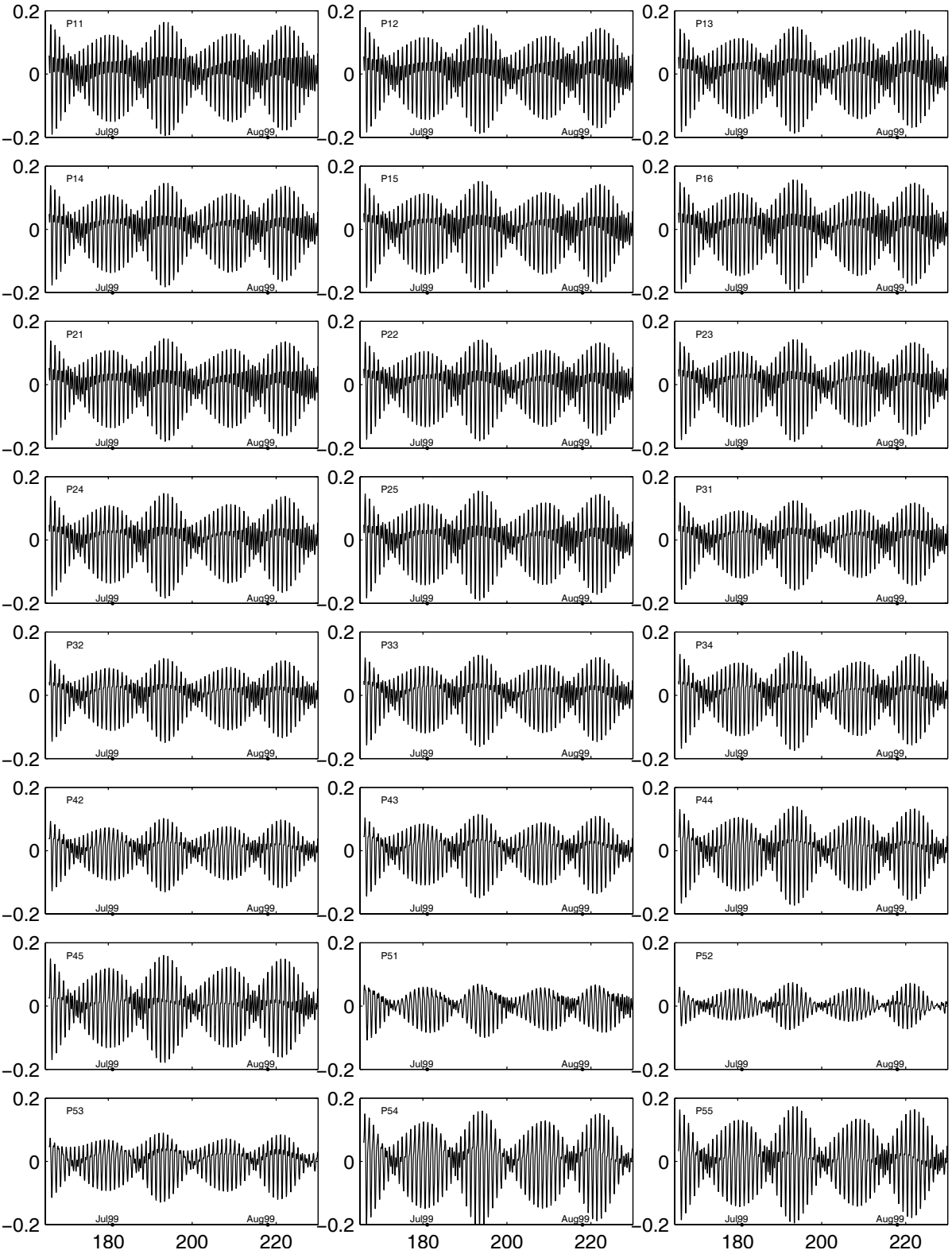

Figure 16: **P1-1–P2-2 Residual Pressure Records Including Drift.**

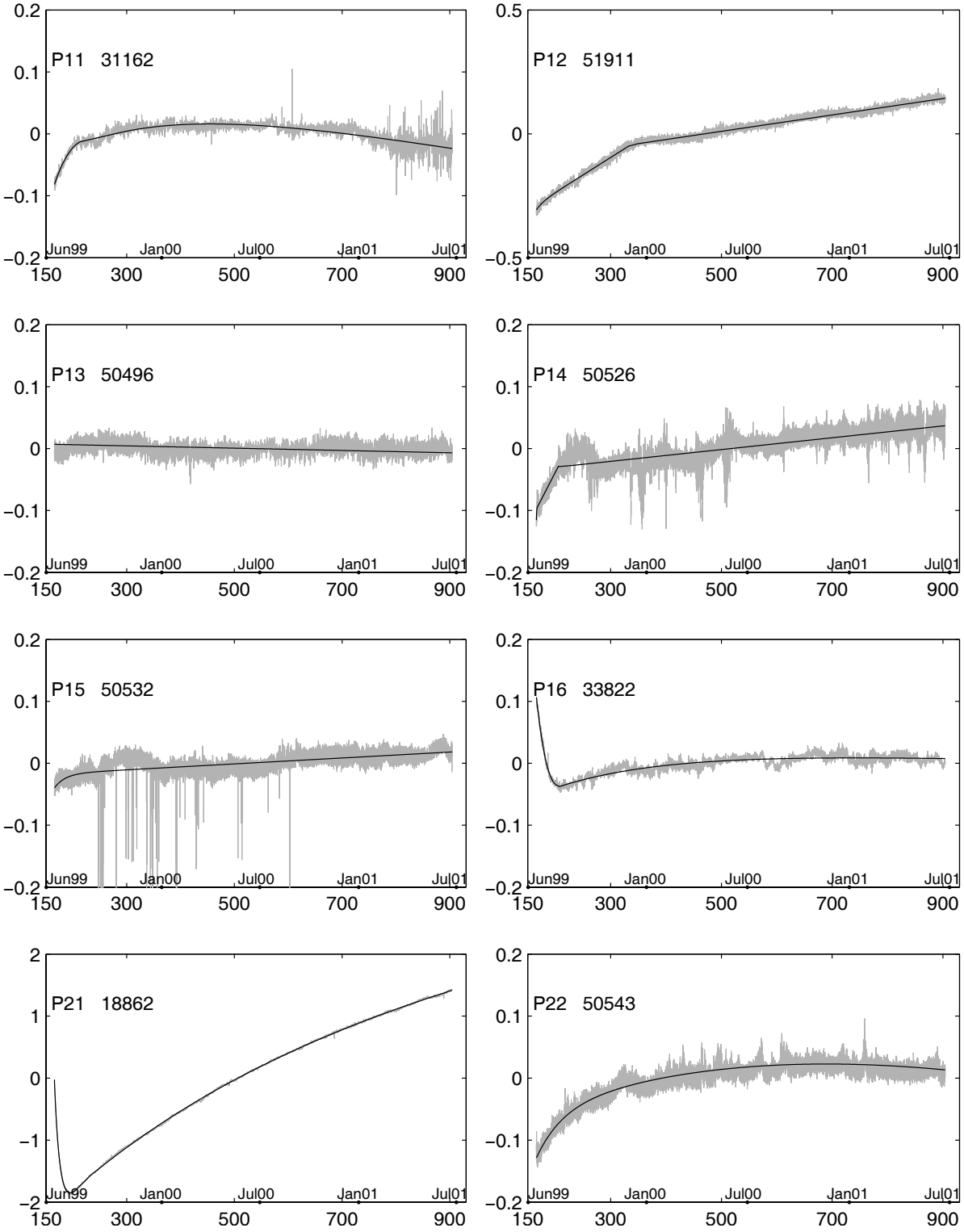

Figure 17: **P2-3–P4-3 Residual Pressure Records Including Drift.**

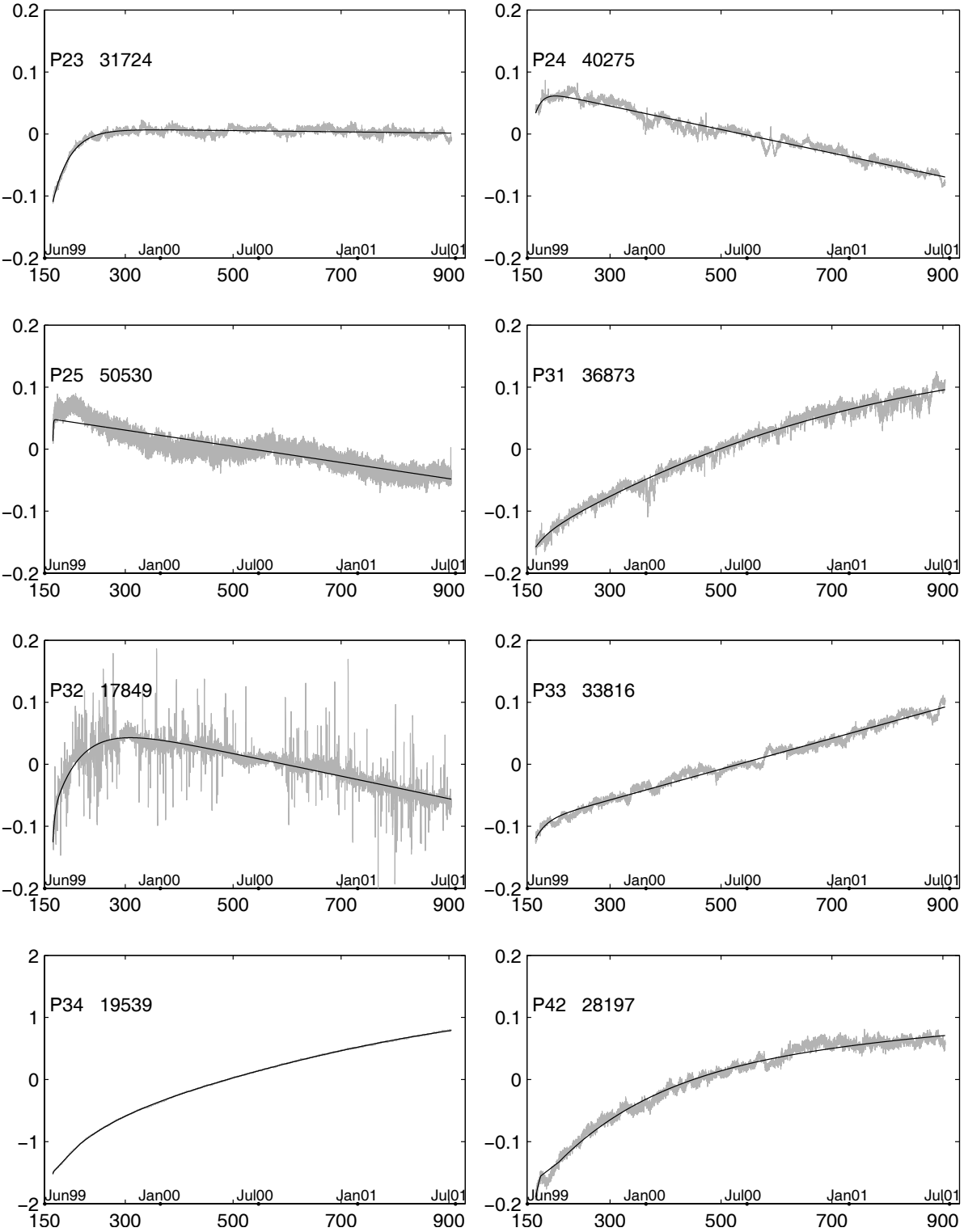

Figure 18: **P4-4–P5-5 Residual Pressure Records Including Drift.**

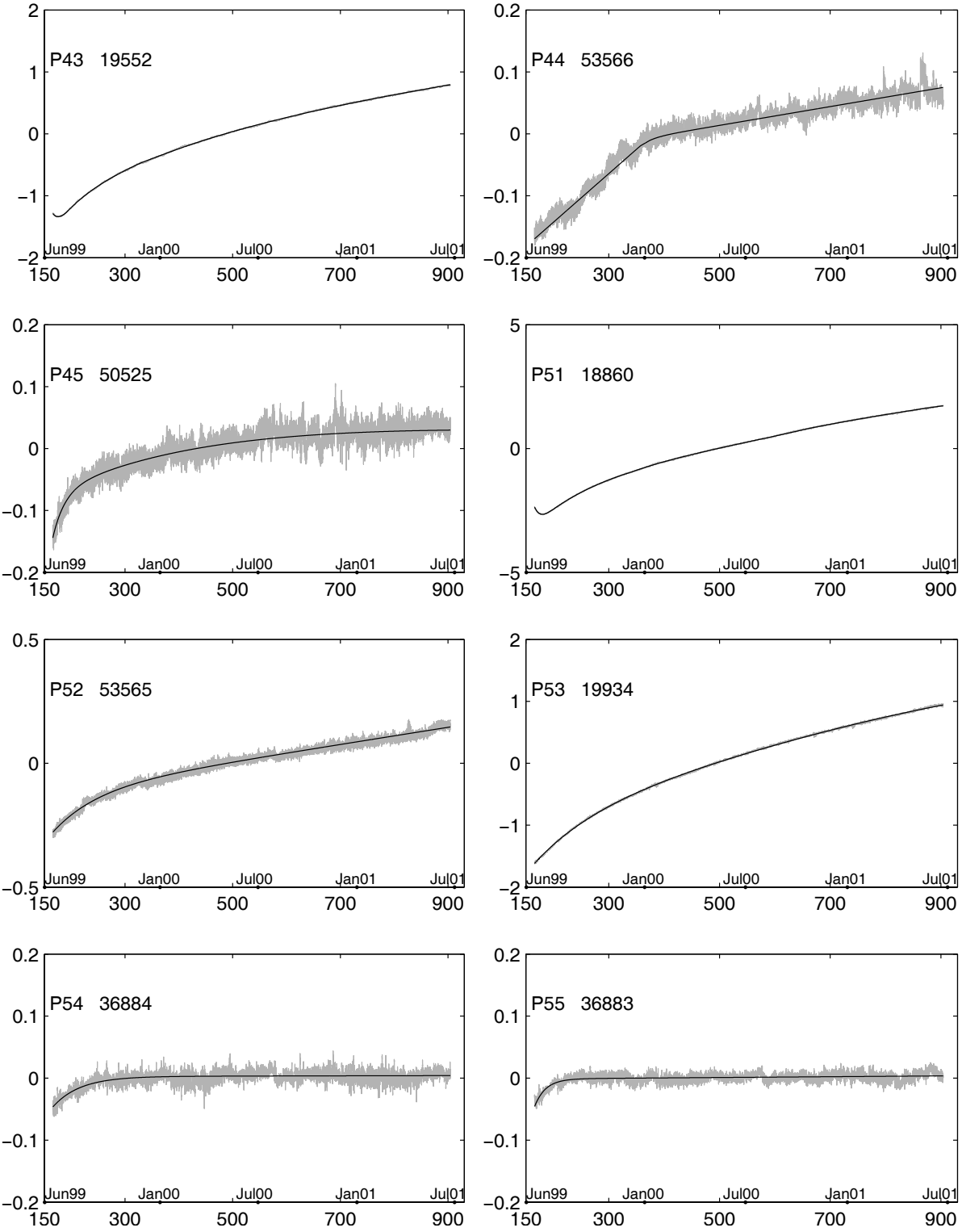

Figure 19: **P1-1–P2-2 Hourly Pressures.**

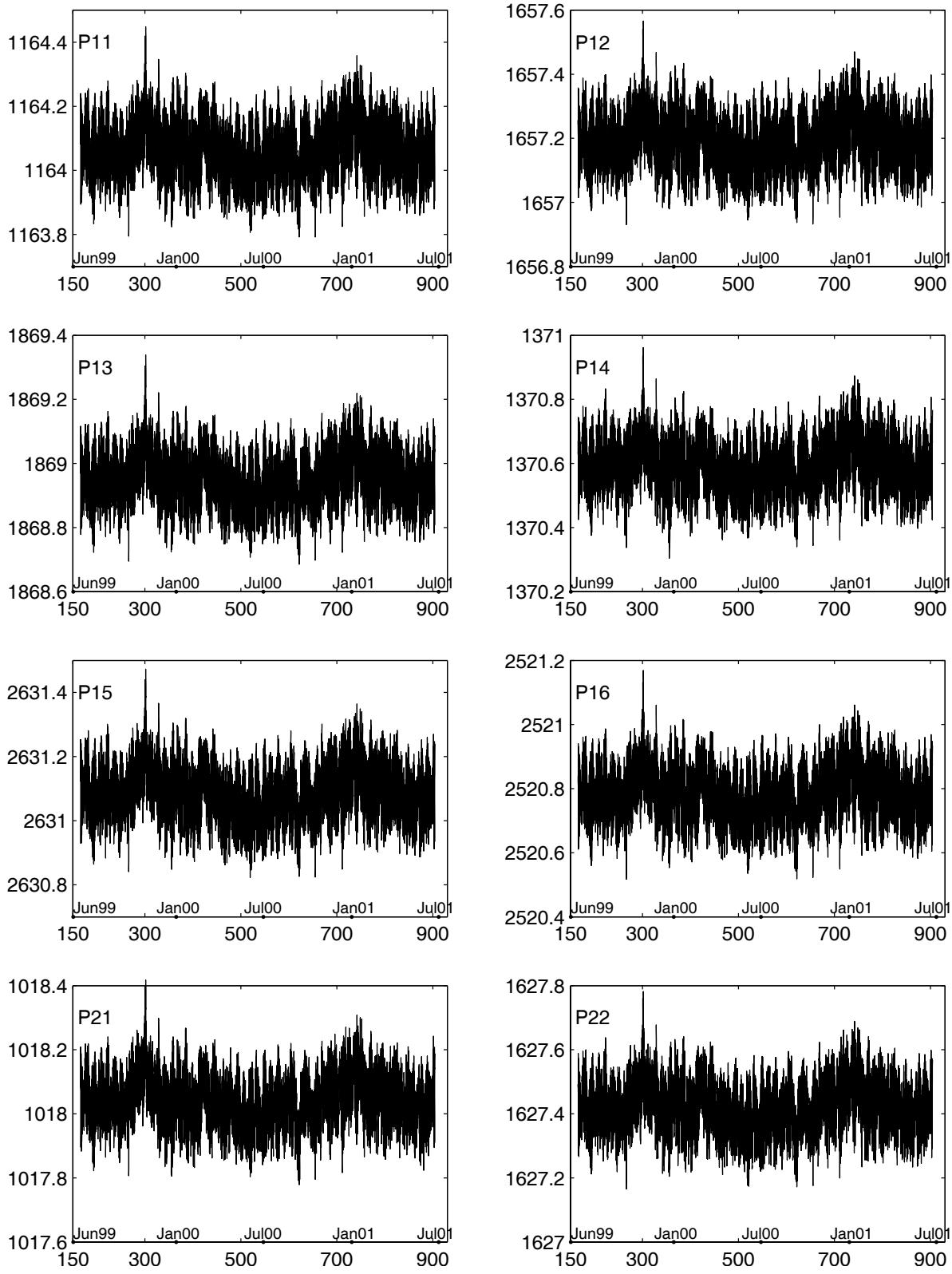

Figure 20: **P2-3–P4-3 Hourly Pressures.**

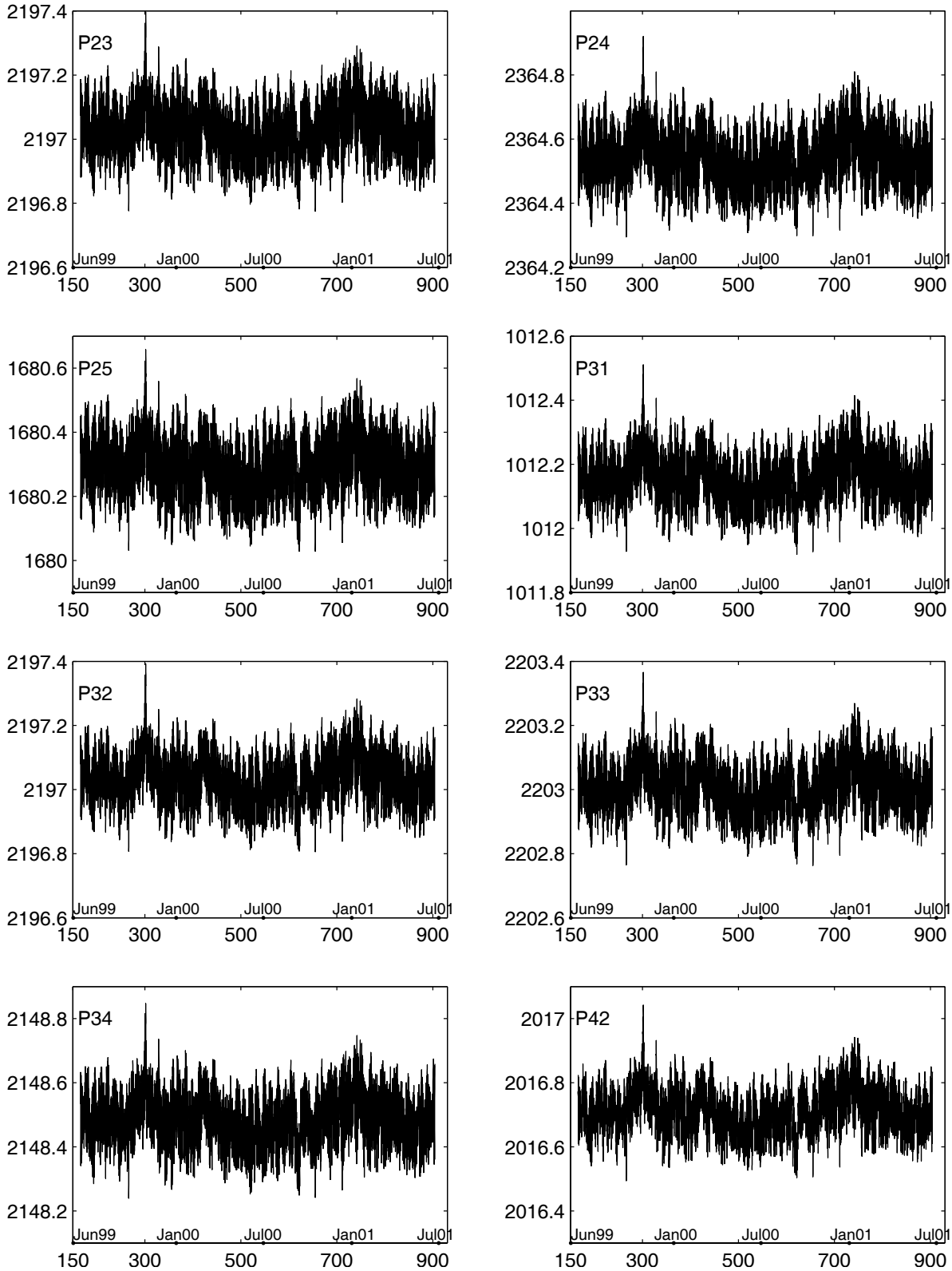

Figure 21: **P4-4–P5-5 Hourly Pressures.**

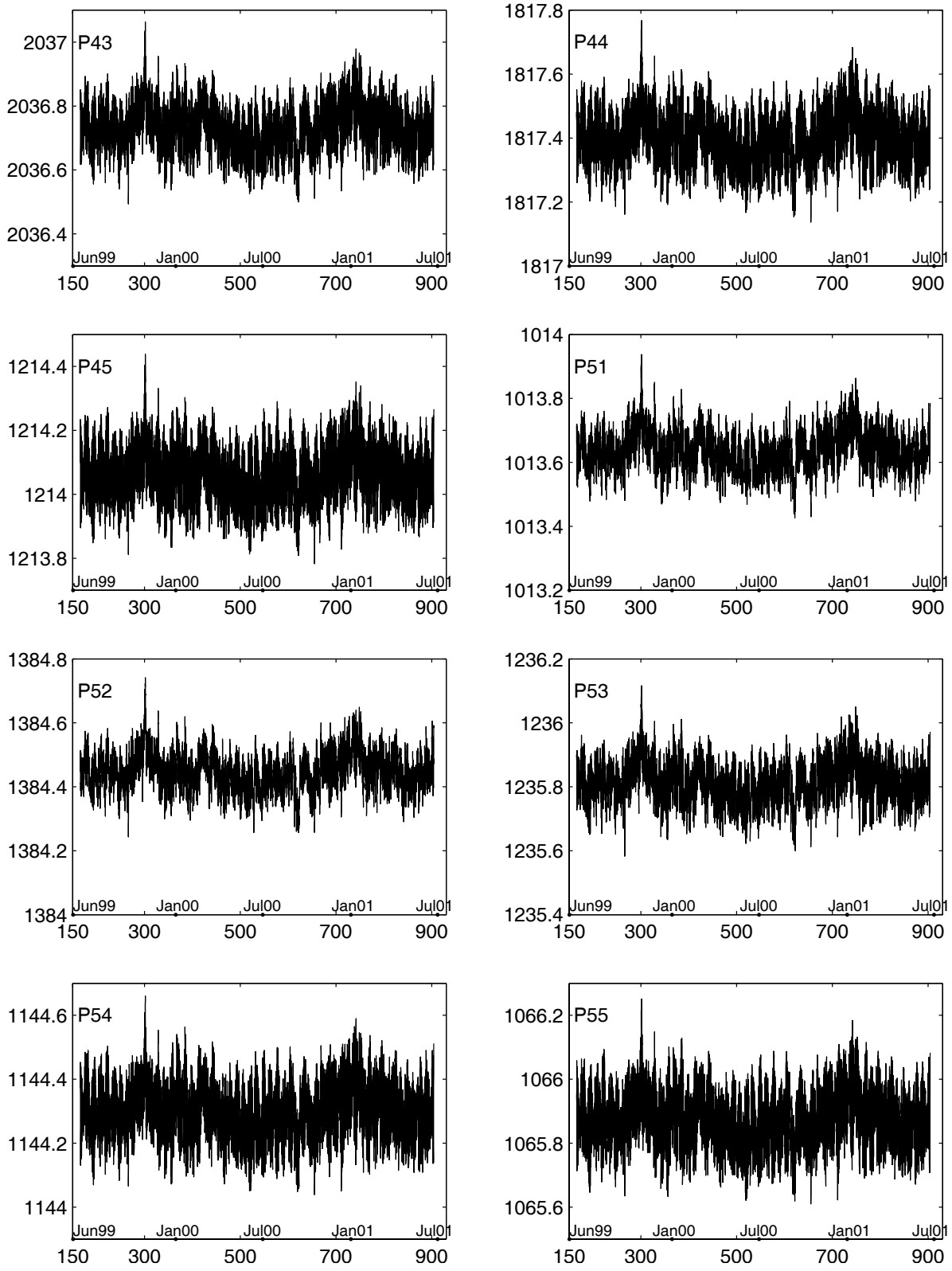

Figure 22: **P1-1 Hourly and 120-hrlp Leveled Pressures**

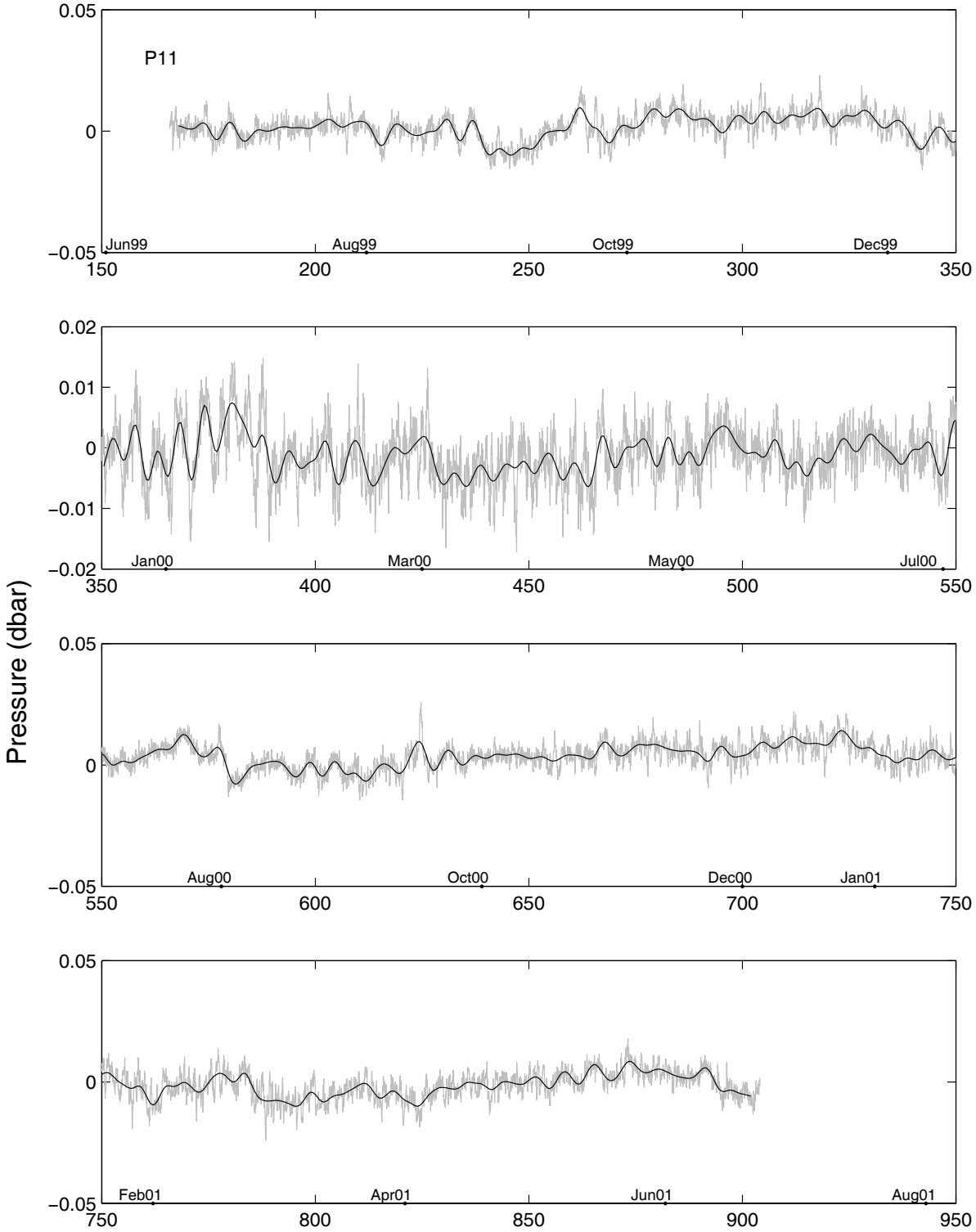

Figure 23: **P1-2 Hourly and 120-hrlp Leveled Pressures**

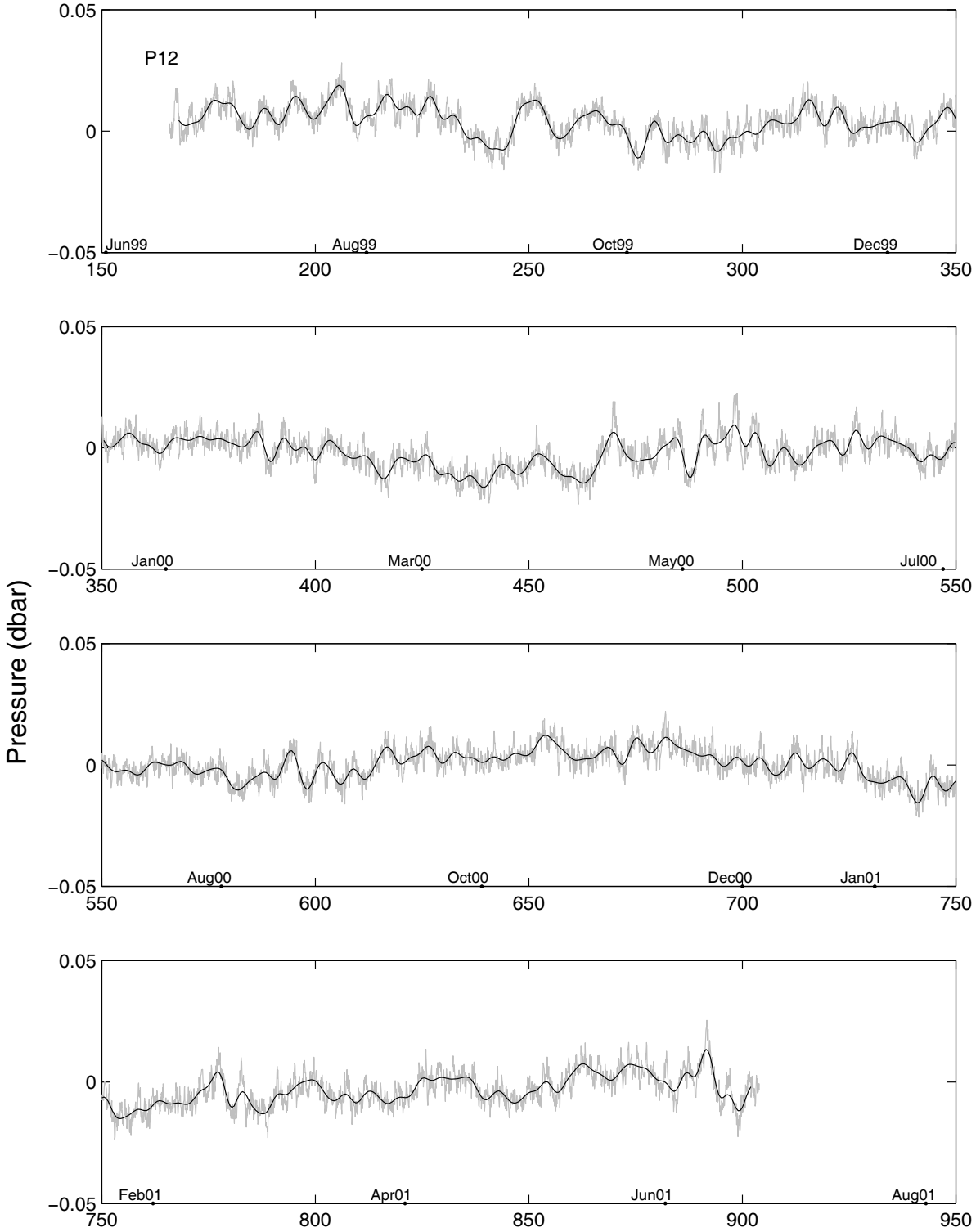

Figure 24: **P1-3 Hourly and 120-hrlp Leveled Pressures**

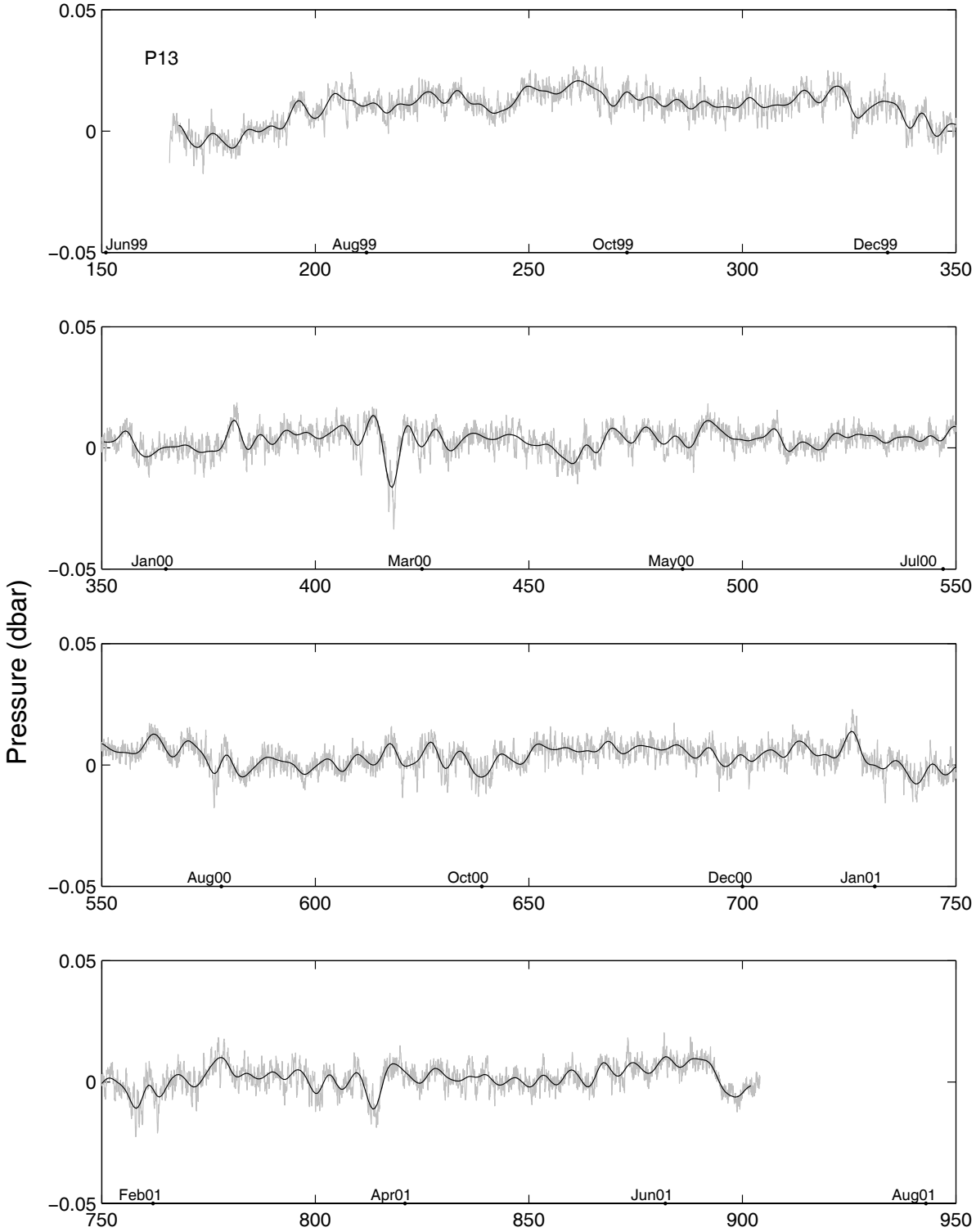

Figure 25: **P1-4 Hourly and 120-hrlp Leveled Pressures**

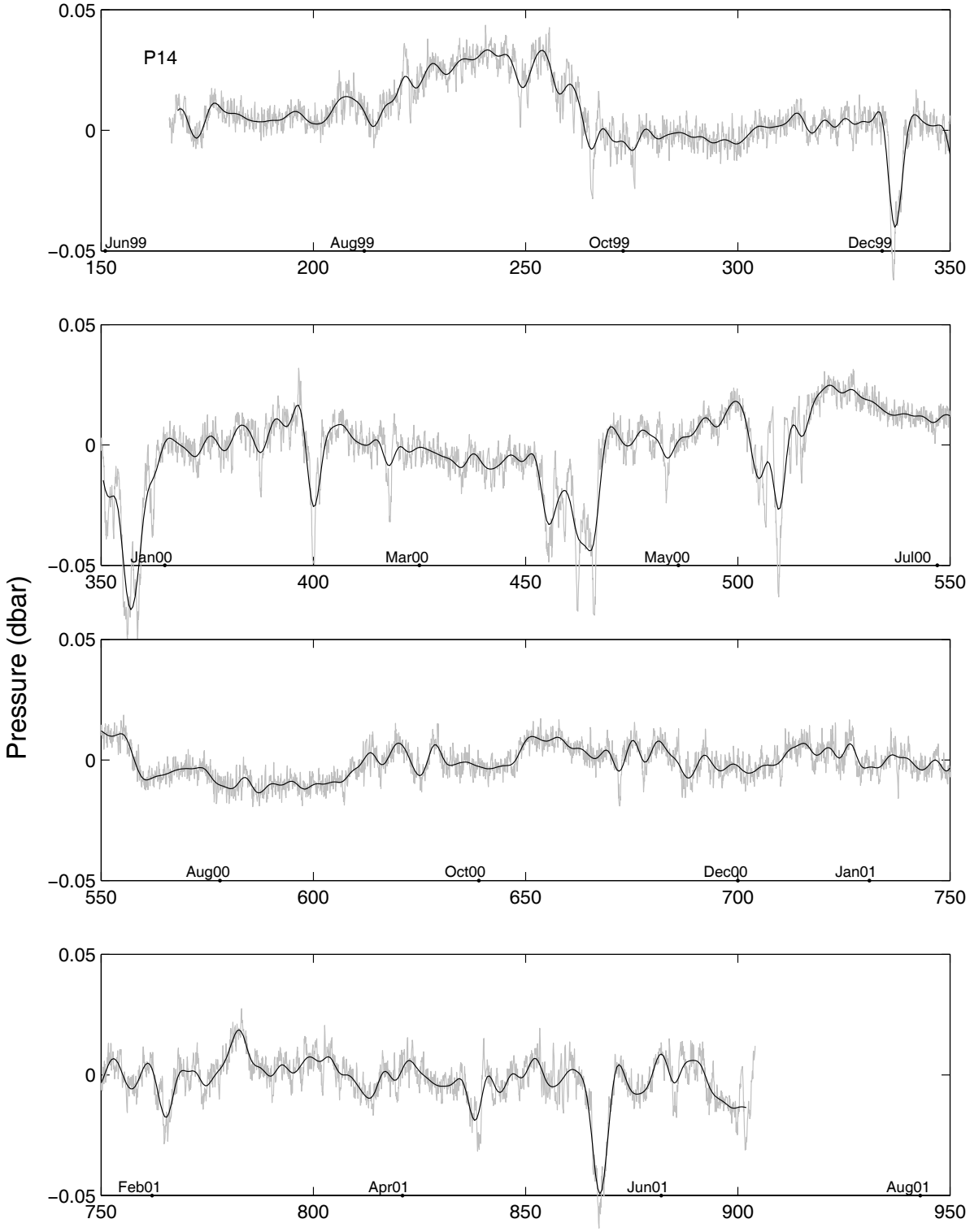

Figure 26: **P1-5 Hourly and 120-hrlp Leveled Pressures**

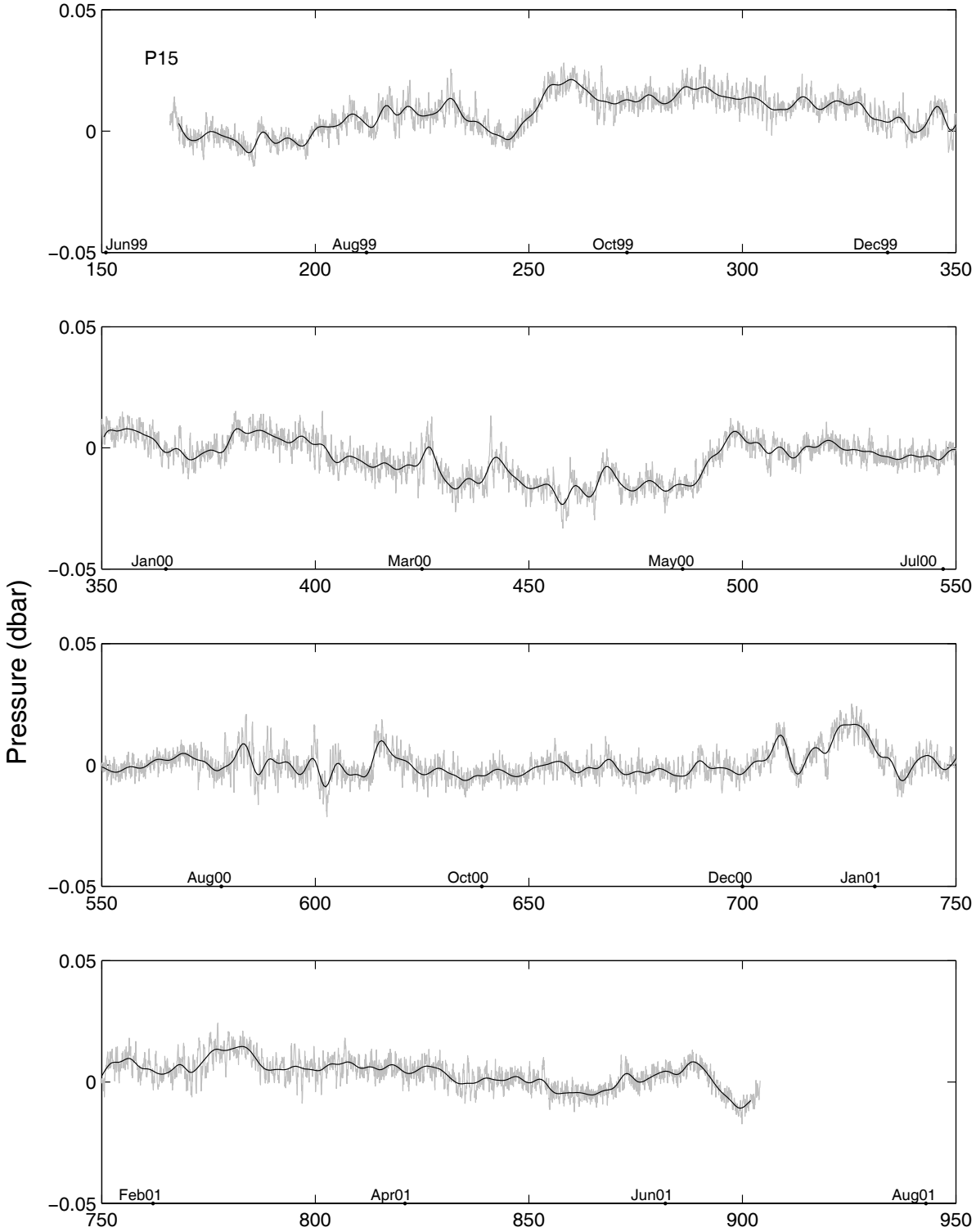

Figure 27: **P1-6 Hourly and 120-hrlp Leveled Pressures**

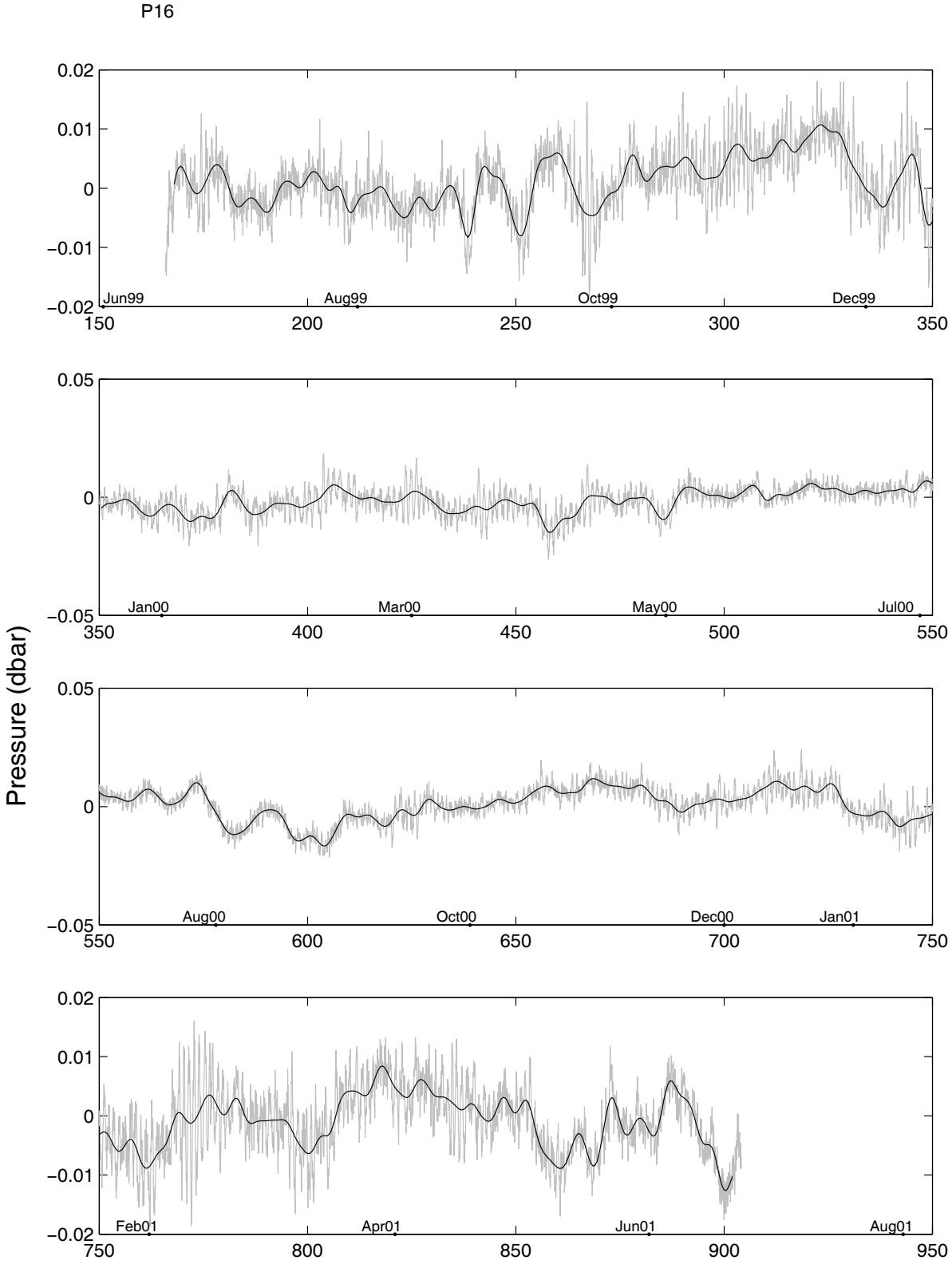

Figure 28: **P2-1 Hourly and 120-hrlp Leveled Pressures**

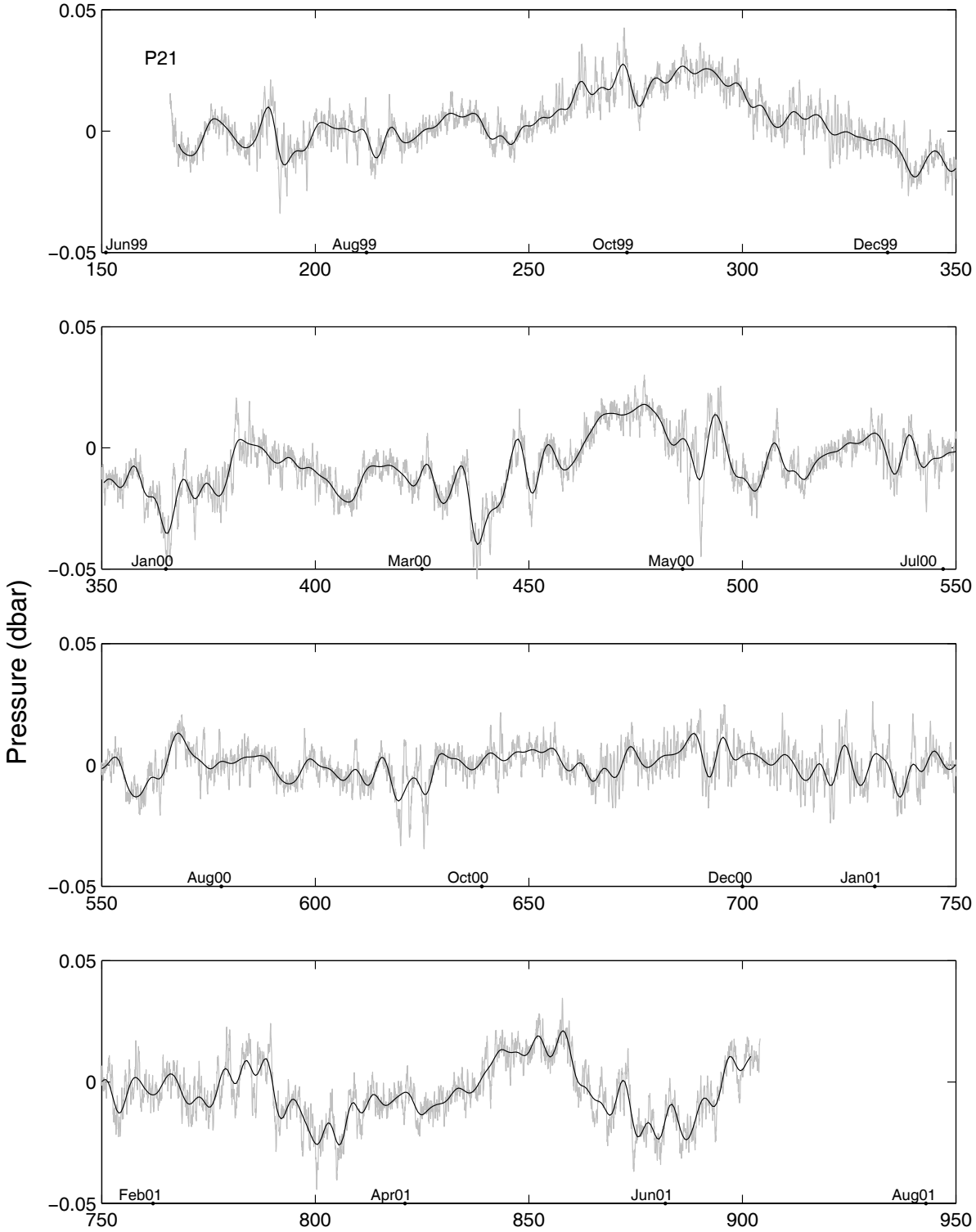

Figure 29: **P2-2 Hourly and 120-hrlp Leveled Pressures**

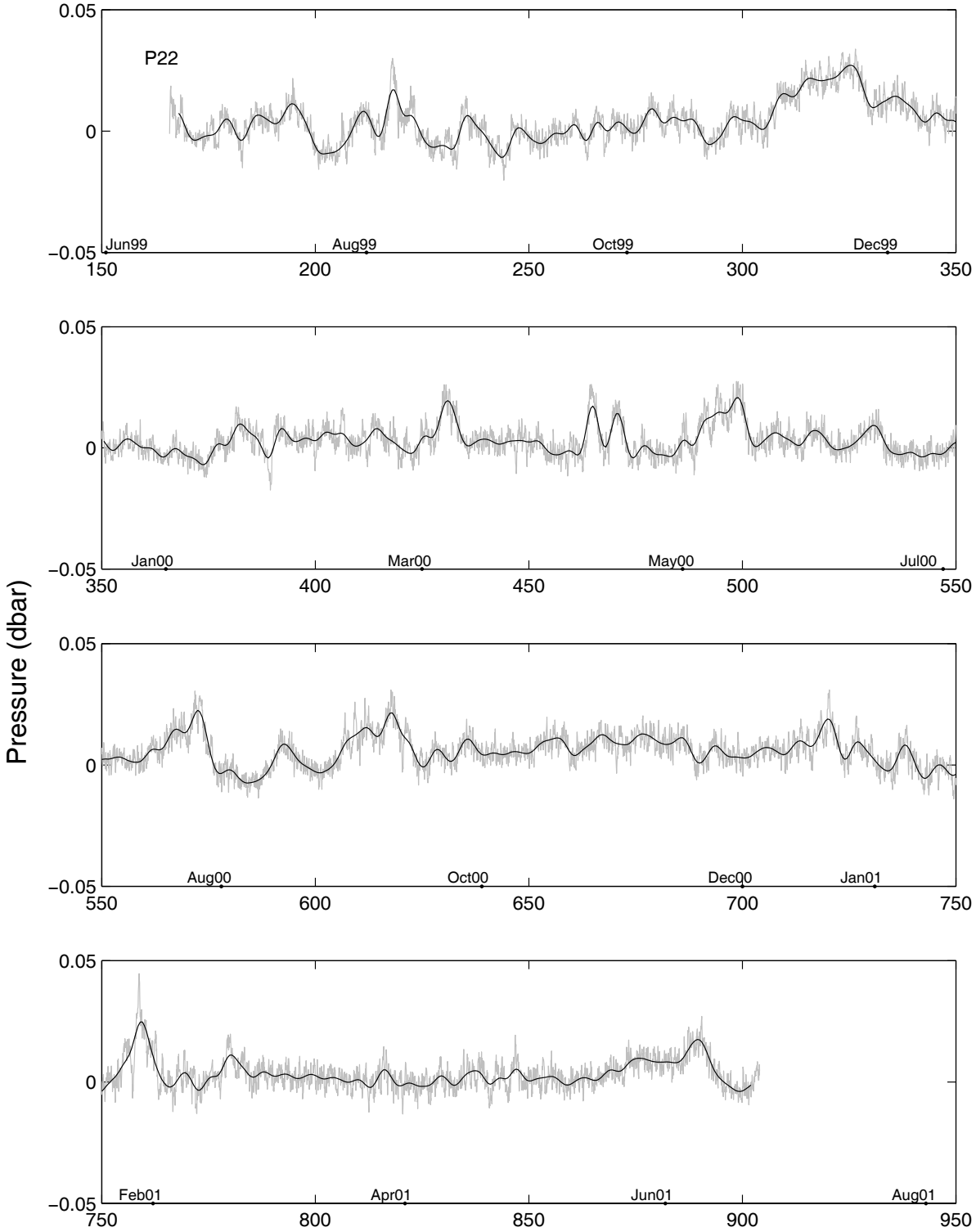

Figure 30: **P2-3 Hourly and 120-hrlp Leveled Pressures**

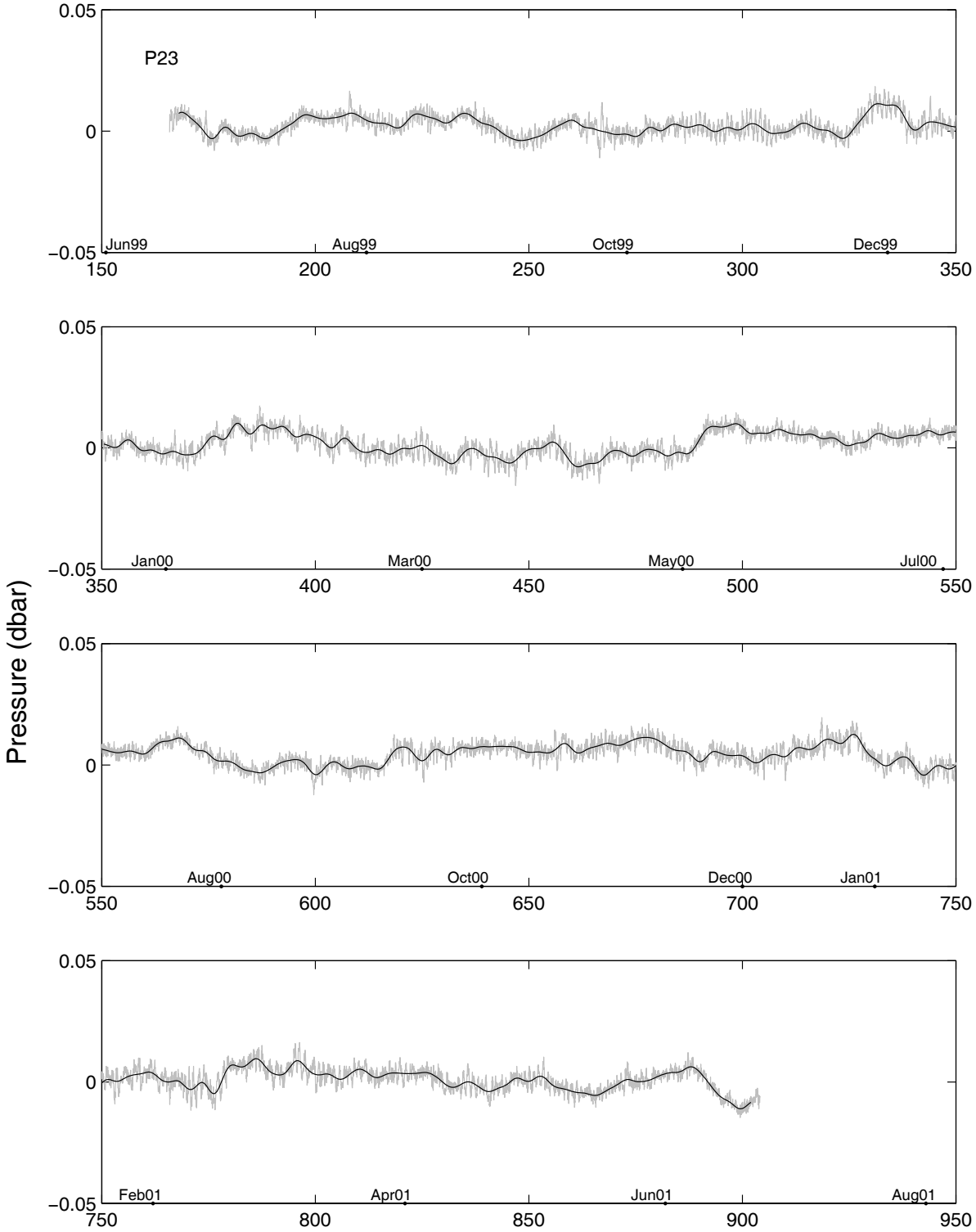

Figure 31: **P2-4 Hourly and 120-hrlp Leveled Pressures**

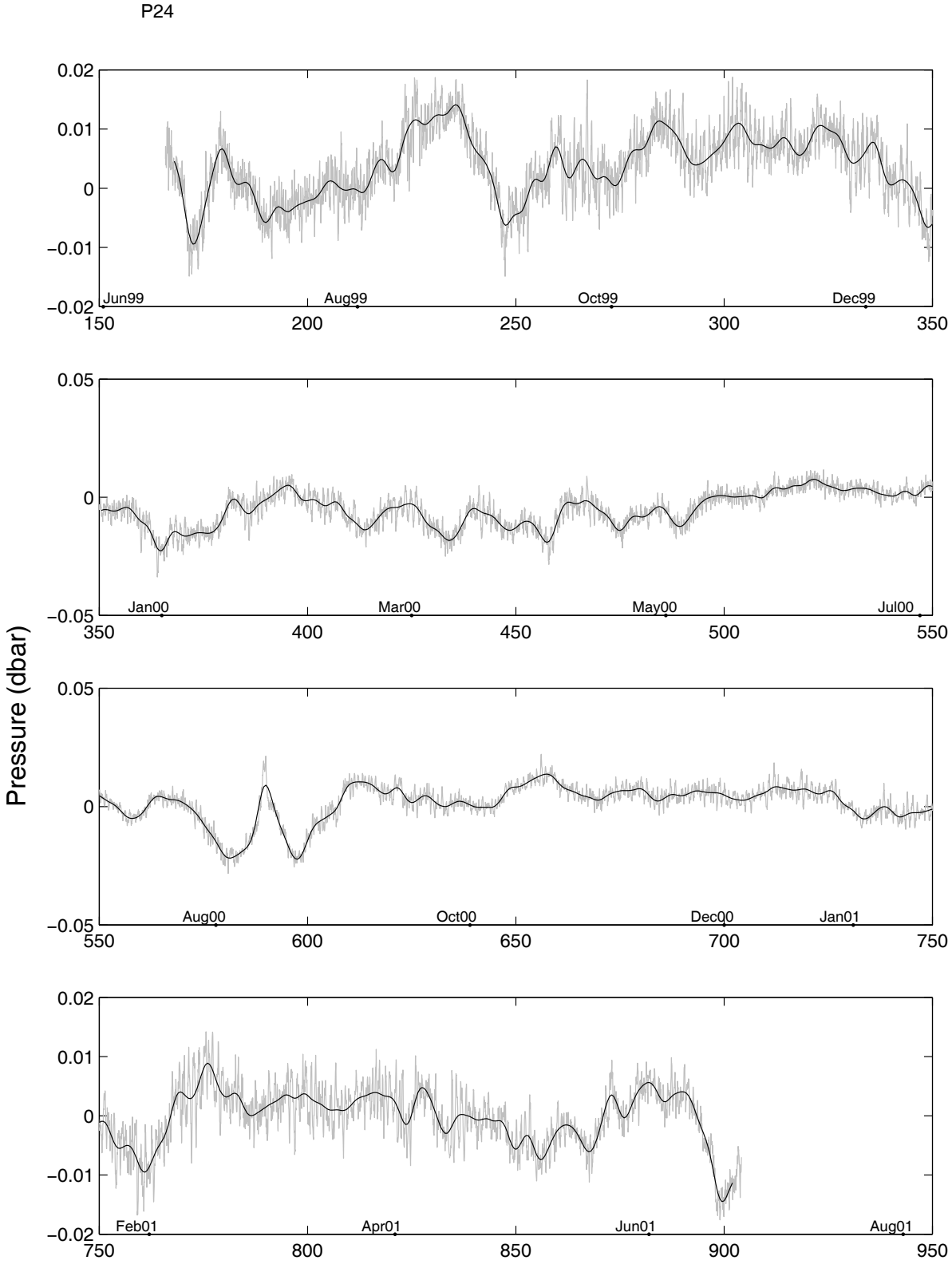

Figure 32: **P2-5 Hourly and 120-hrlp Leveled Pressures**

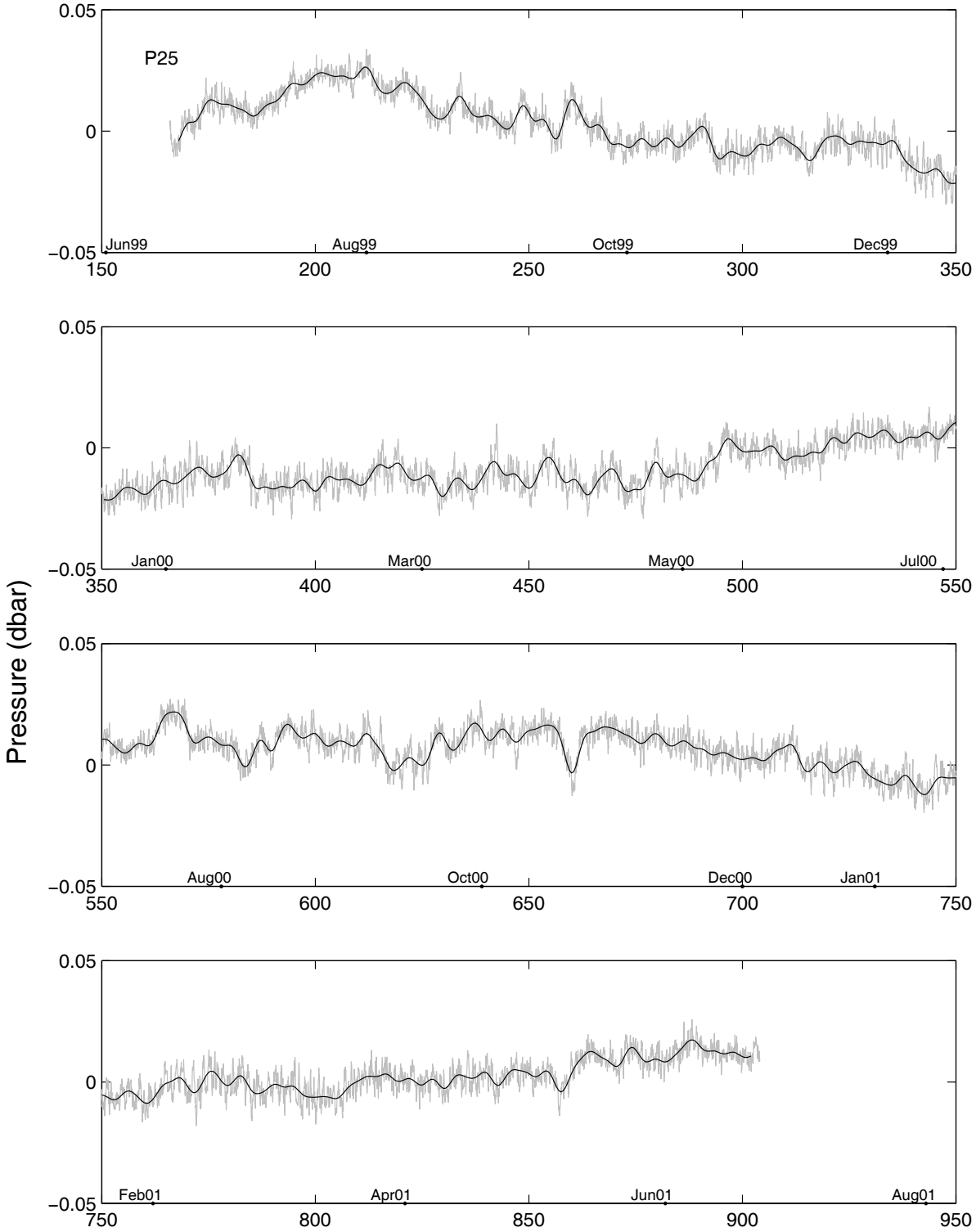

Figure 33: **P3-1 Hourly and 120-hrlp Leveled Pressures**

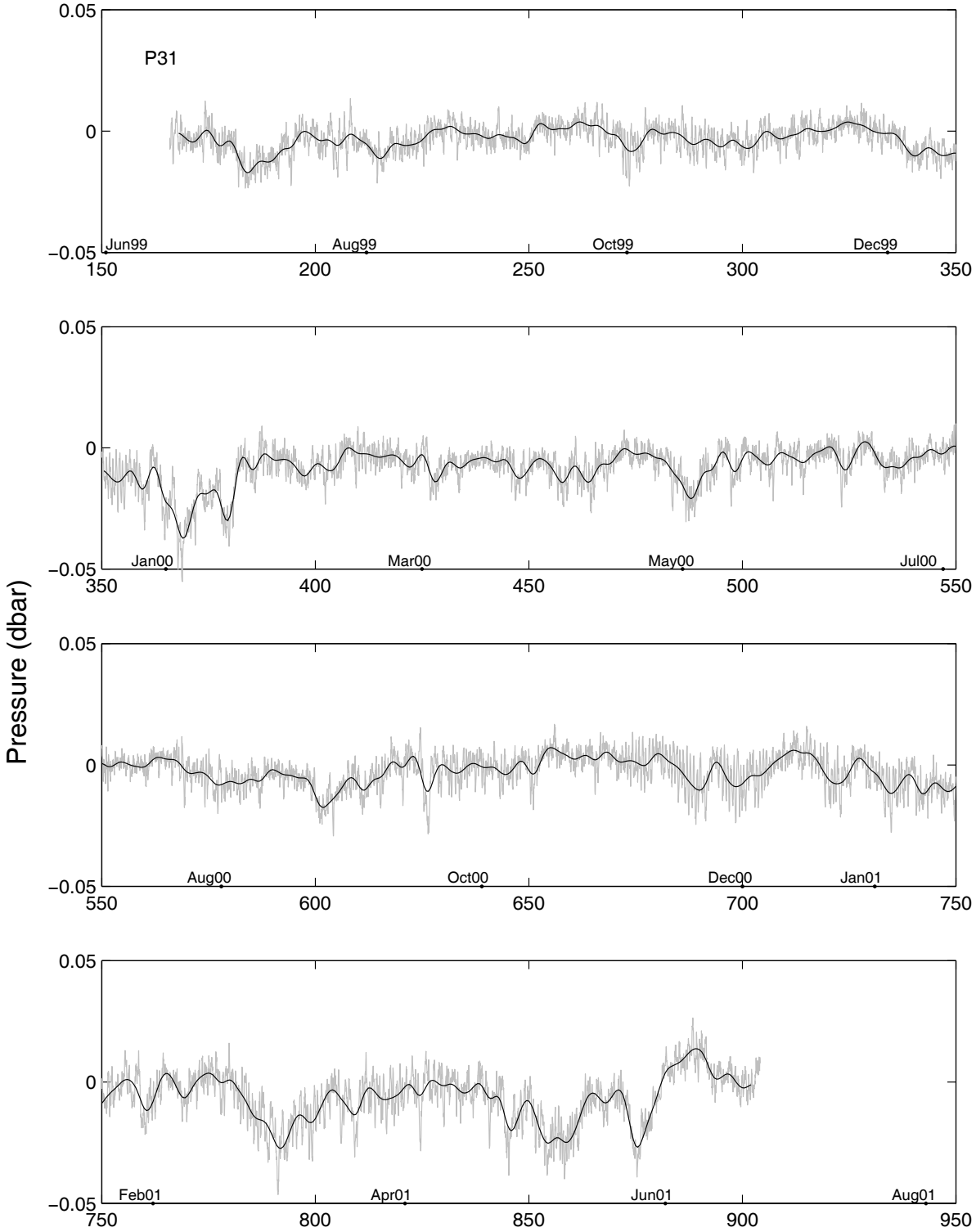

Figure 34: **P3-2 Hourly and 120-hrlp Leveled Pressures**

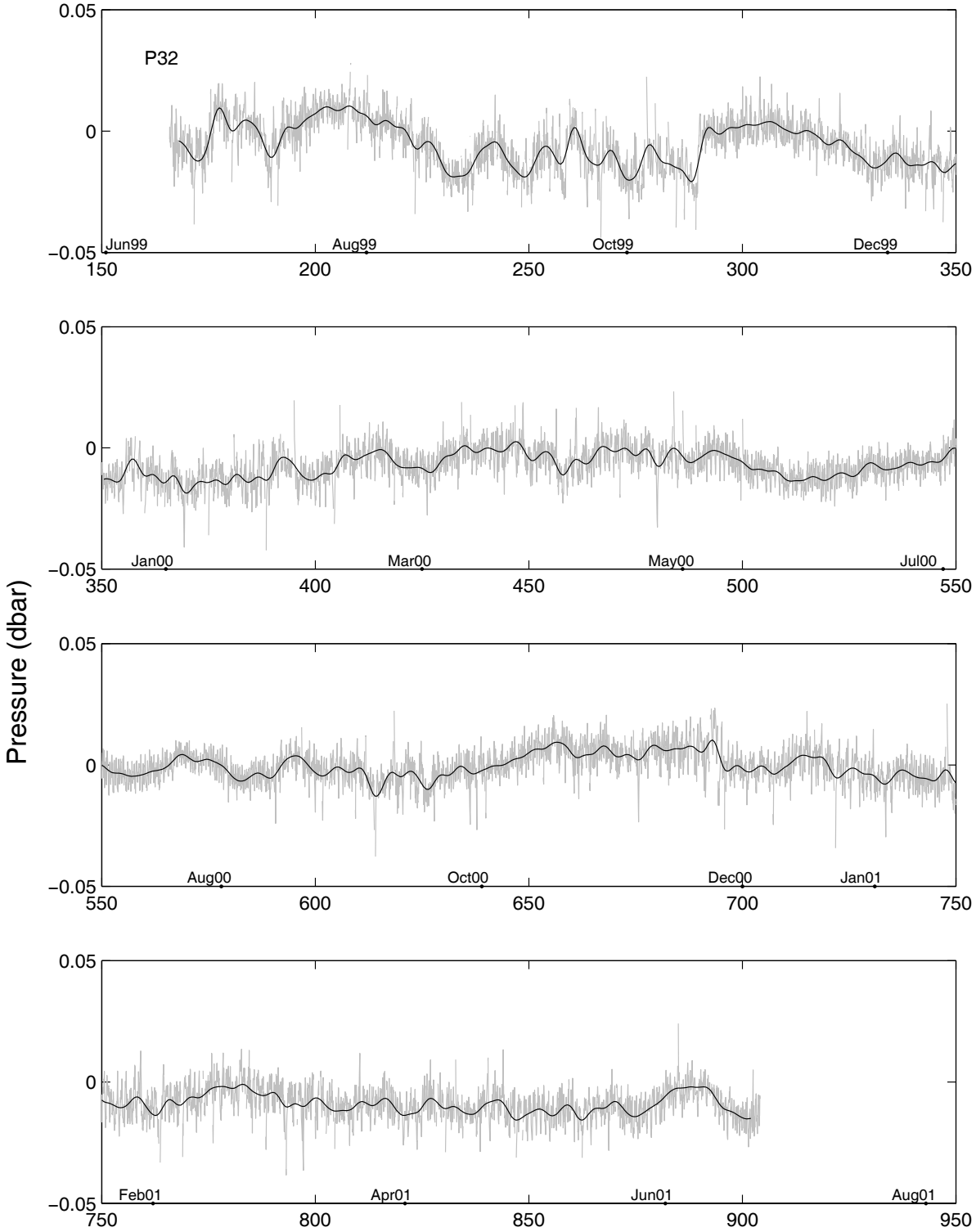

Figure 35: **P3-3 Hourly and 120-hrlp Leveled Pressures**

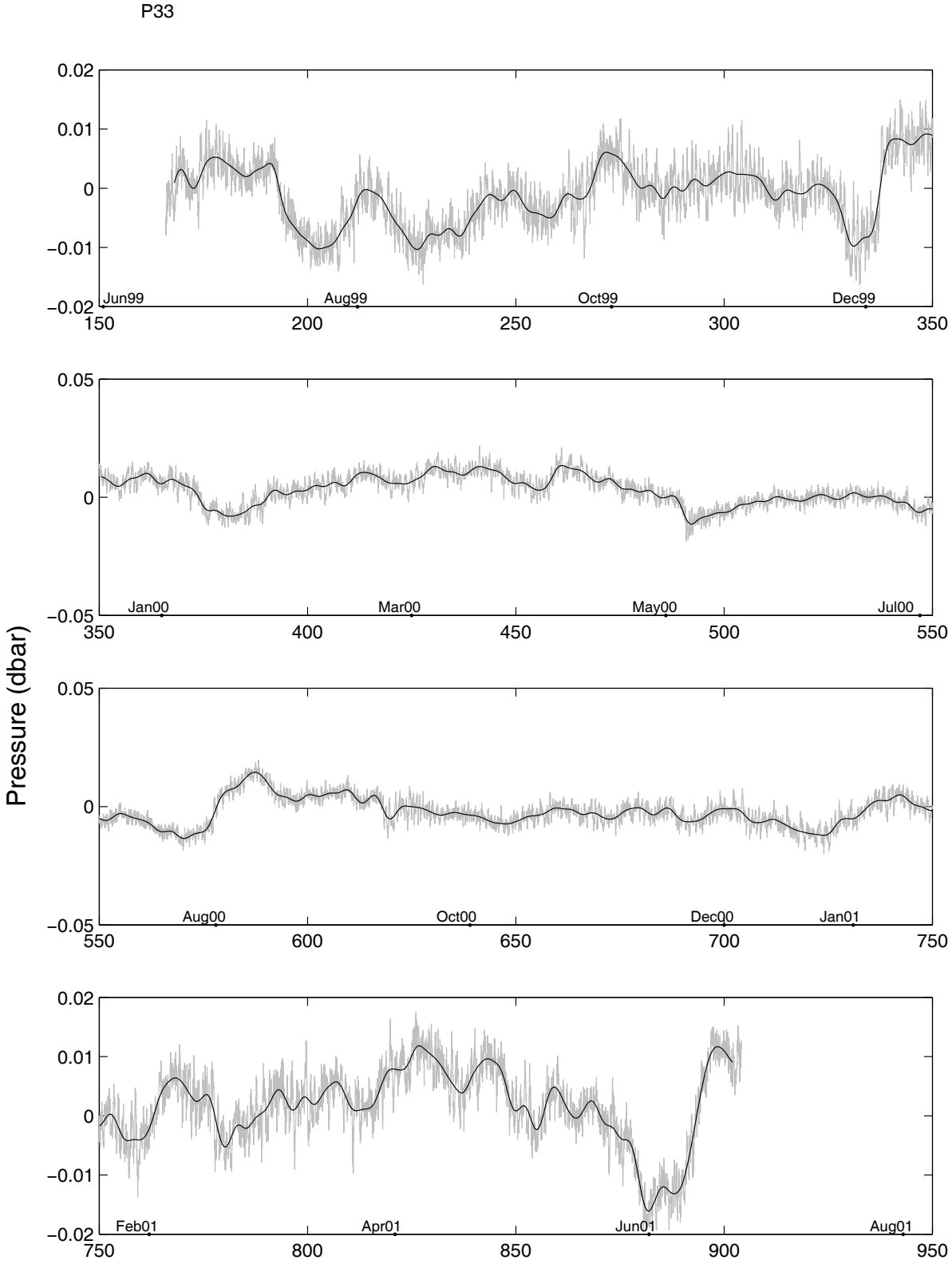

Figure 36: **P3-4 Hourly and 120-hrlp Leveled Pressures**

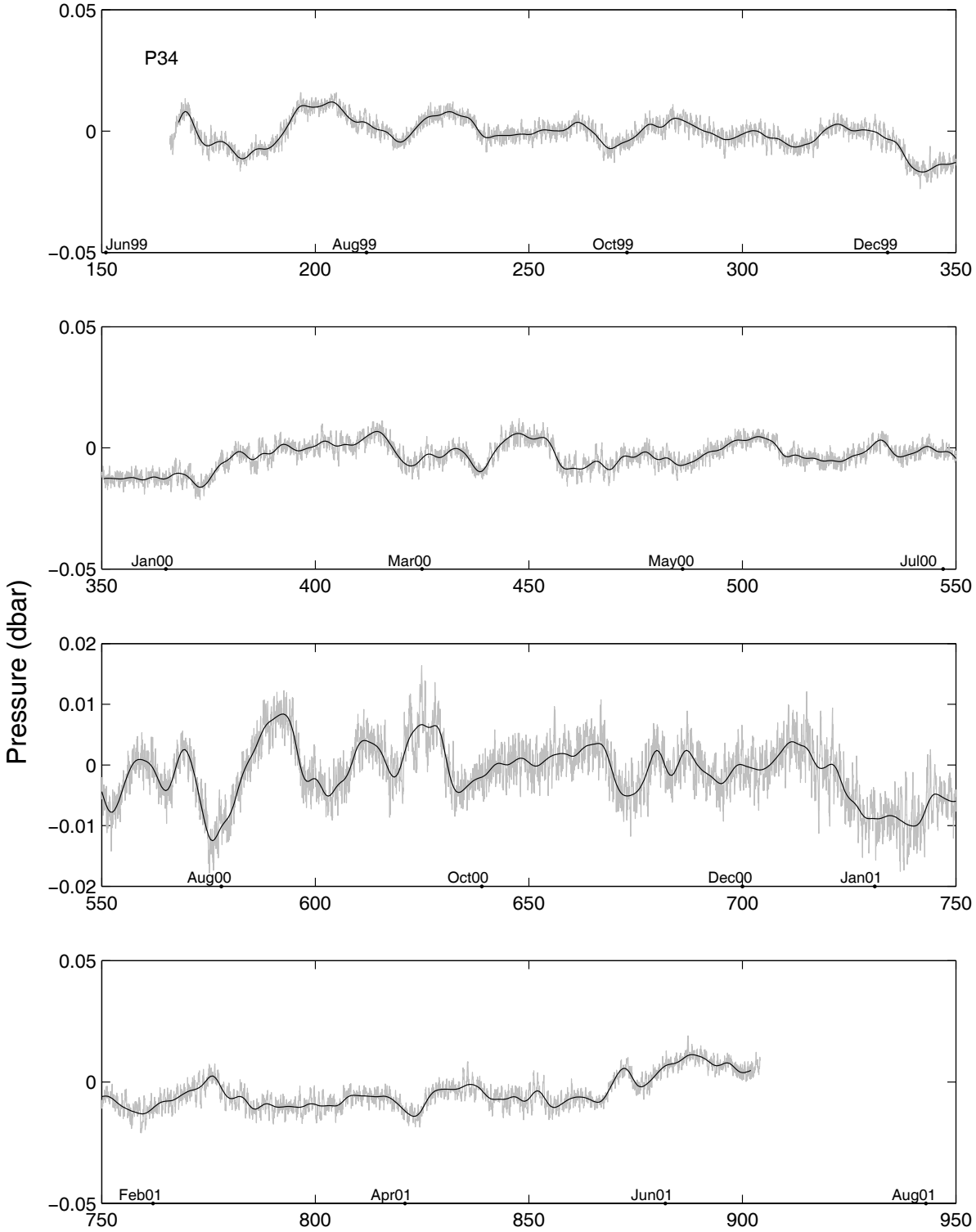

Figure 37: **P4-2 Hourly and 120-hrlp Leveled Pressures**

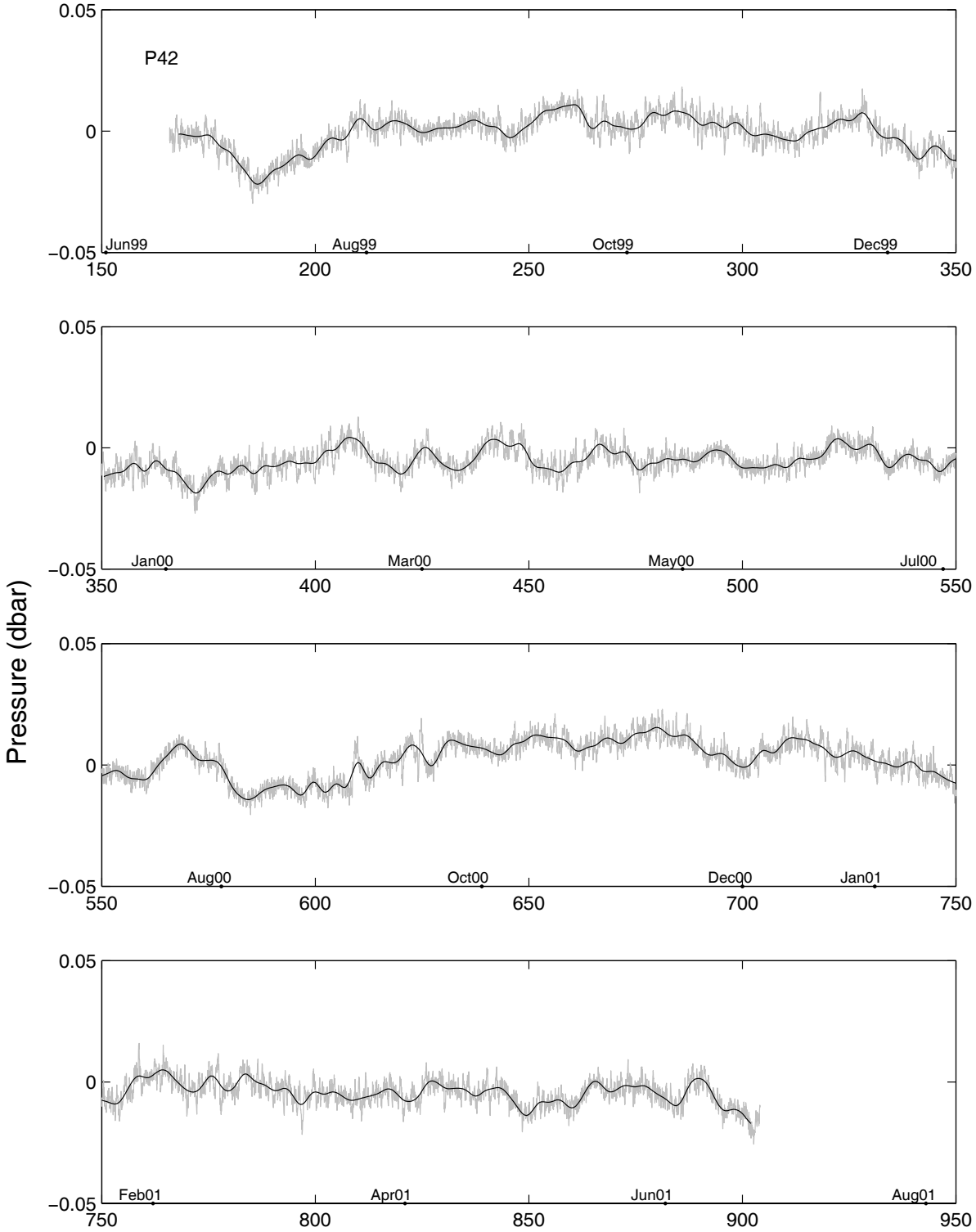

Figure 38: **P4-3 Hourly and 120-hrlp Leveled Pressures**

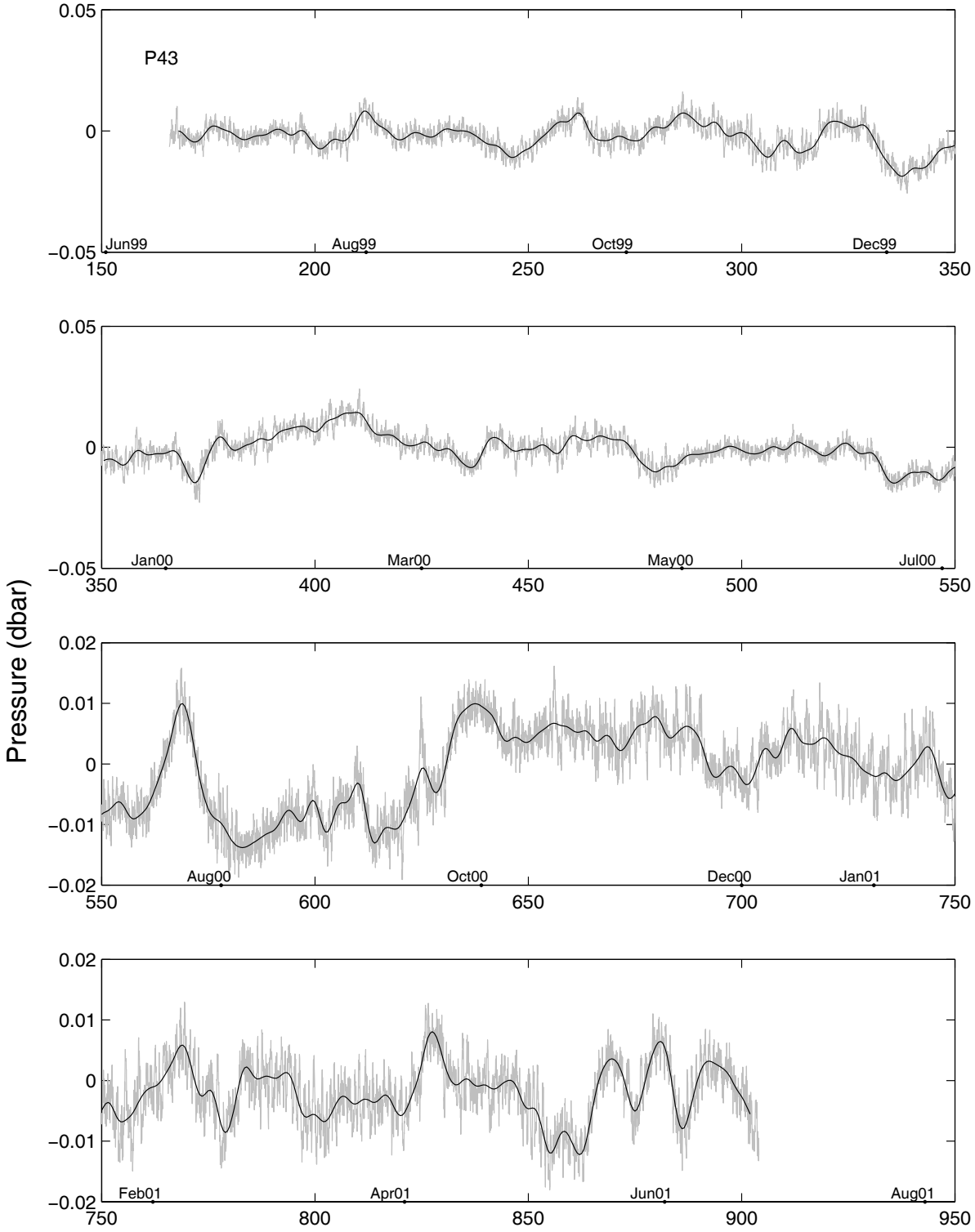

Figure 39: **P4-4 Hourly and 120-hrlp Leveled Pressures**

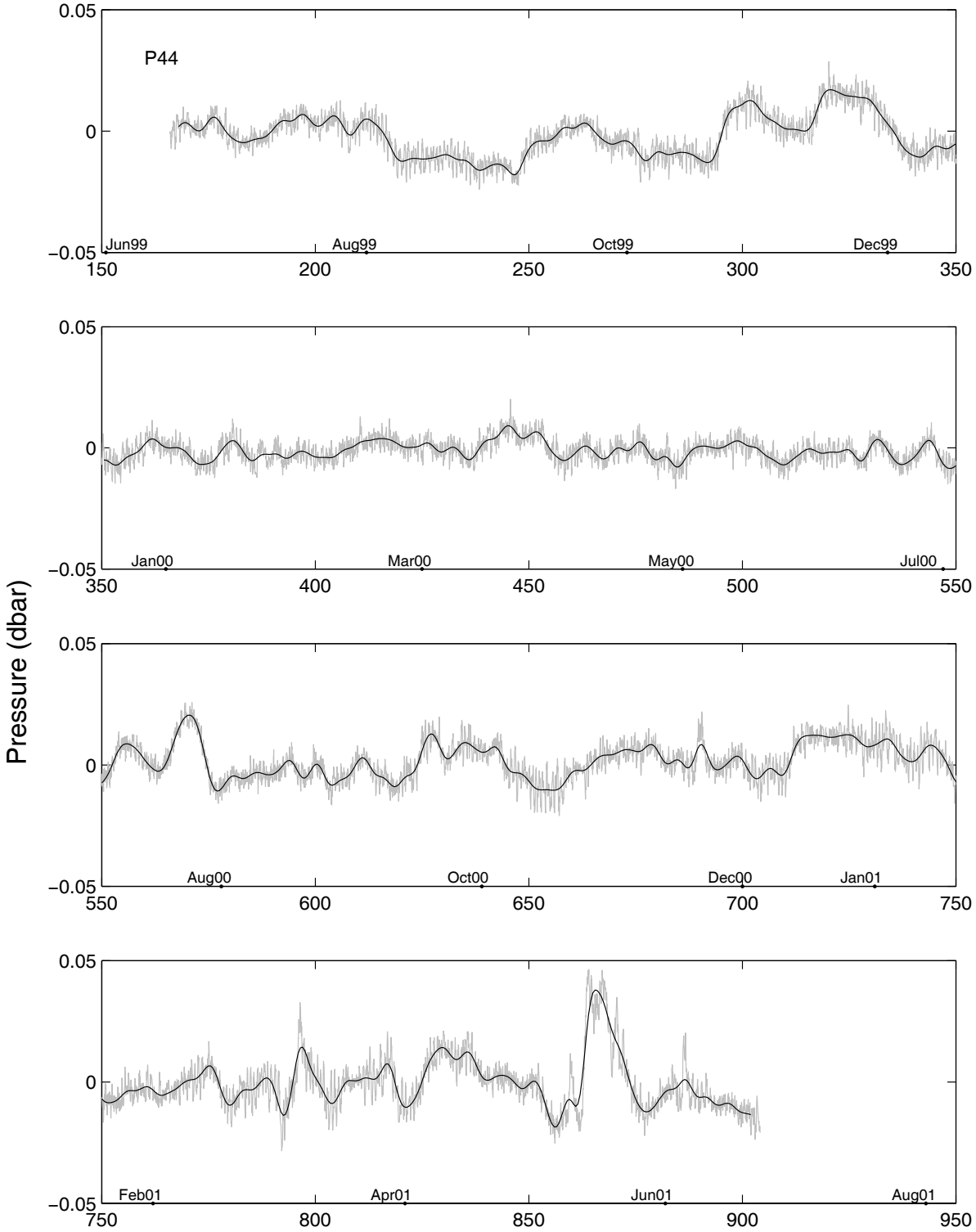

Figure 40: **P4-5 Hourly and 120-hrlp Leveled Pressures**

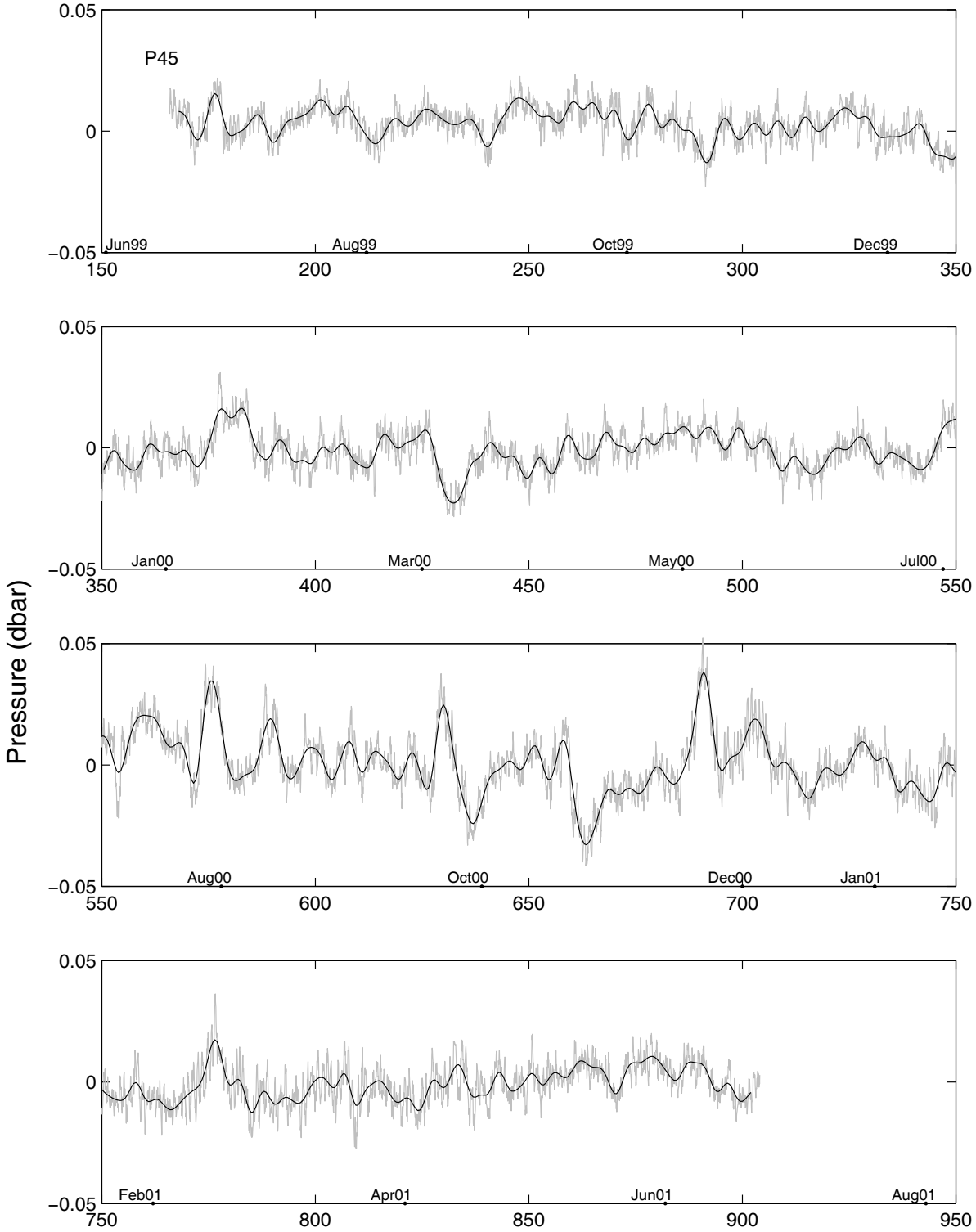

Figure 41: **P5-1 Hourly and 120-hrlp Leveled Pressures**

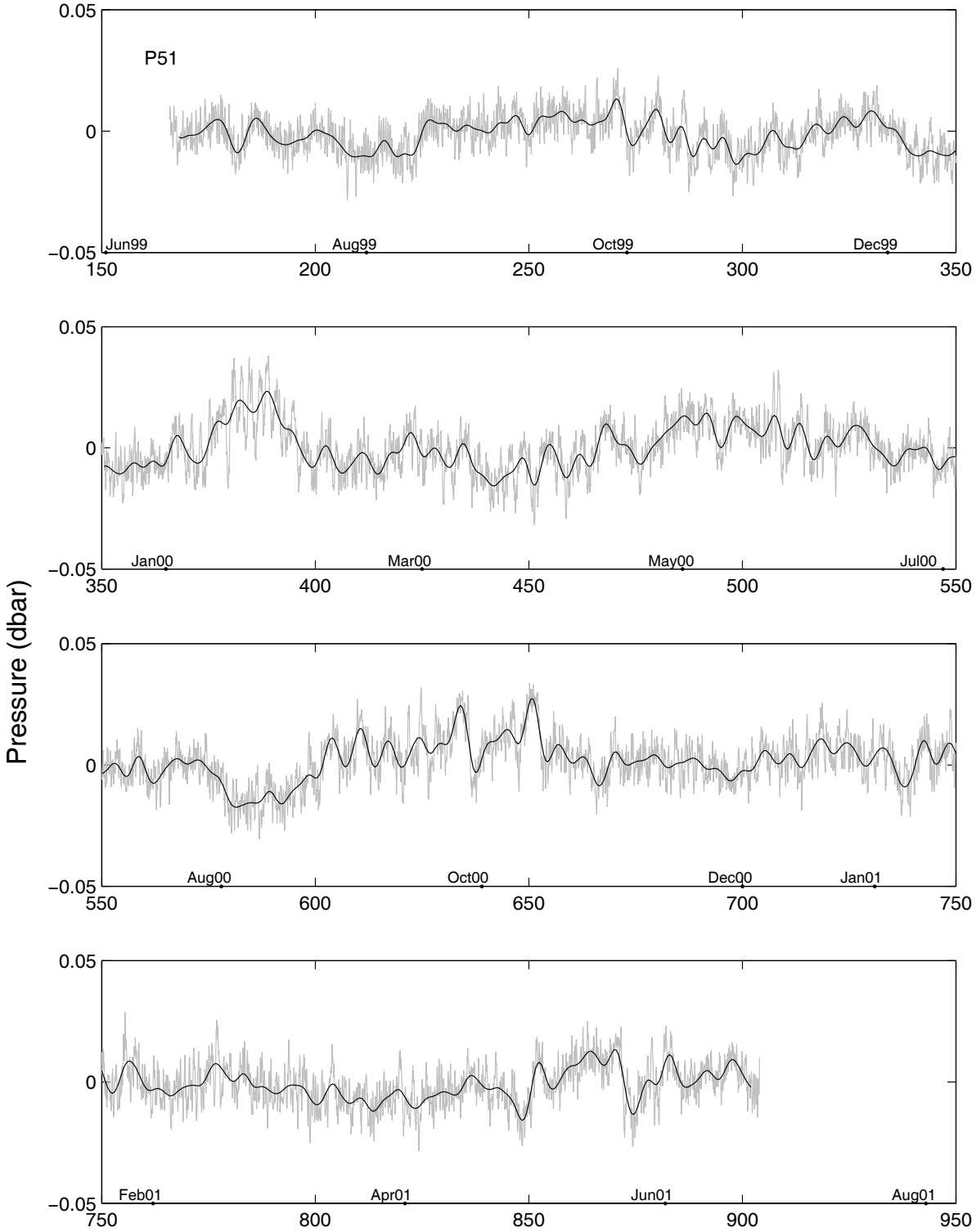

Figure 42: **P5-2 Hourly and 120-hrlp Leveled Pressures**

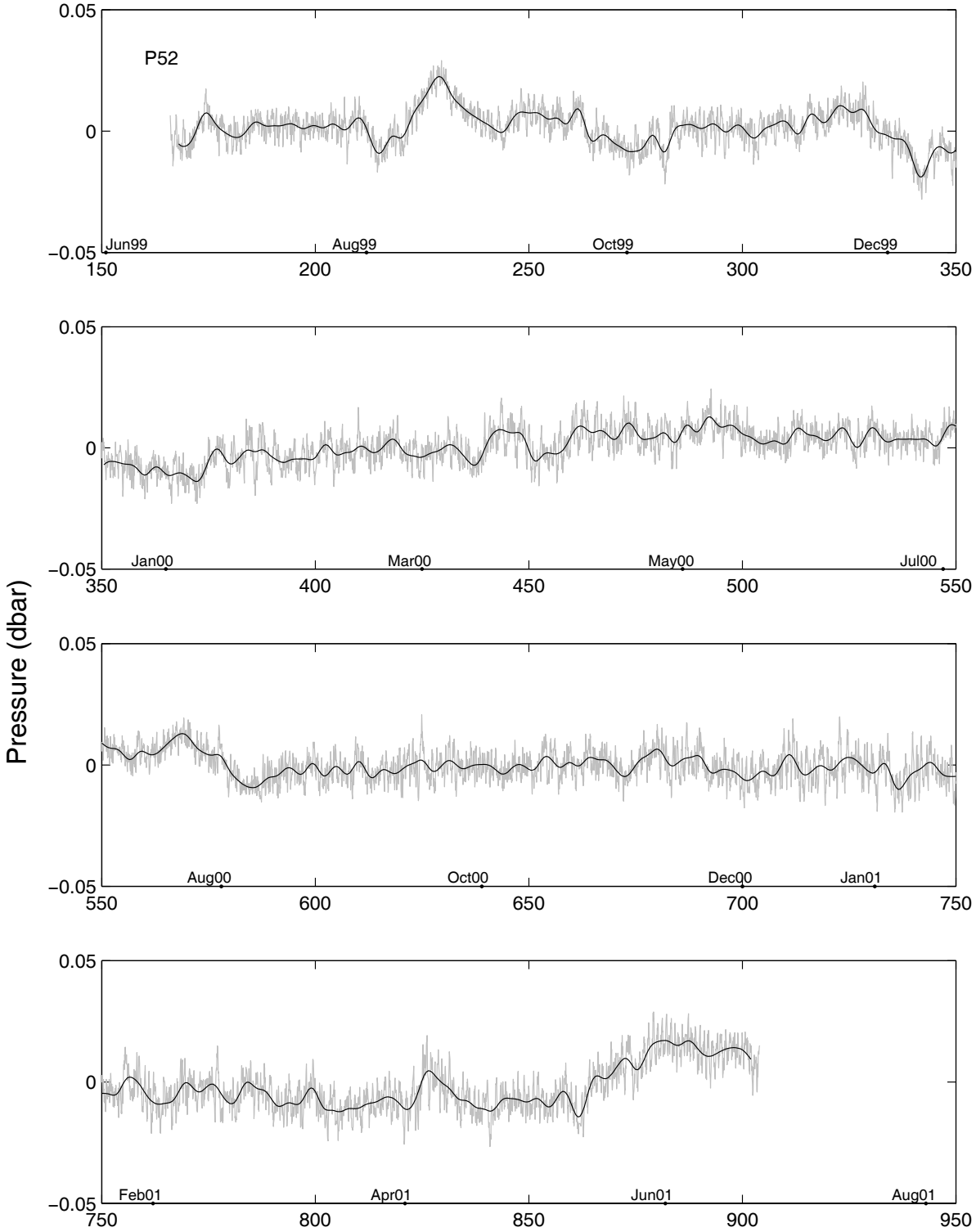

Figure 43: **P5-3 Hourly and 120-hrlp Leveled Pressures**

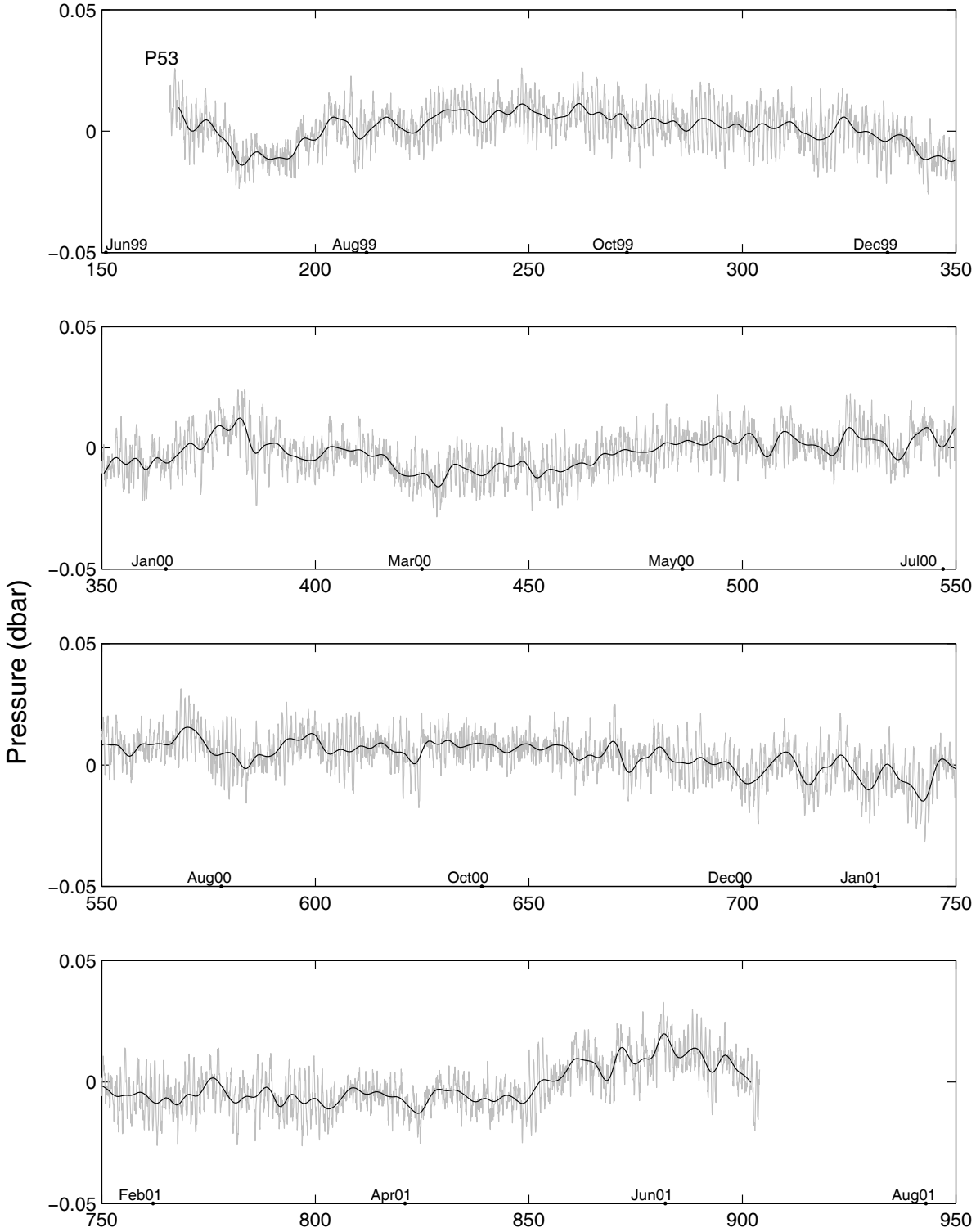

Figure 44: **P5-4 Hourly and 120-hrlp Leveled Pressures**

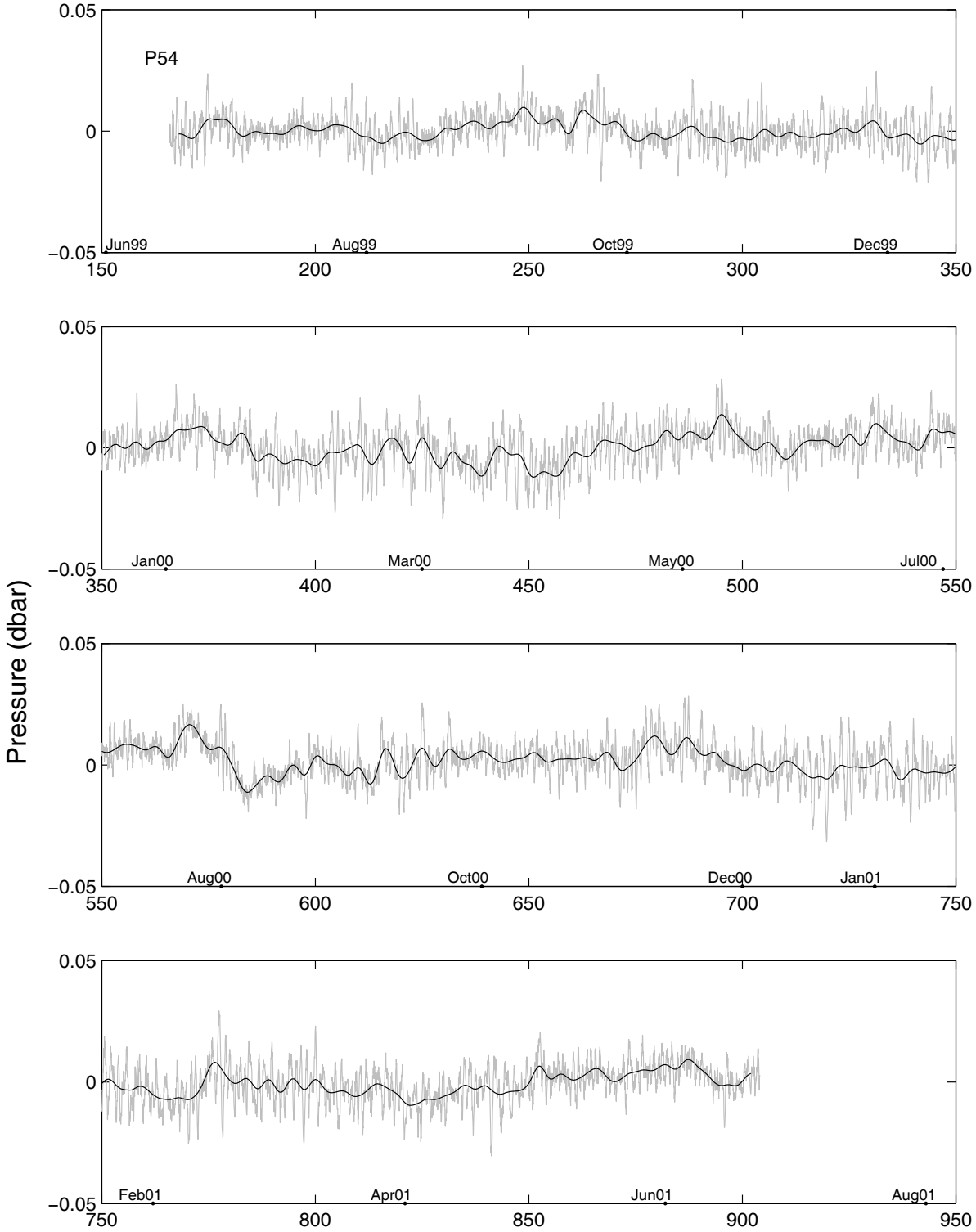

Figure 45: **P5-5 Hourly and 120-hrlp Leveled Pressures**

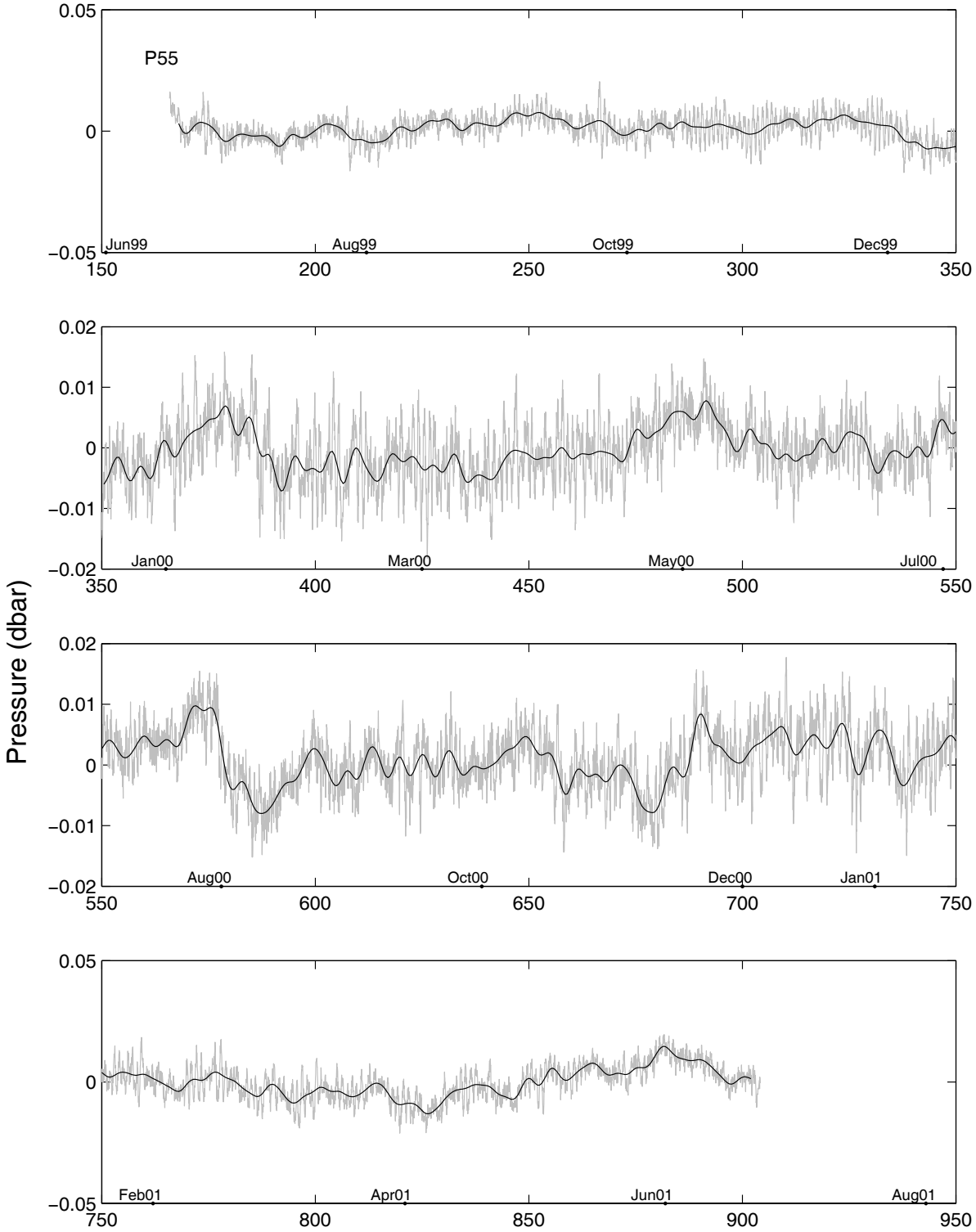

4 Travel Time Records for Each Instrument

Figures 46–48 present the raw travel time records. These illustrate the data quality, including the sizes of the travel time jumps and the number of early echoes caused by biological interference. Because the complete data sets are quite large, only subsampled records are displayed. Every sixth hourly sample is shown and of the 24 echo returns taken during those samples, only six values are shown. Travel times units are the internally recorded counts, not time in seconds. Time in hours since deployment is plotted along the x-axis with selected dates indicated. The site designation and serial number are labeled in each panel.

Hourly travel times are plotted separately for each site in Figures 49–71. These records have had large data spikes (outliers) removed and replaced with linearly interpolated values. Additionally, data gaps left by early echoes have also been replaced with linearly interpolated values. All records have been interpolated onto a common time base. The statistics are listed in Table 6. These records are provided on the accompanying CD-ROM.

The measured travel times were projected onto a common pressure level of 500 dbar and low-pass filtered. The resulting τ_{500} records are plotted in Figures 72–77. These records have a time interval of 12 hours. These records are provided on the accompanying CD-ROM.

Table 6: Statistics on the hourly travel time records shown in Figures 49–71. The mean, minimum (min), maximum (max), and standard deviations (STD) of the travel times are reported along with the start and ending times of each data record.

Site	Start Time (UT)	End Time (UT)	Time Interval (hours)	Mean (sec)	Min (sec)	Max (sec)	STD (sec)
11	July June 1999 00:00:00	1 July 2001 23:59:60	1.000	1.566	1.563	1.569	0.001
12	7 June 1999 00:00:00	1 July 2001 23:59:60	1.000	2.224	2.218	2.228	0.002
13	7 June 1999 00:00:00	1 July 2001 23:59:60	1.000	2.507	2.502	2.512	0.003
14	7 June 1999 00:00:00	1 July 2001 23:59:60	1.000	1.839	1.833	1.844	0.003
15	7 June 1999 00:00:00	4 September 1999 7:59:60	1.000	3.517	3.514	3.521	0.002
16	7 June 1999 00:00:00	1 July 2001 23:59:60	1.000	3.374	3.369	3.379	0.002
21	7 June 1999 00:00:00	1 July 2001 23:59:60	1.000	1.384	1.380	1.387	0.002
22	7 June 1999 00:00:00	1 July 2001 23:59:60	1.000	2.183	2.179	2.189	0.002
23	7 June 1999 00:00:00	1 July 2001 23:59:60	1.000	2.939	2.933	2.946	0.003
24	7 June 1999 00:00:00	1 July 2001 23:59:60	1.000	3.168	3.160	3.173	0.003
25	7 June 1999 00:00:00	1 July 2001 23:59:60	1.000	2.255	2.250	2.259	0.001
31	7 June 1999 00:00:00	1 July 2001 23:59:60	1.000	1.356	1.353	1.360	0.001
32	7 June 1999 00:00:00	2 July 2001 00:00:00	1.000	1.356	1.353	1.360	0.001
33	7 June 1999 00:00:00	1 July 2001 23:59:60	1.000	2.947	2.943	2.955	0.002
34	7 June 1999 00:00:00	1 July 2001 23:59:60	1.000	2.888	2.882	2.893	0.002
42	7 June 1999 00:00:00	1 July 2001 23:59:60	1.000	2.710	2.705	2.715	0.002
43	7 June 1999 00:00:00	1 July 2001 23:59:60	1.000	2.735	2.732	2.740	0.001
44	7 June 1999 00:00:00	1 July 2001 23:59:60	1.000	2.442	2.439	2.445	0.001
45	7 June 1999 00:00:00	1 July 2001 23:59:60	1.000	1.628	1.624	1.632	0.001
51	7 June 1999 00:00:00	1 July 2001 23:59:60	1.000	1.366	1.362	1.369	0.001
52	7 June 1999 00:00:00	1 July 2001 23:59:60	1.000	1.859	1.855	1.863	0.002
53	7 June 1999 00:00:00	1 July 2001 23:59:60	1.000	1.670	1.666	1.675	0.001
54	7 June 1999 00:00:00	1 July 2001 23:59:60	1.000	1.537	1.533	1.541	0.001
55	7 June 1999 00:00:00	1 July 2001 23:59:60	1.000	1.431	1.427	1.436	0.001

Figure 46: **P1-1–P2-2 Raw Travel Time Records.**

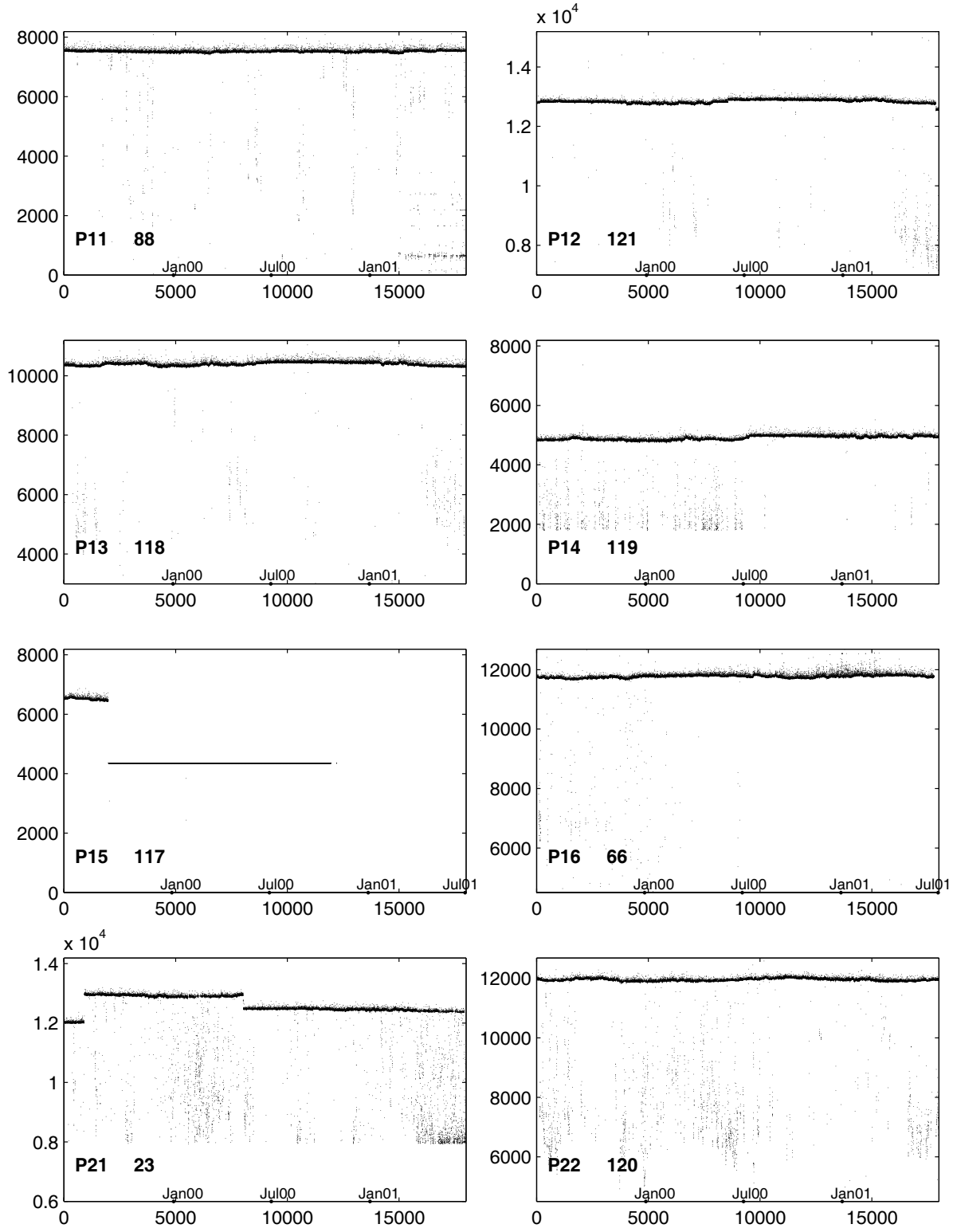

Figure 47: **P2-3–P4-2 Raw Travel Time Records.**

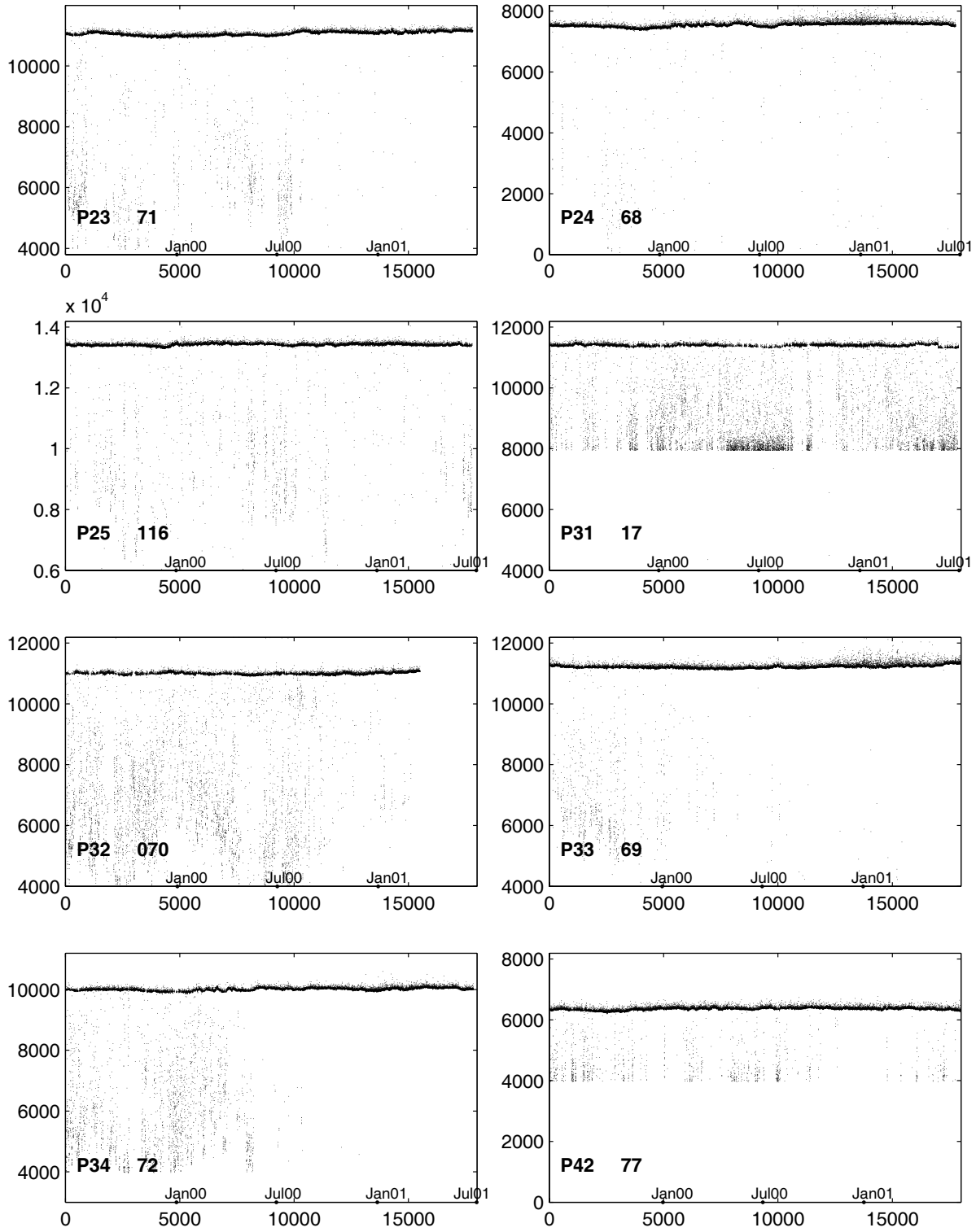

Figure 48: **P4-3–P5-5 Raw Travel Time Records.**

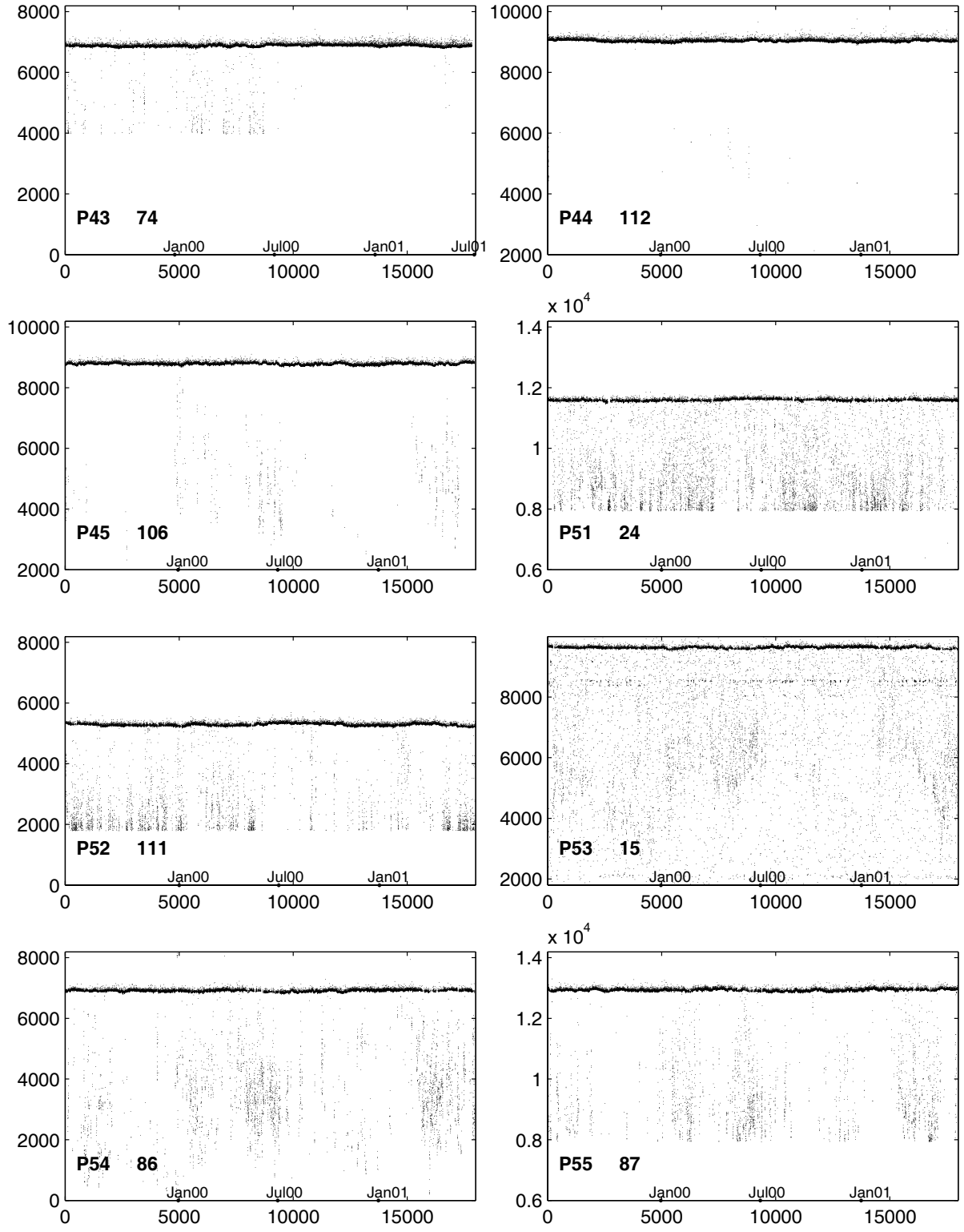

Figure 49: **P1-1 Hourly Travel Times**

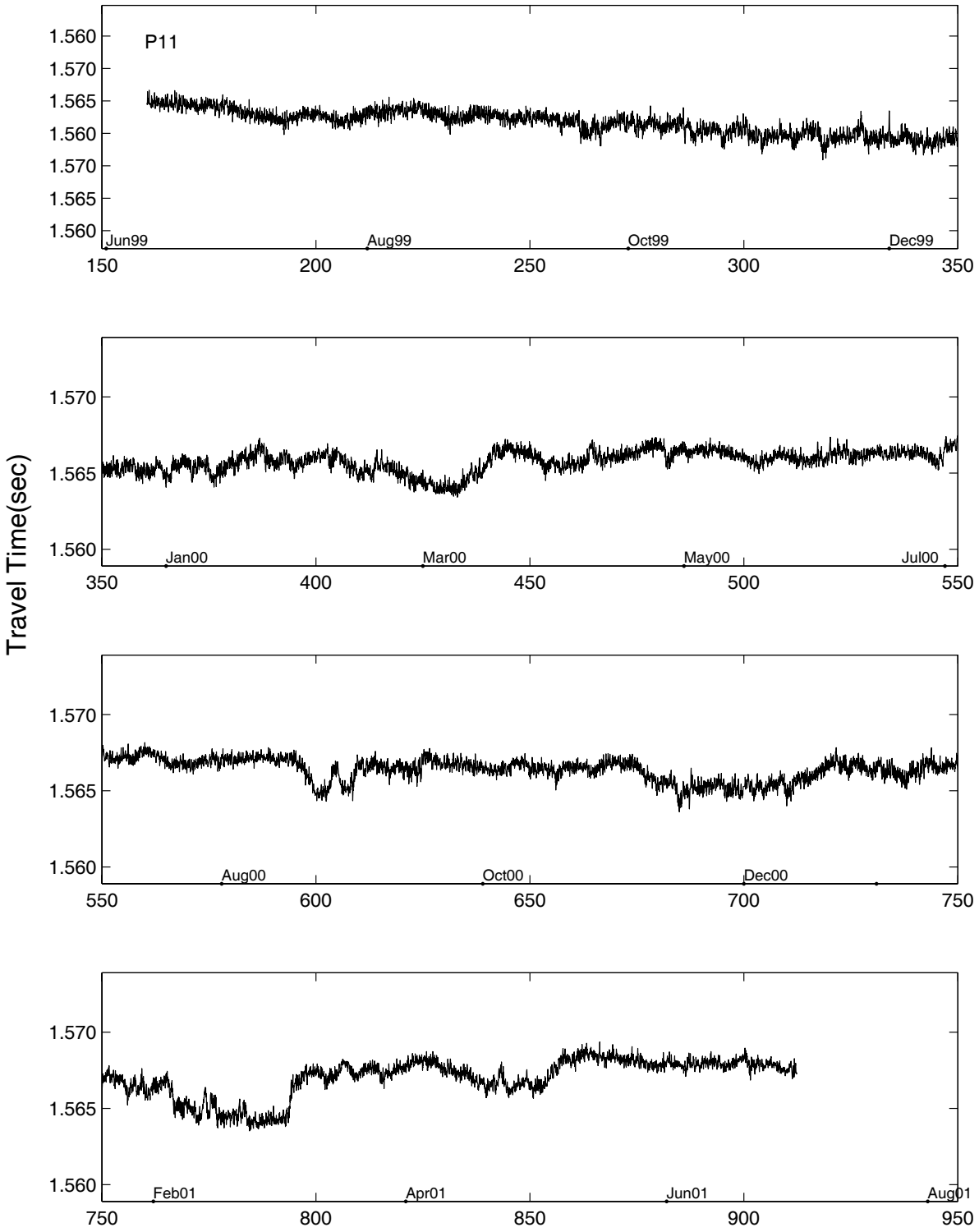

Figure 50: **P1-2 Hourly Travel Times**

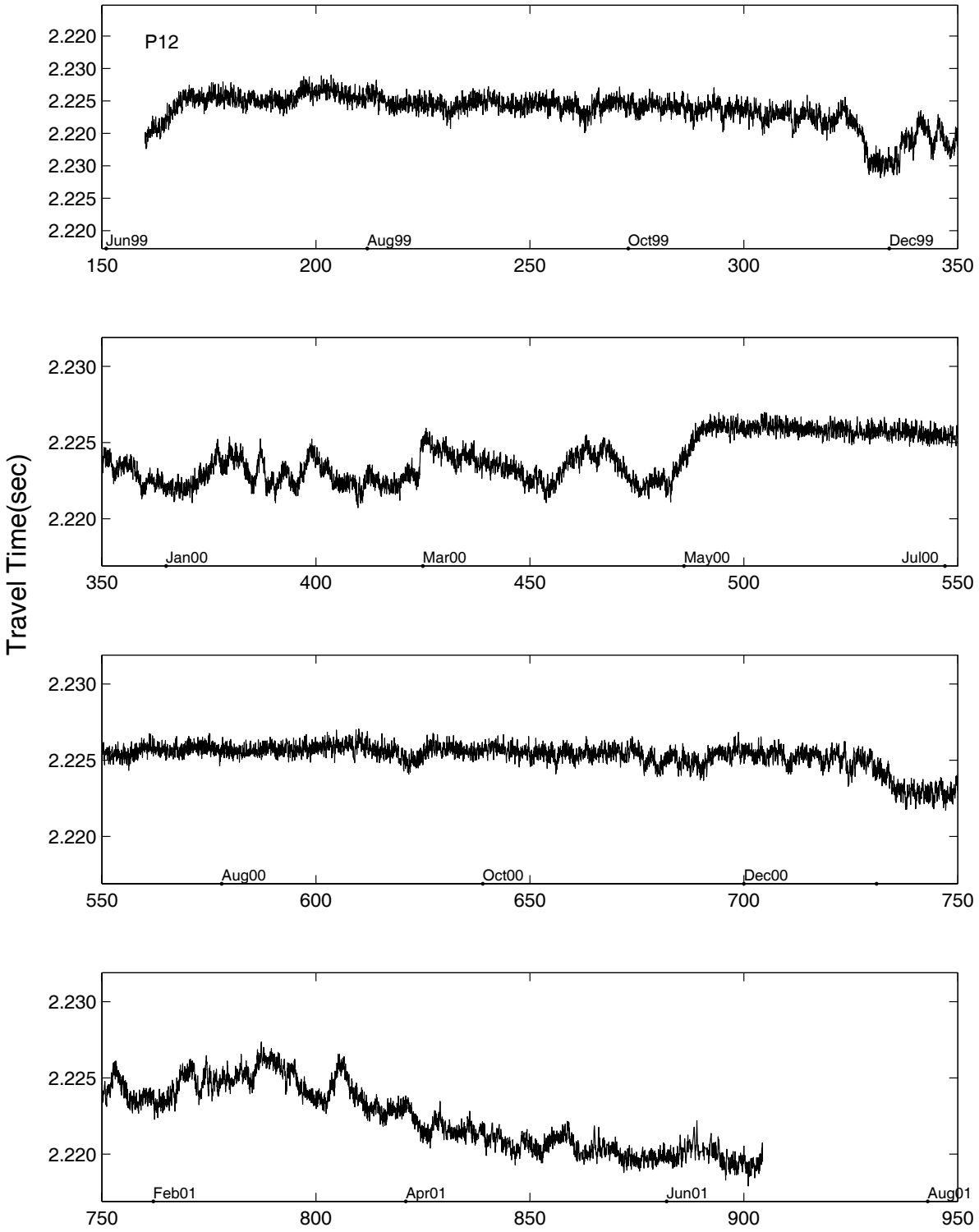

Figure 51: **P1-3 Hourly Travel Times**

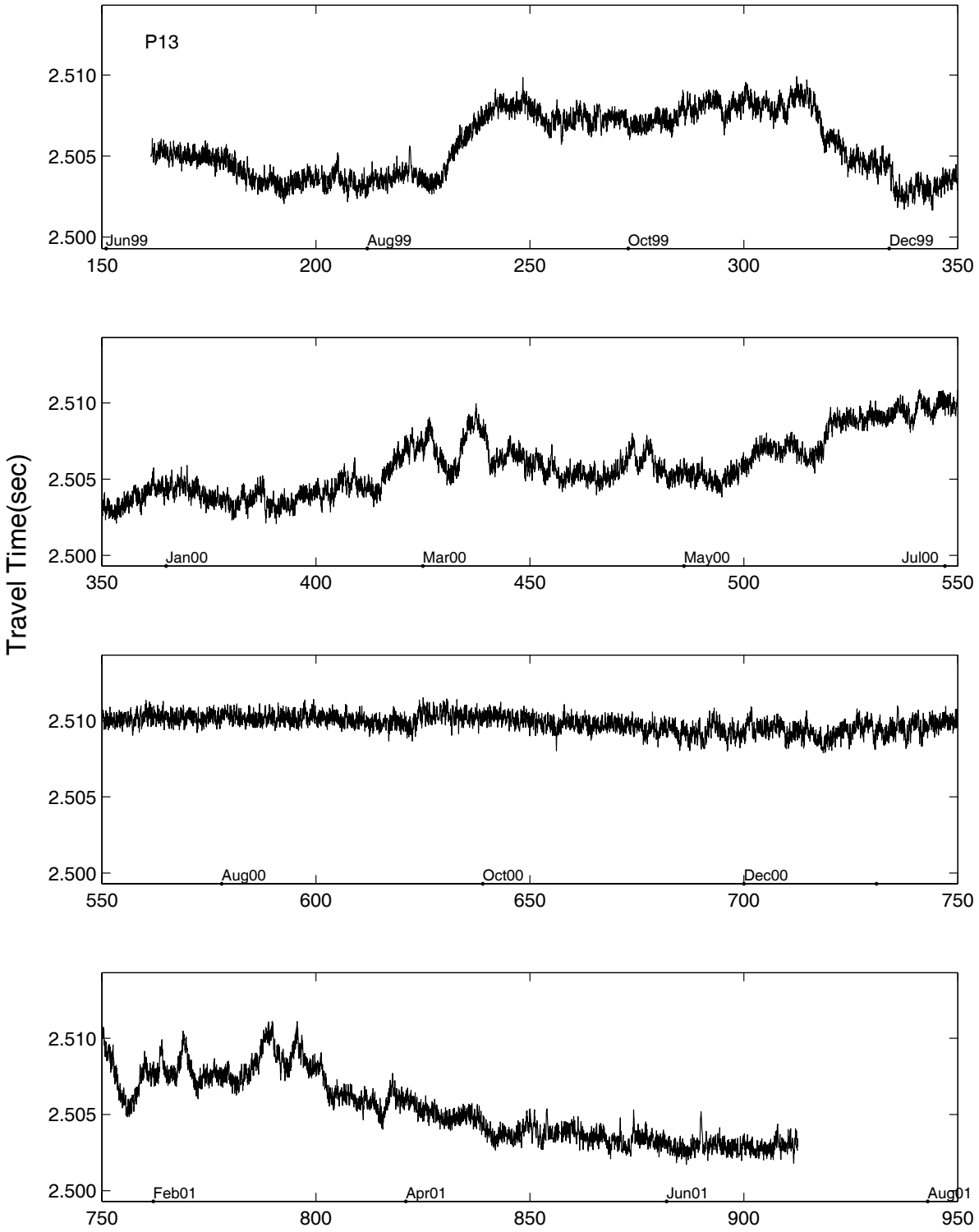

Figure 52: **P1-4 Hourly Travel Times**

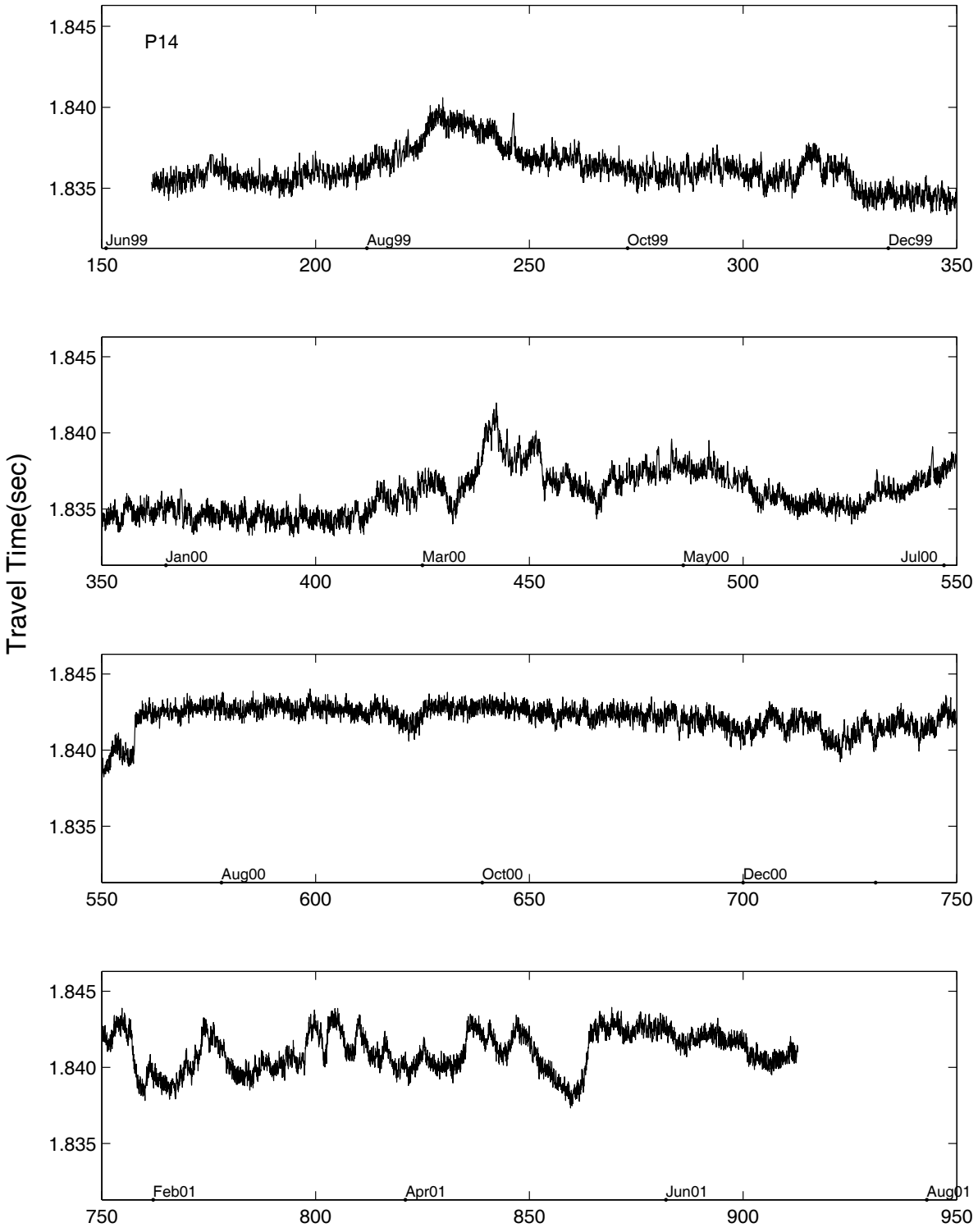

Figure 53: **P1-5 Hourly Travel Times**

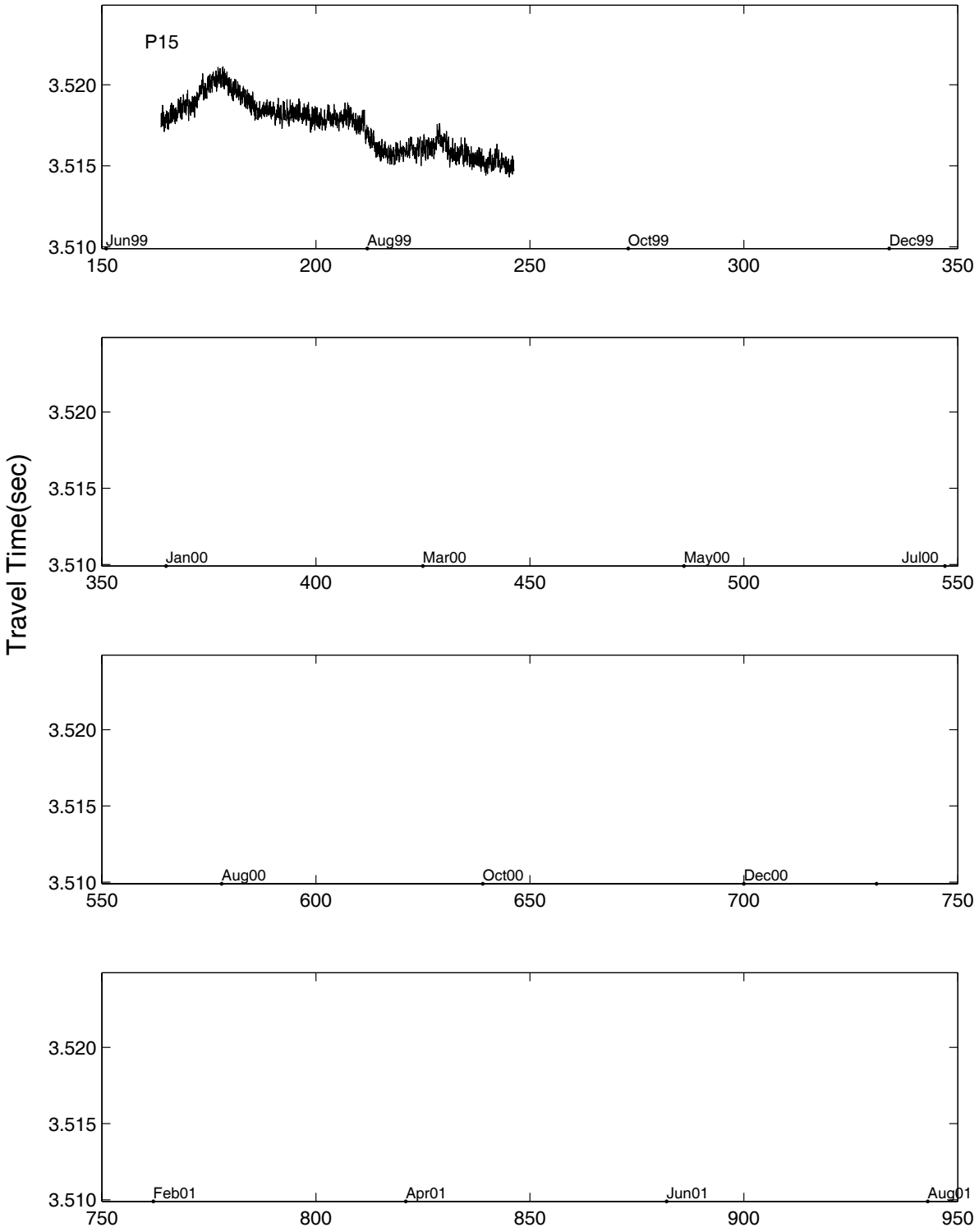

Figure 54: **P1-6 Hourly Travel Times**

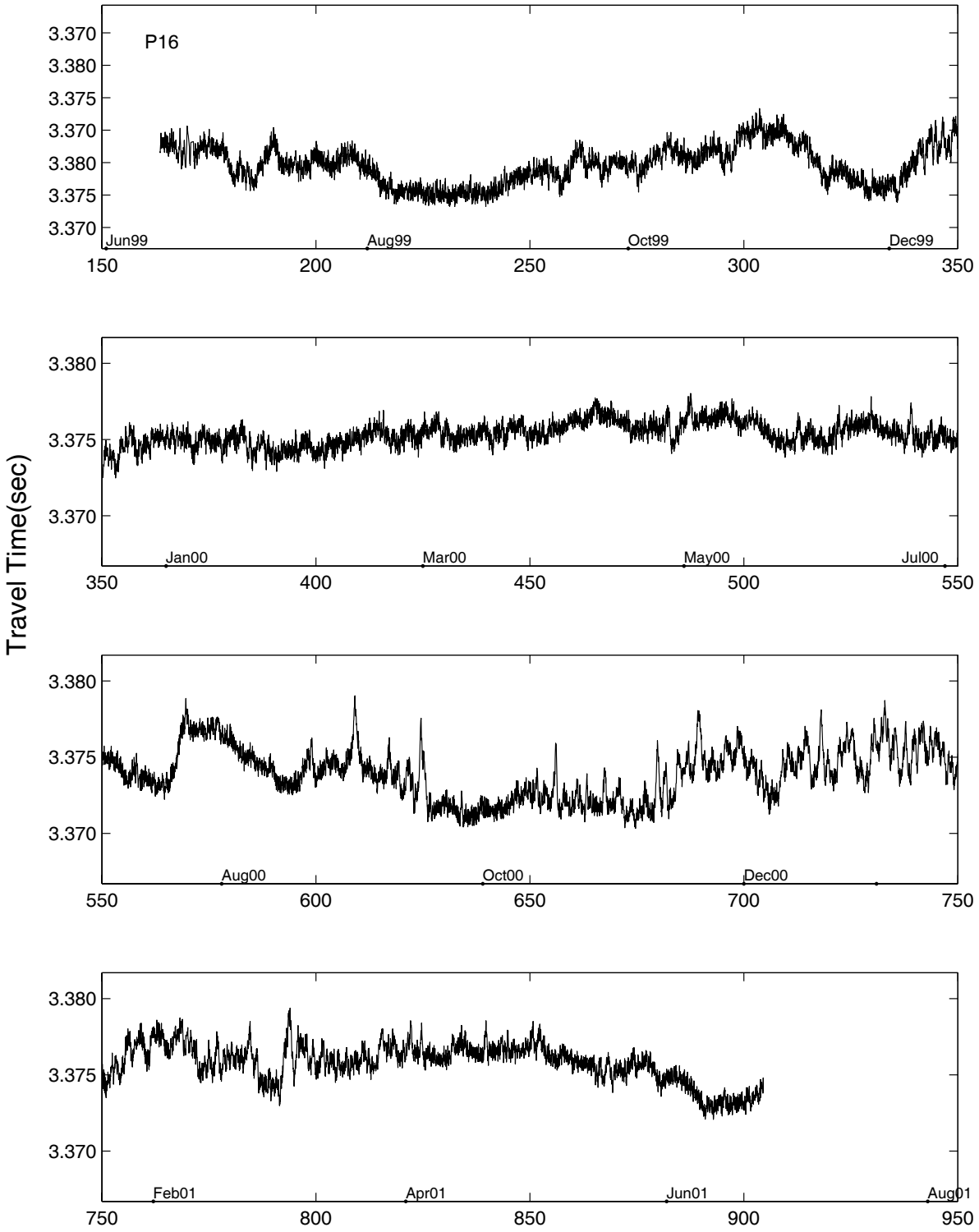

Figure 55: **P2-1 Hourly Travel Times**

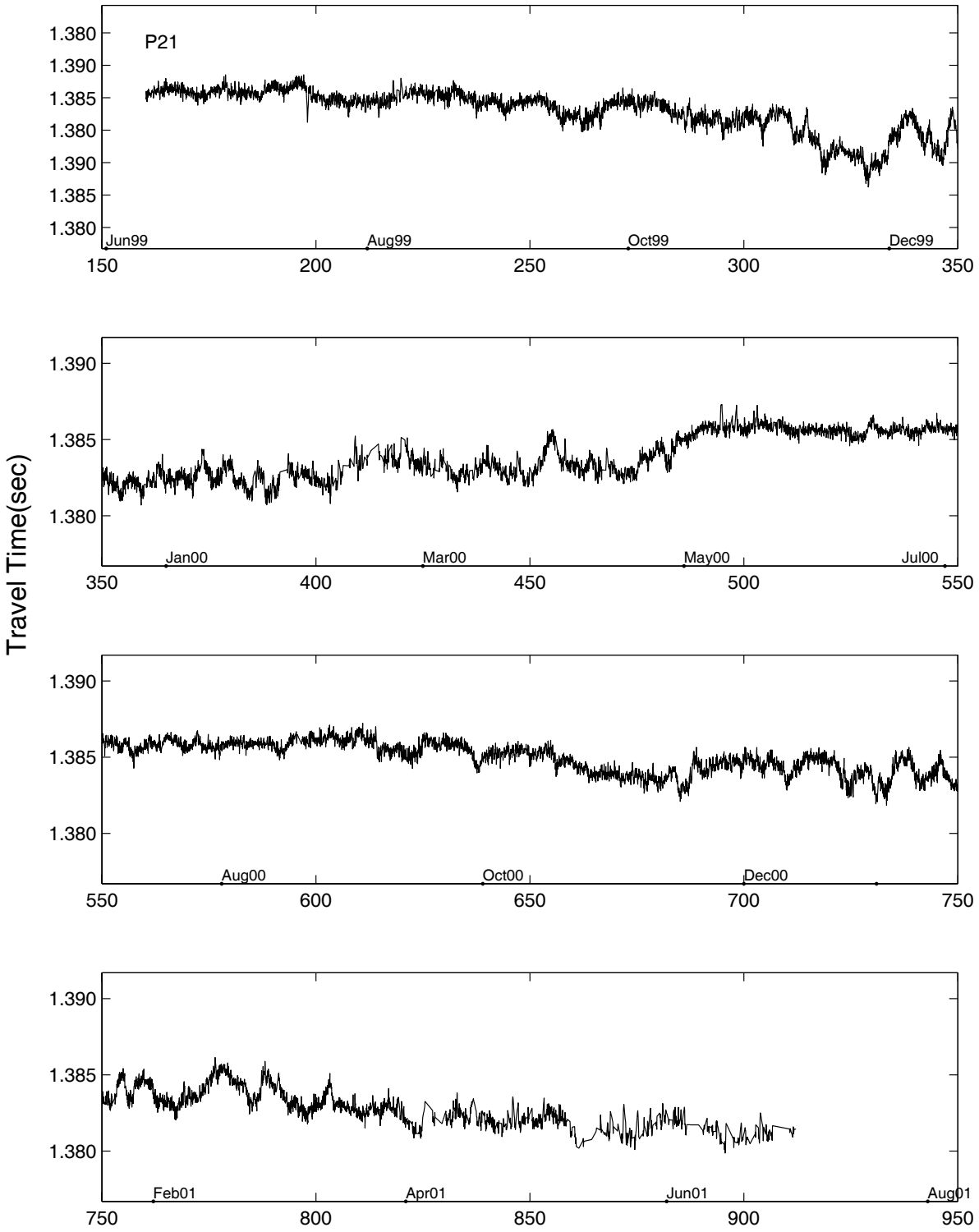

Figure 56: **P2-2 Hourly Travel Times**

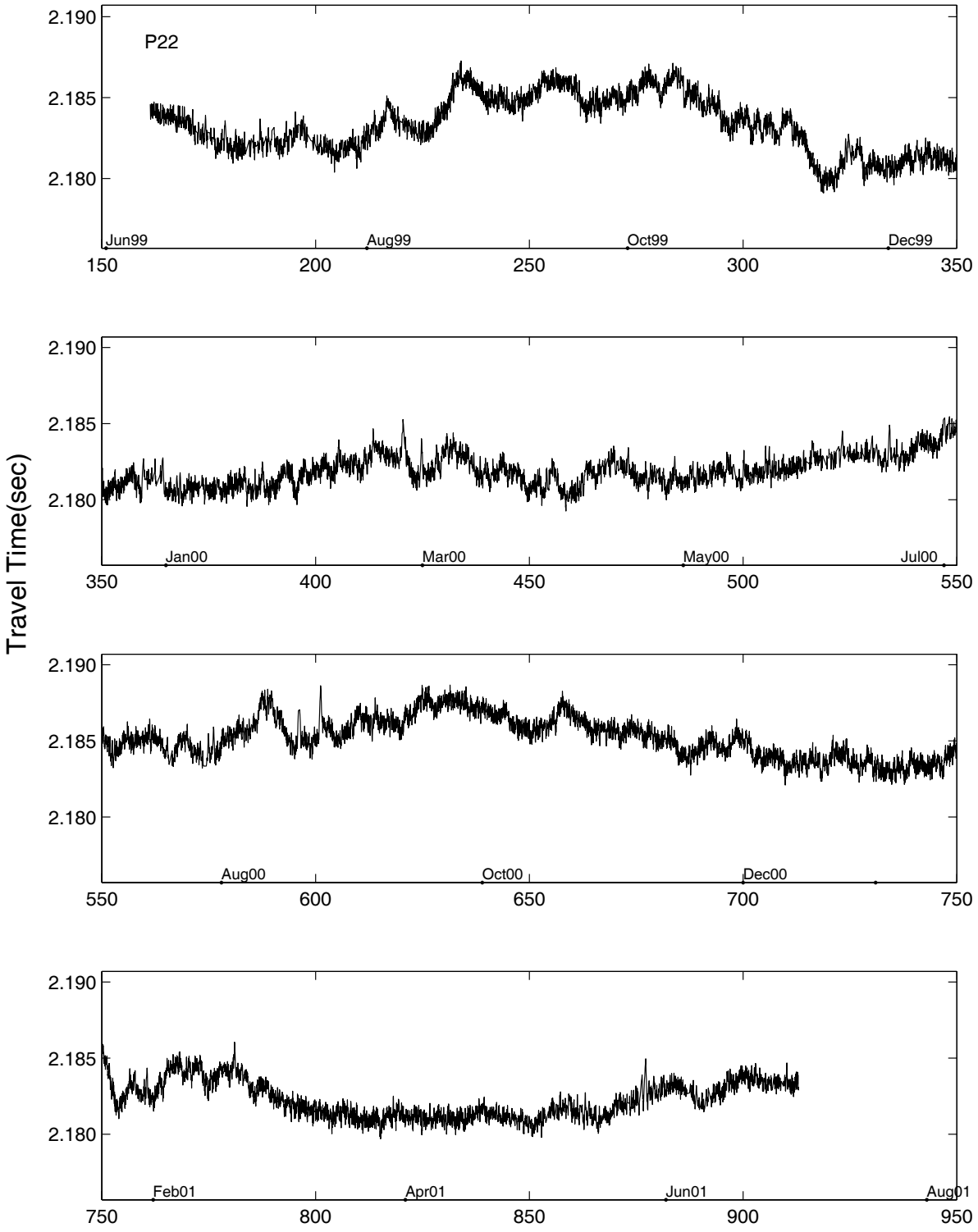

Figure 57: **P2-3 Hourly Travel Times**

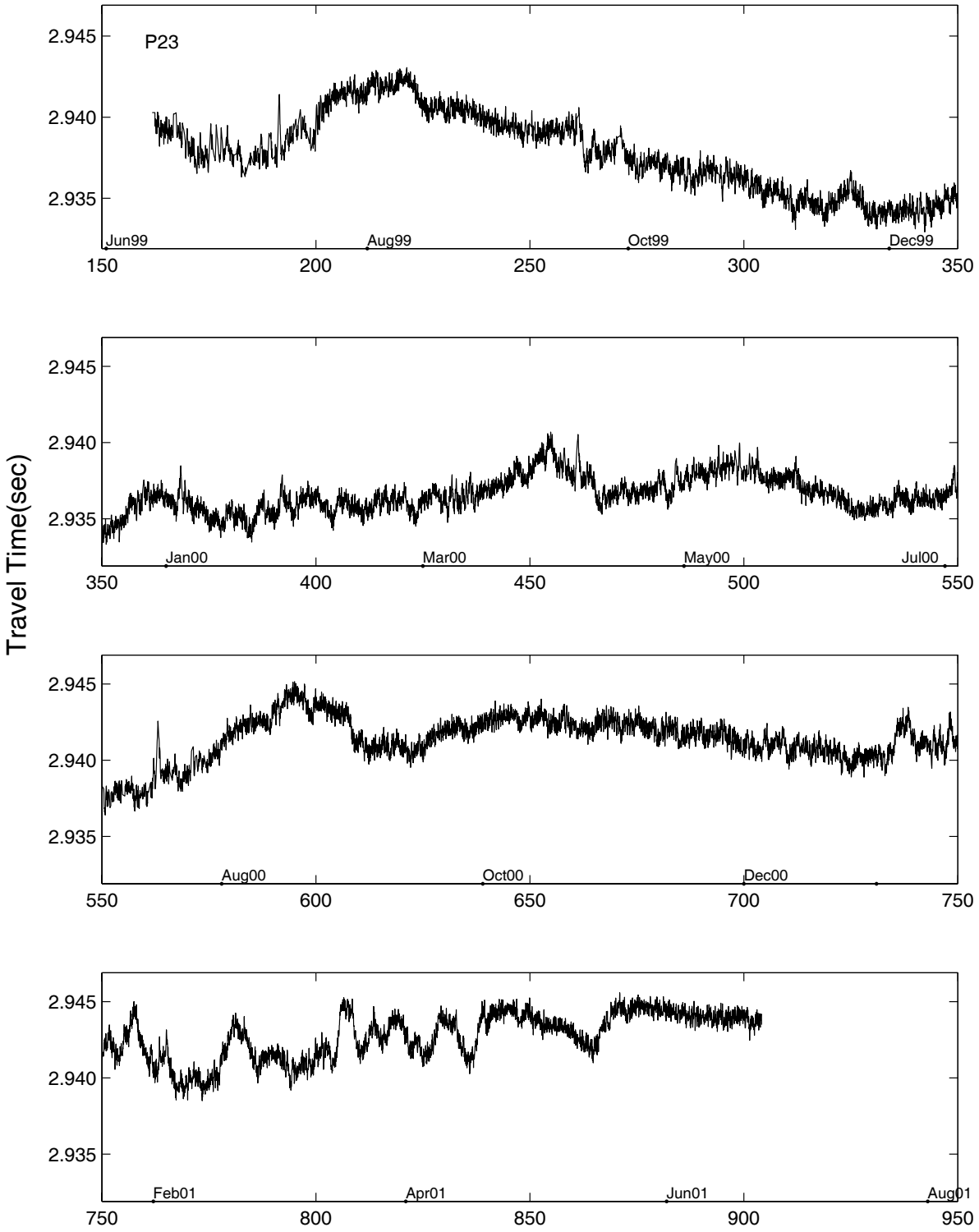

Figure 58: **P2-4 Hourly Travel Times**

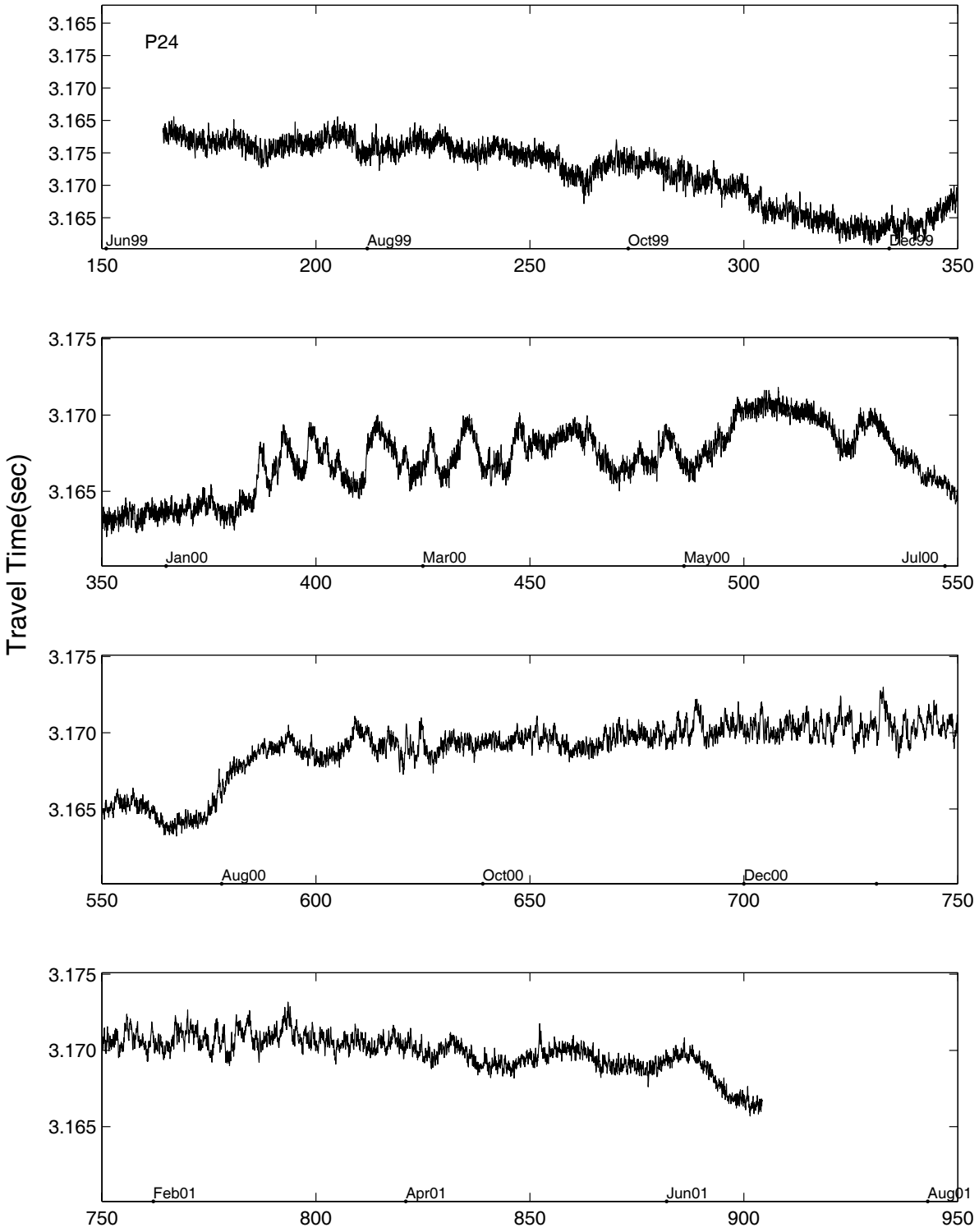

Figure 59: **P2-5 Hourly Travel Times**

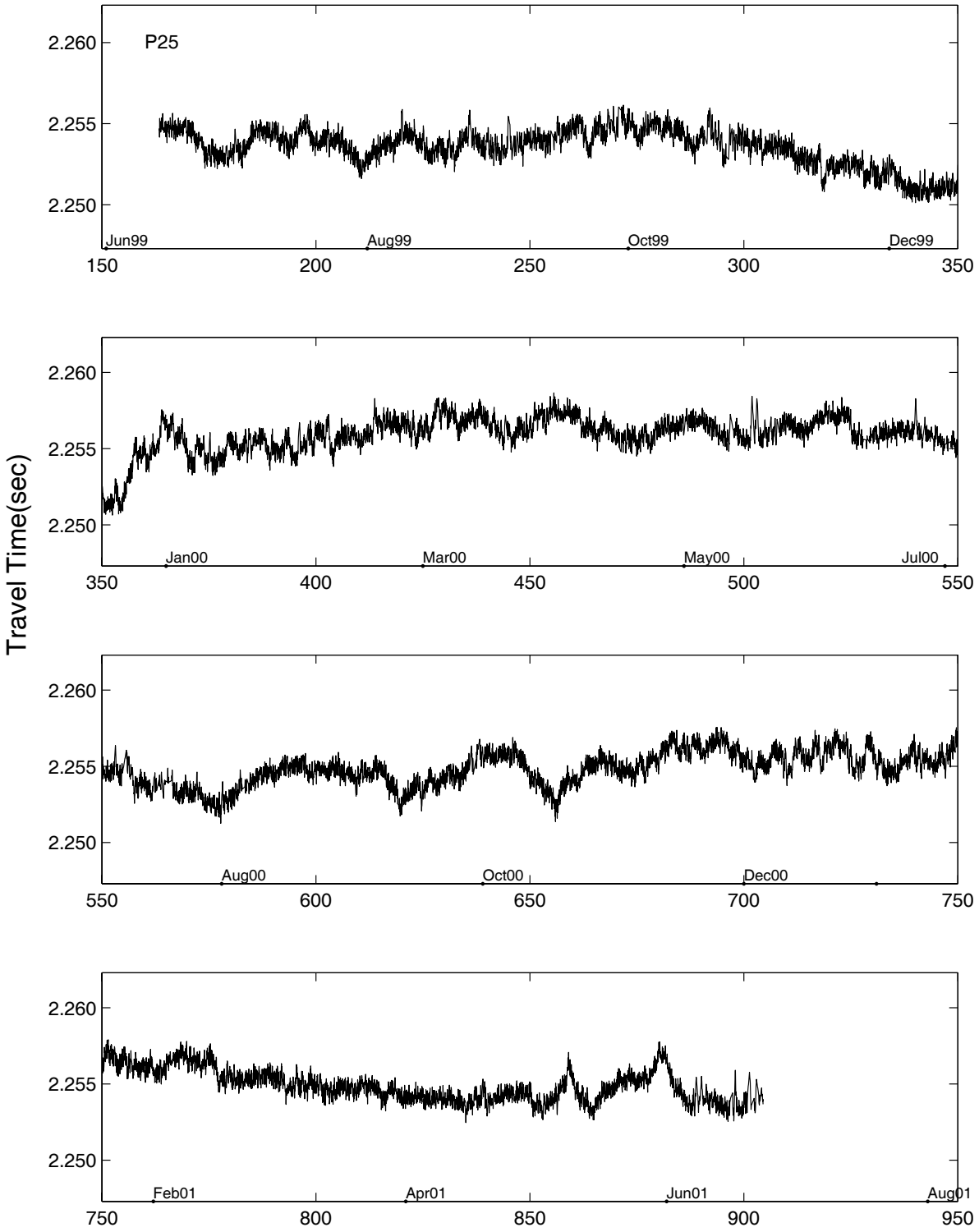

Figure 60: **P3-1 Hourly Travel Times**

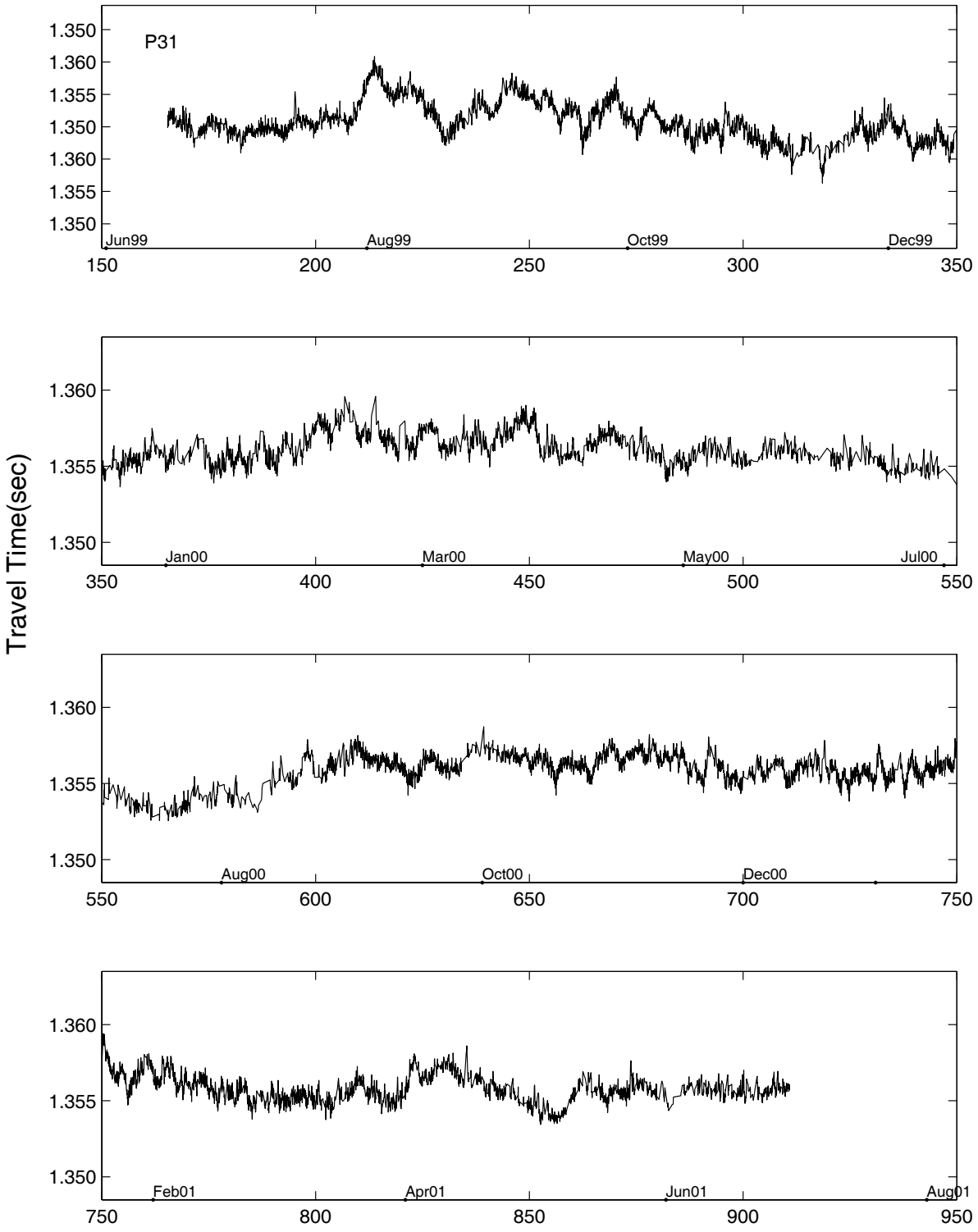

Figure 61: **P3-3 Hourly Travel Times**

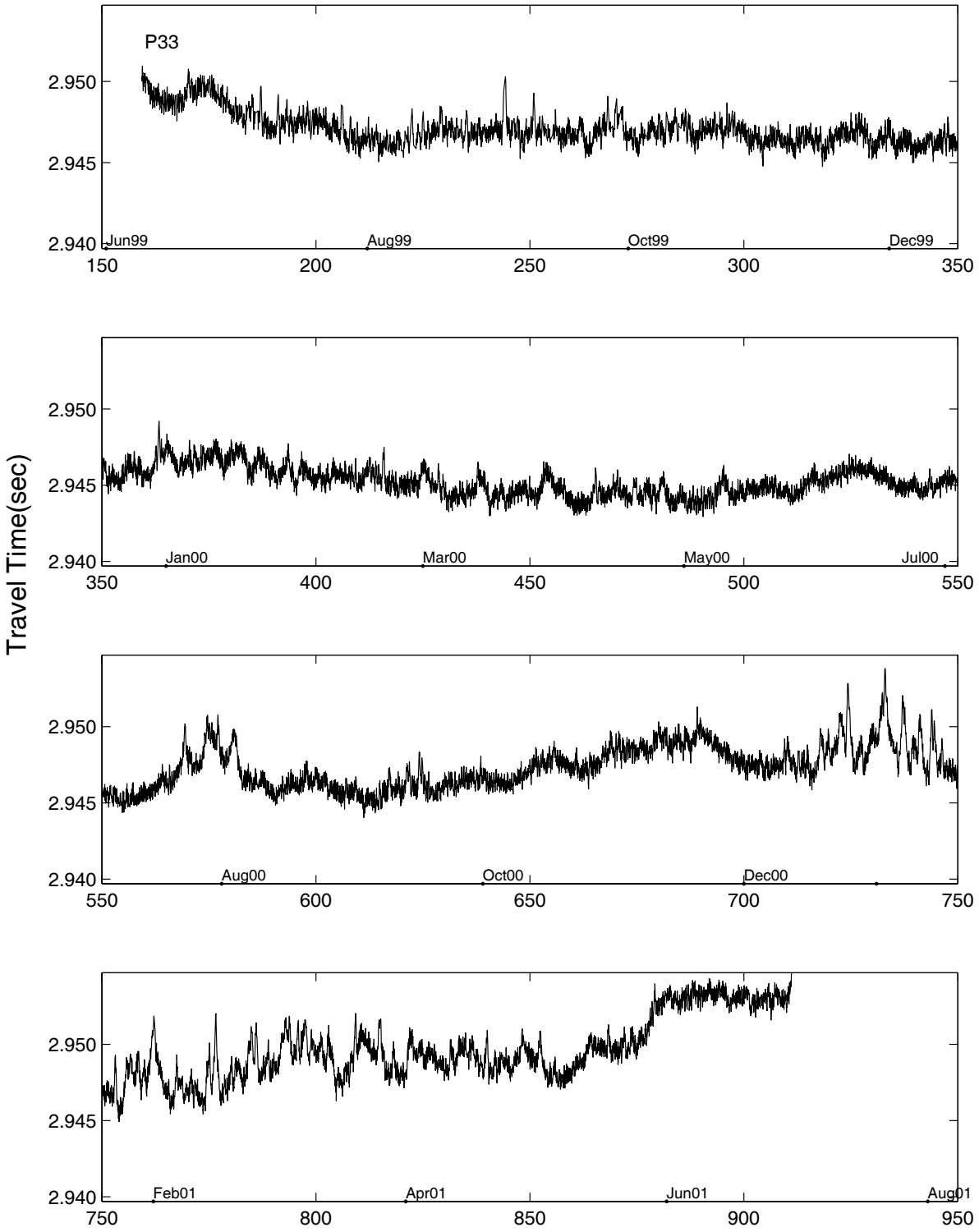

Figure 62: **P3-4 Hourly Travel Times**

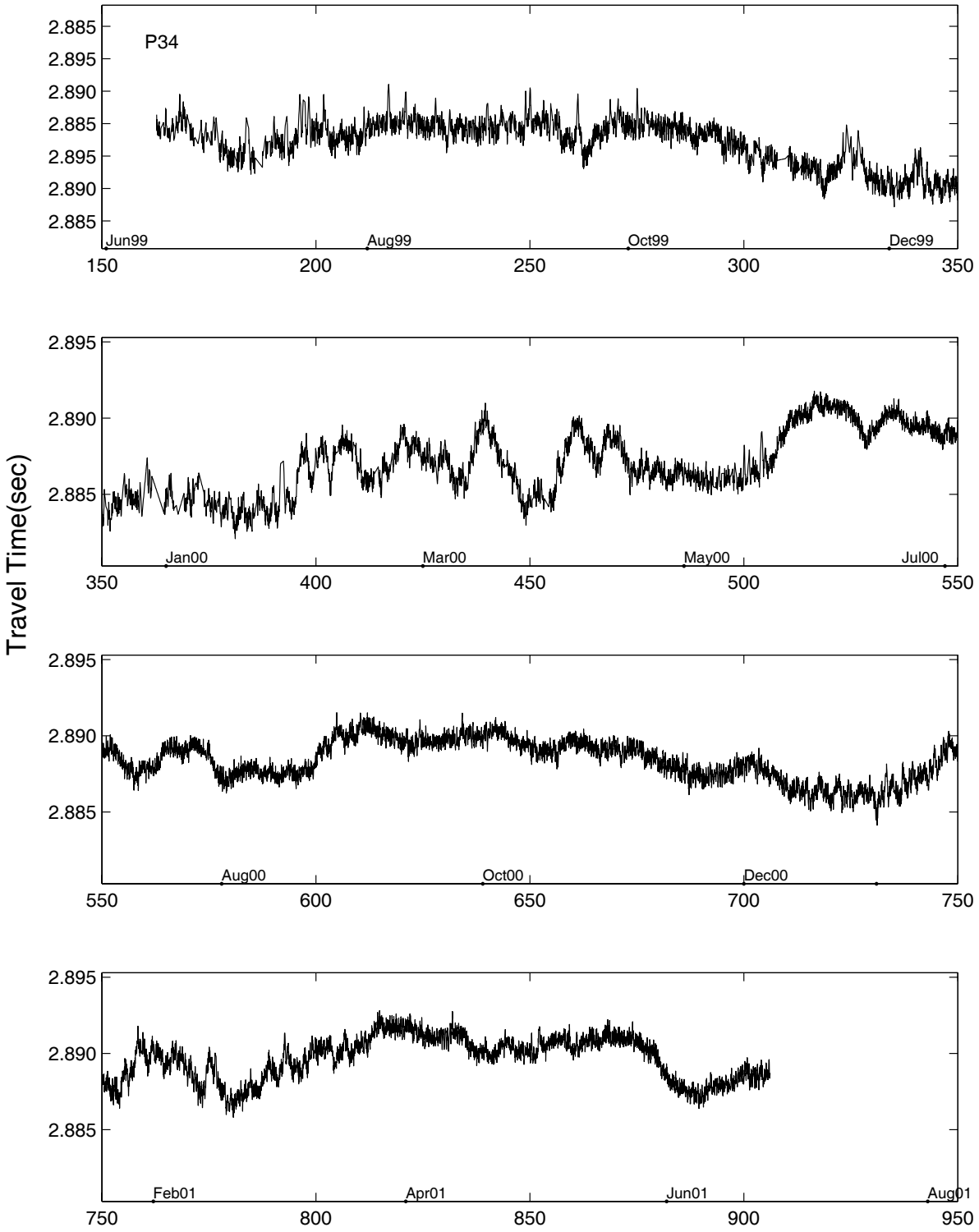

Figure 63: **P4-2 Hourly Travel Times**

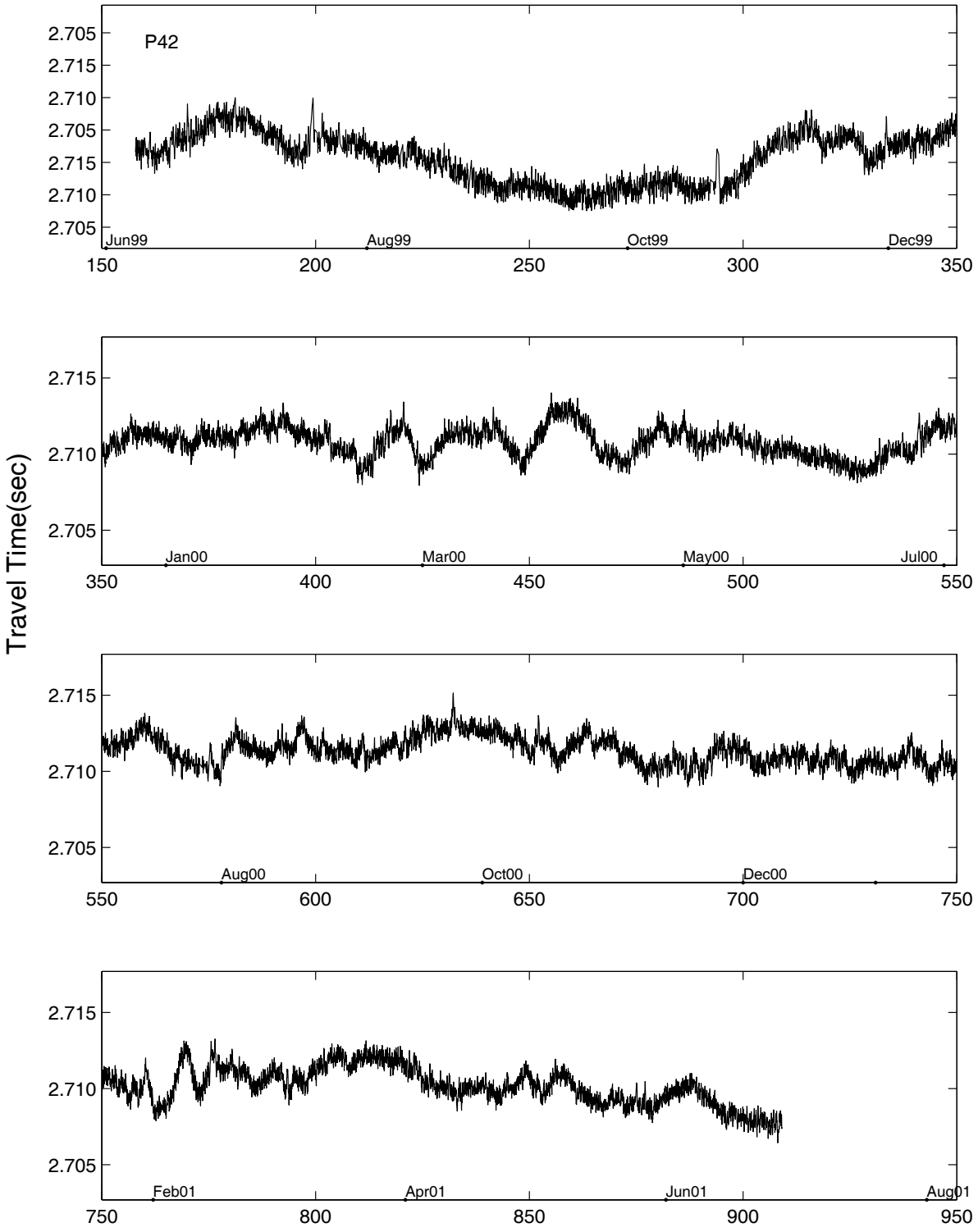

Figure 64: **P4-3 Hourly Travel Times**

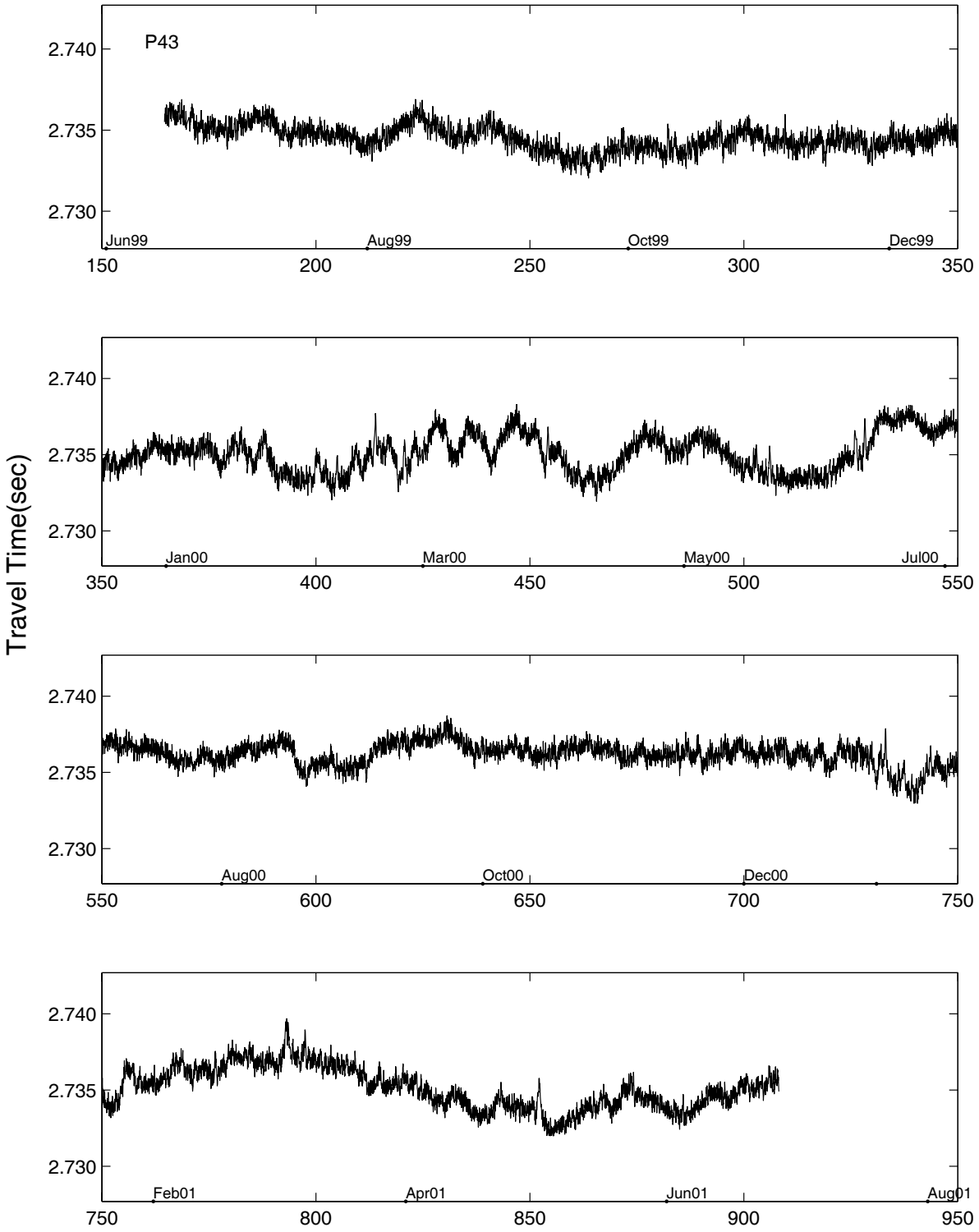

Figure 65: **P4-4 Hourly Travel Times**

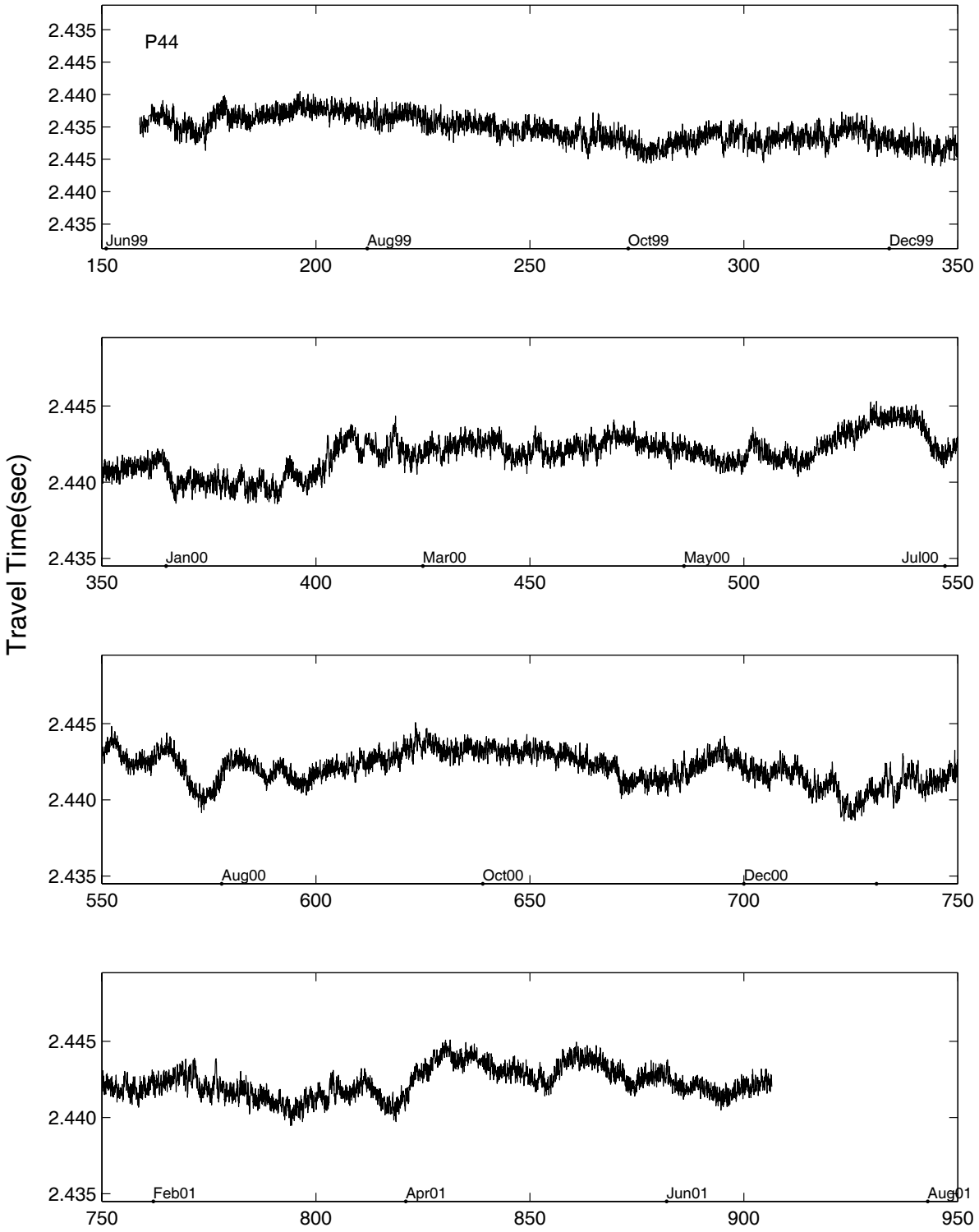

Figure 66: **P4-5 Hourly Travel Times**

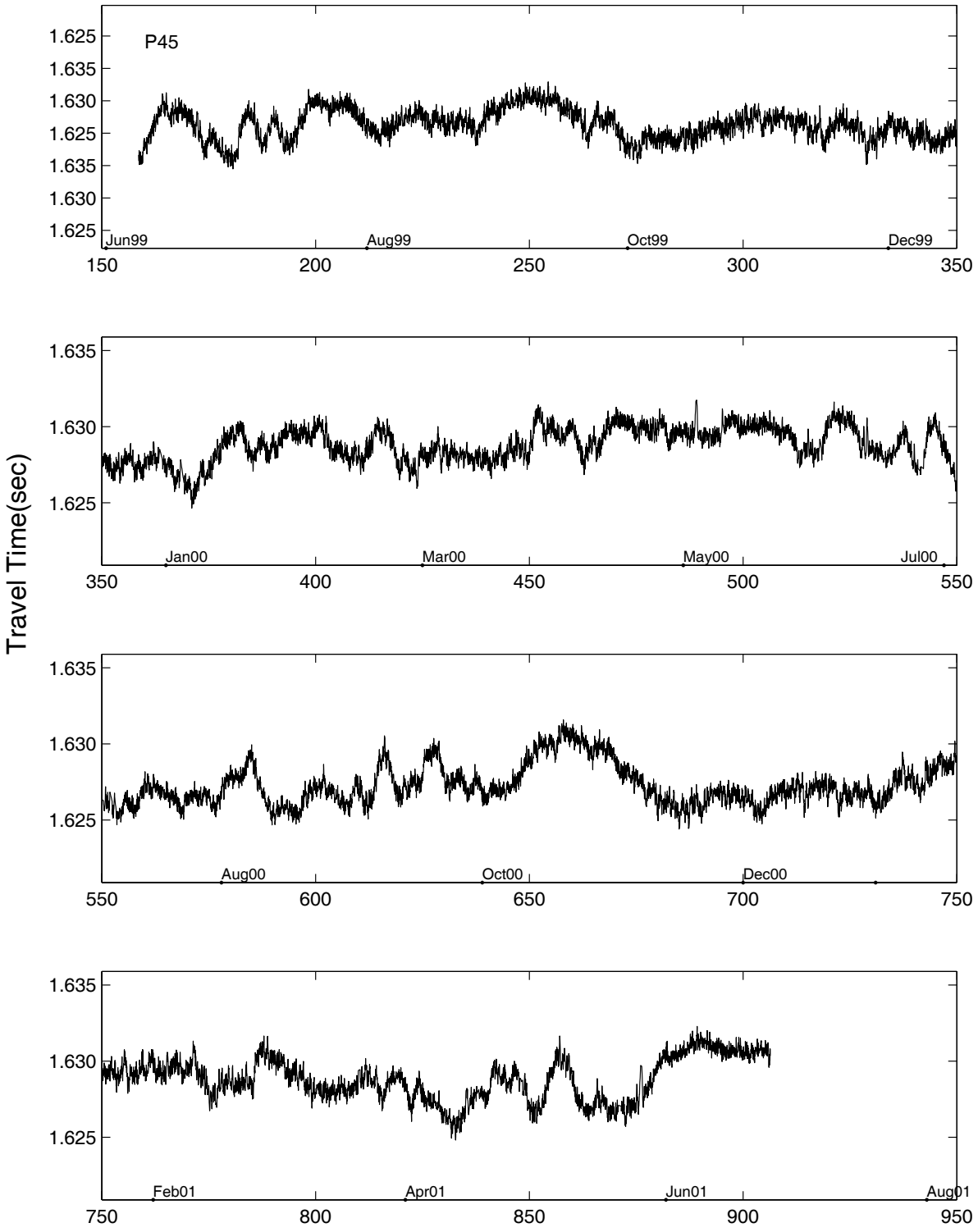

Figure 67: **P5-1 Hourly Travel Times**

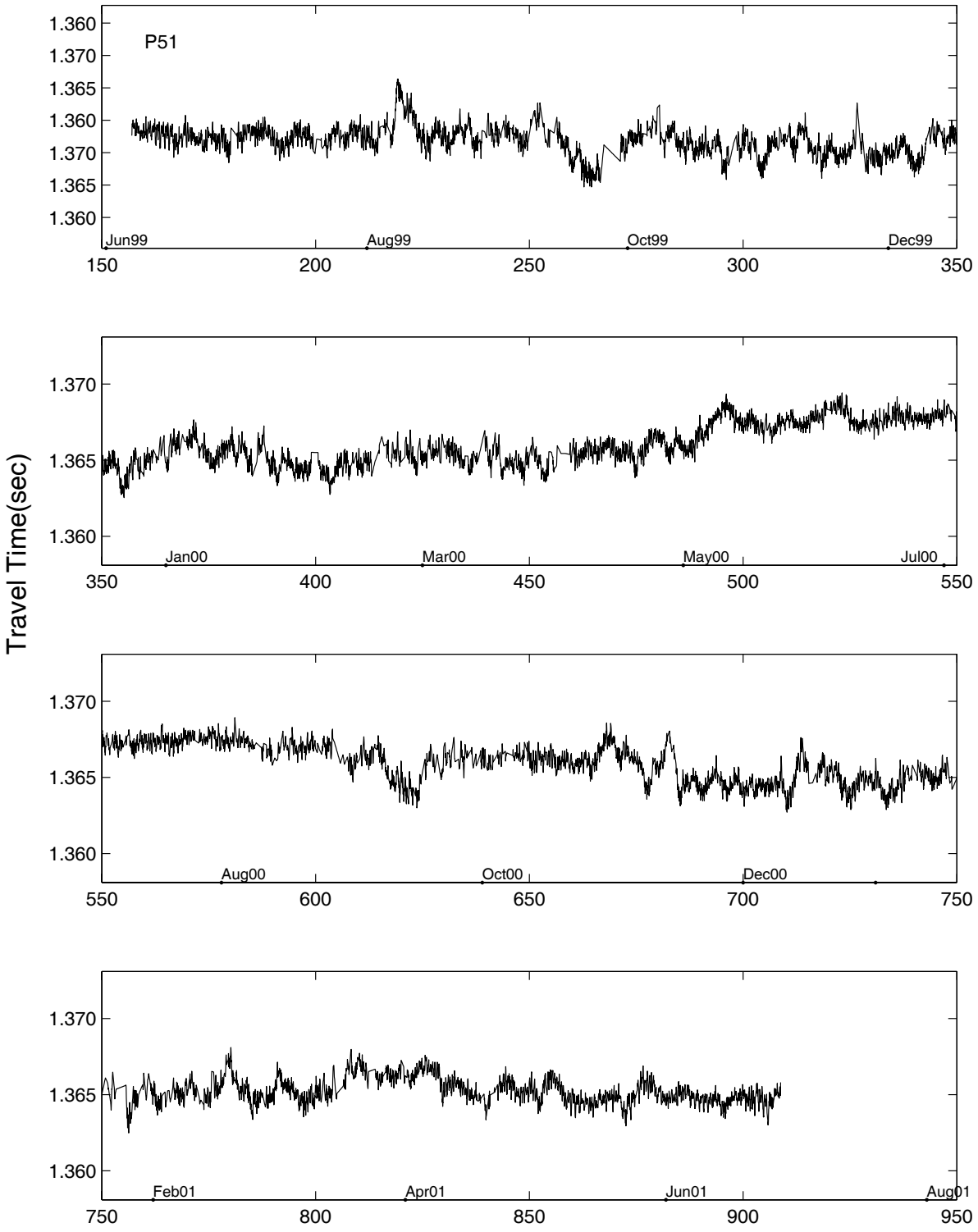

Figure 68: **P5-2 Hourly Travel Times**

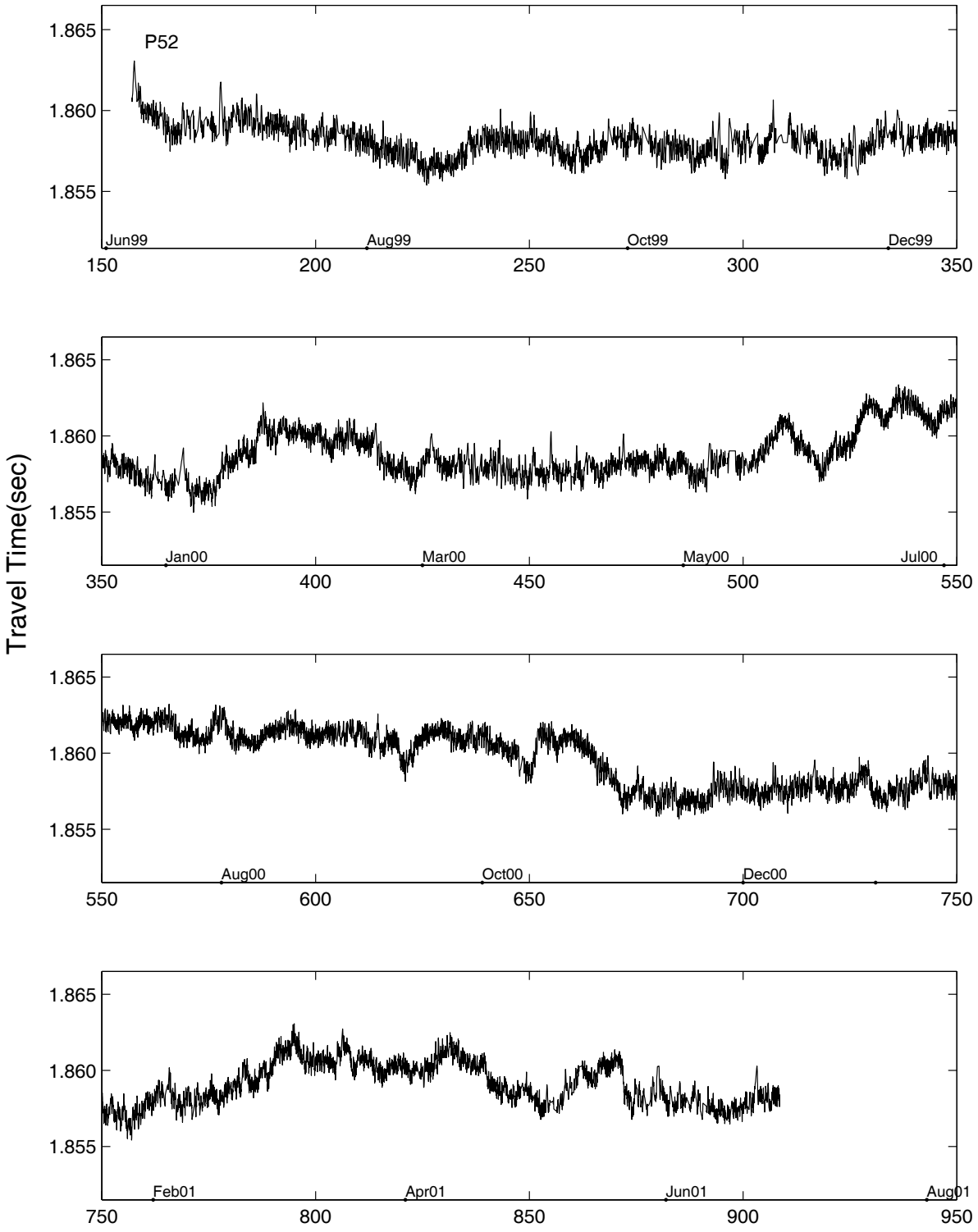

Figure 69: **P5-3 Hourly Travel Times**

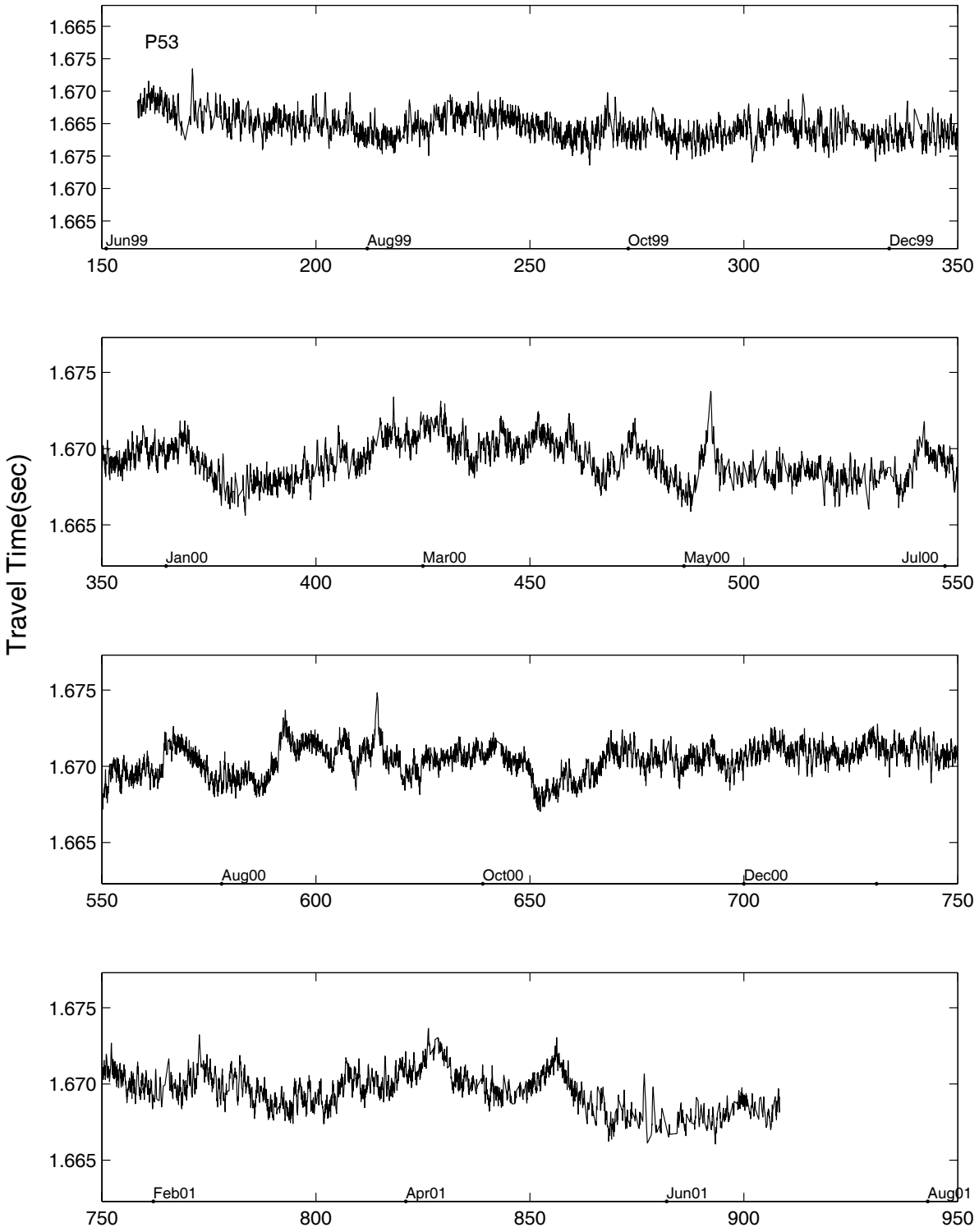

Figure 70: **P5-4 Hourly Travel Times**

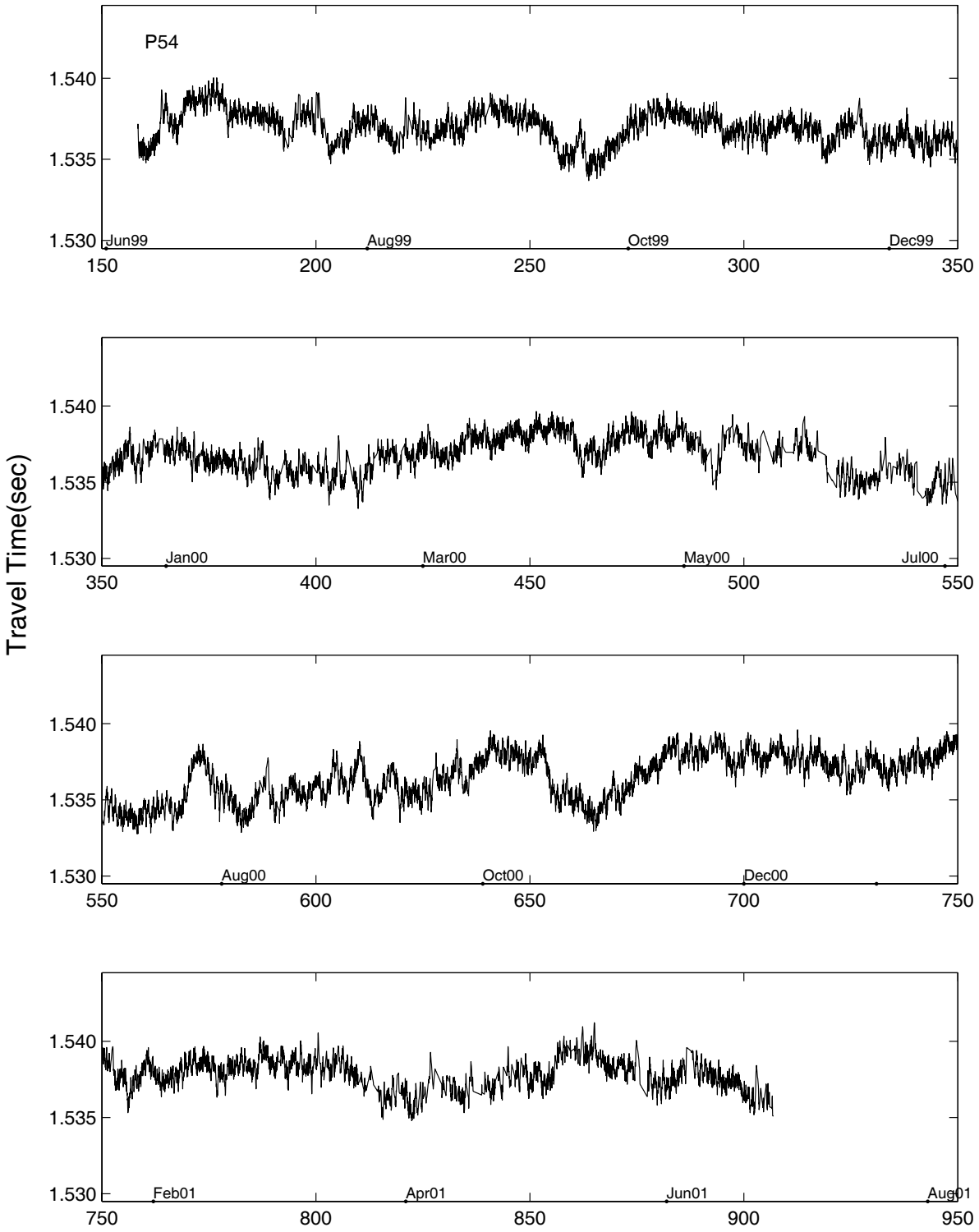

Figure 71: **P5-5 Hourly Travel Times**

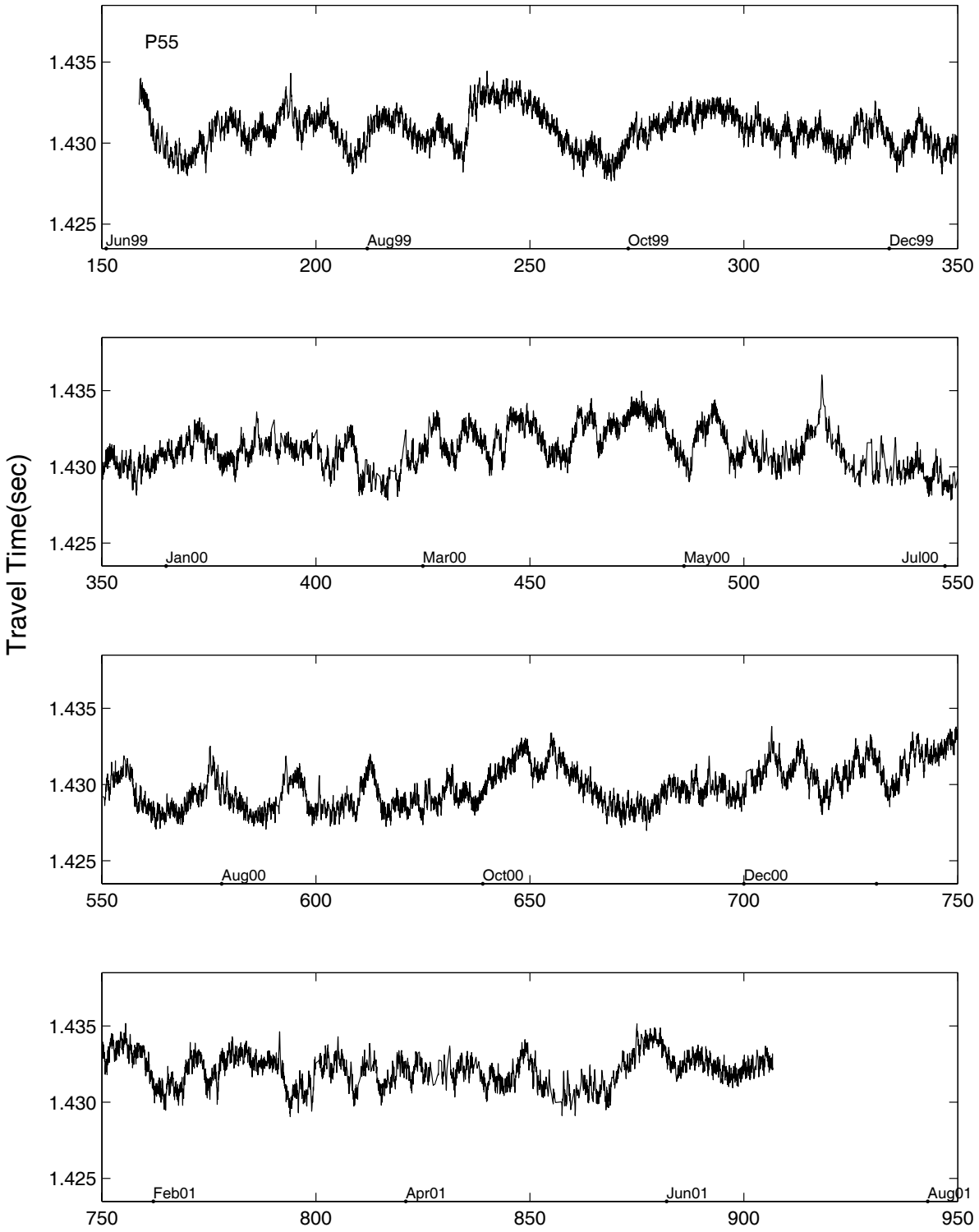

Figure 72: **P1-1–P1-4 120-hrlp** τ_{500}

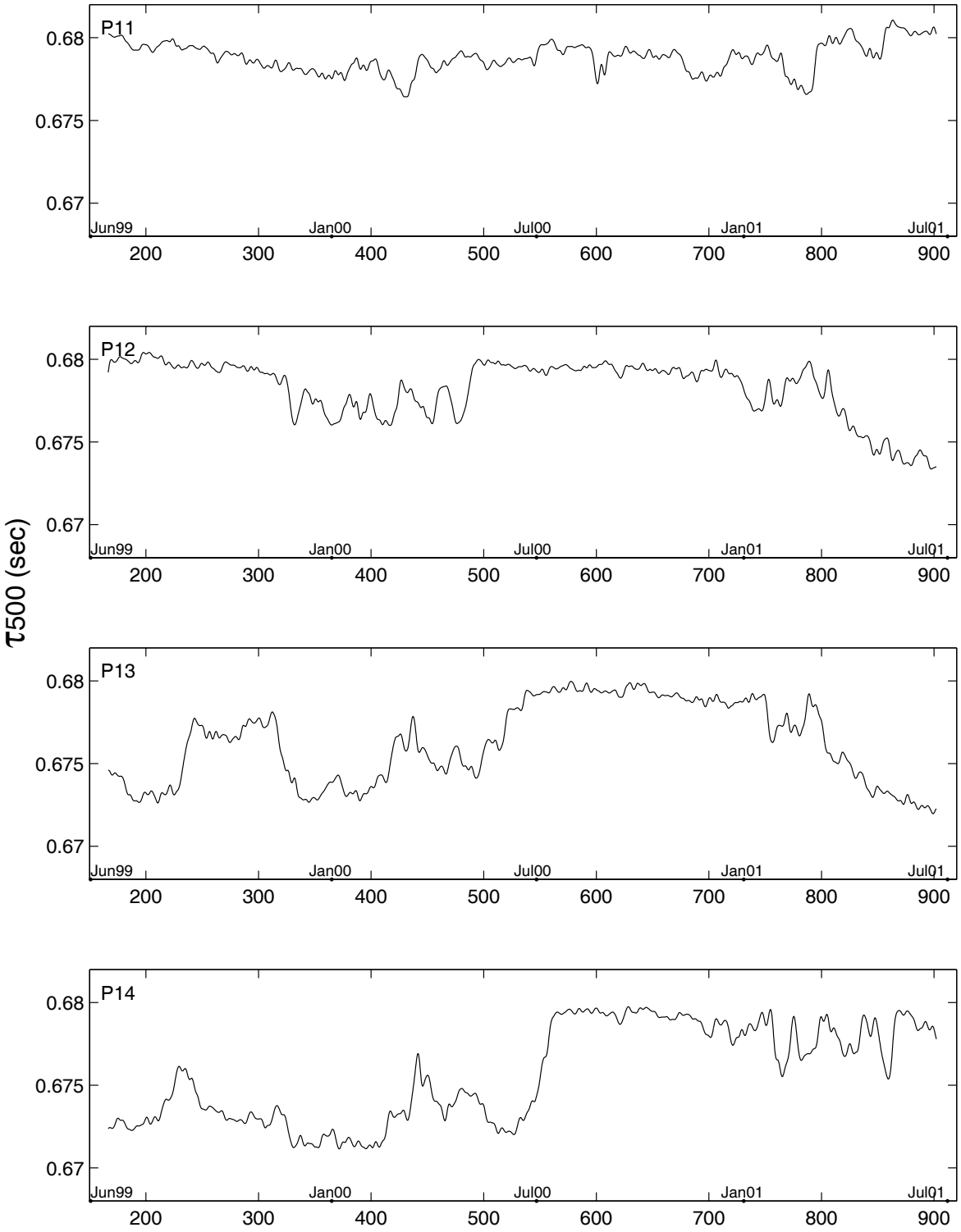

Figure 73: **P1-5–P2-2 120-hrlp** τ_{500}

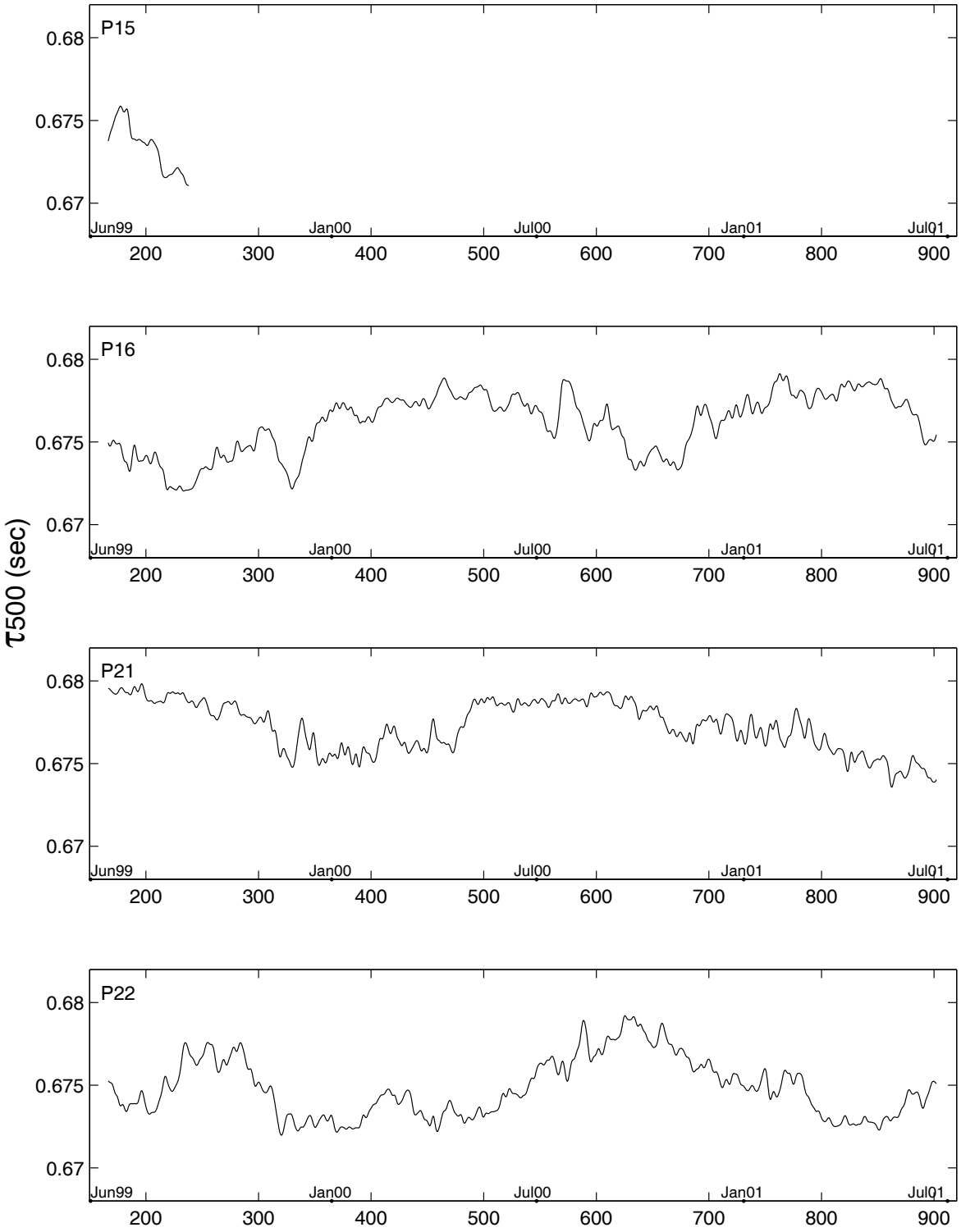

Figure 74: **P2-3–P3-1 120-hrlp** τ_{500}

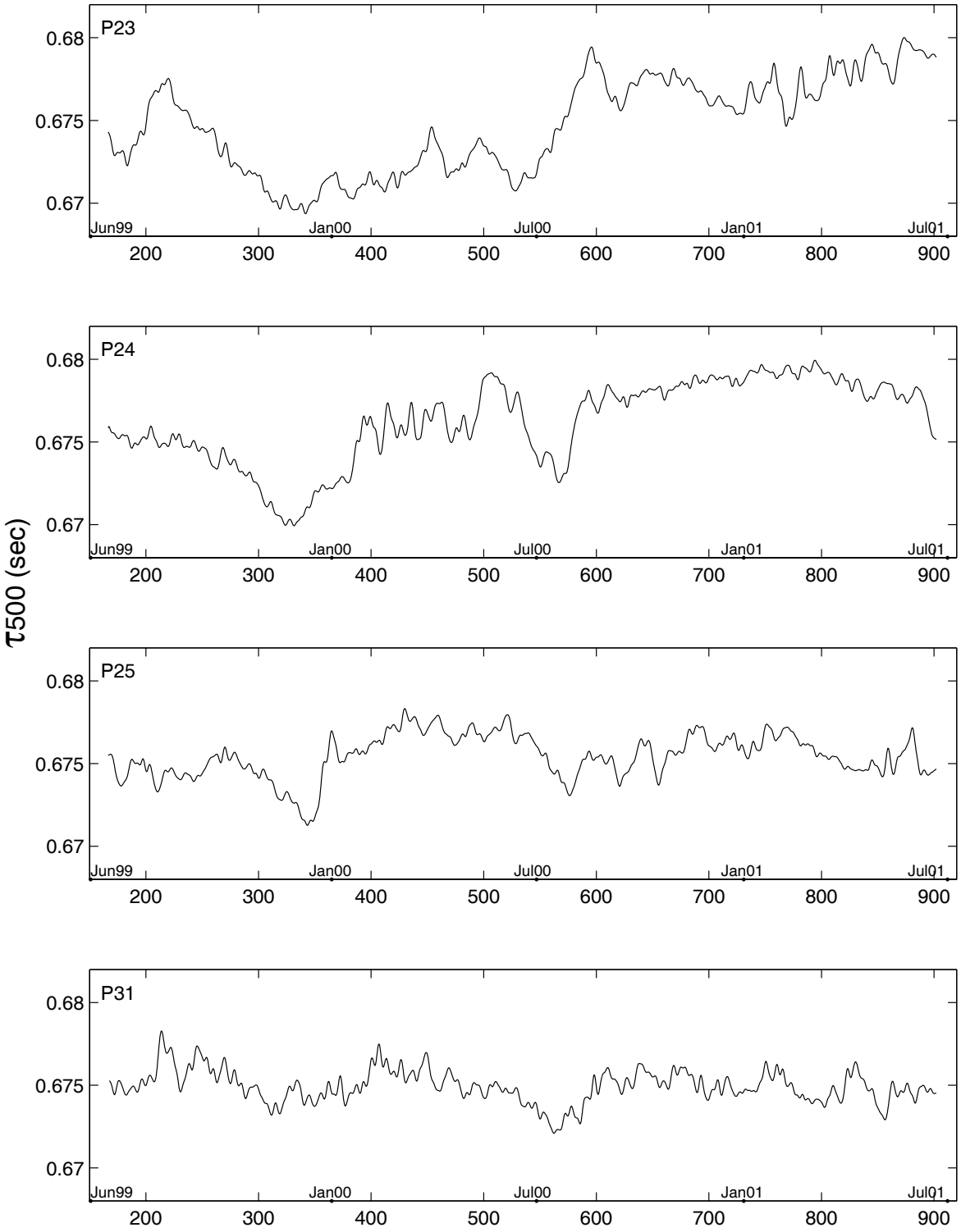

Figure 75: **P3-2–P4-2 120-hrlp** τ_{500}

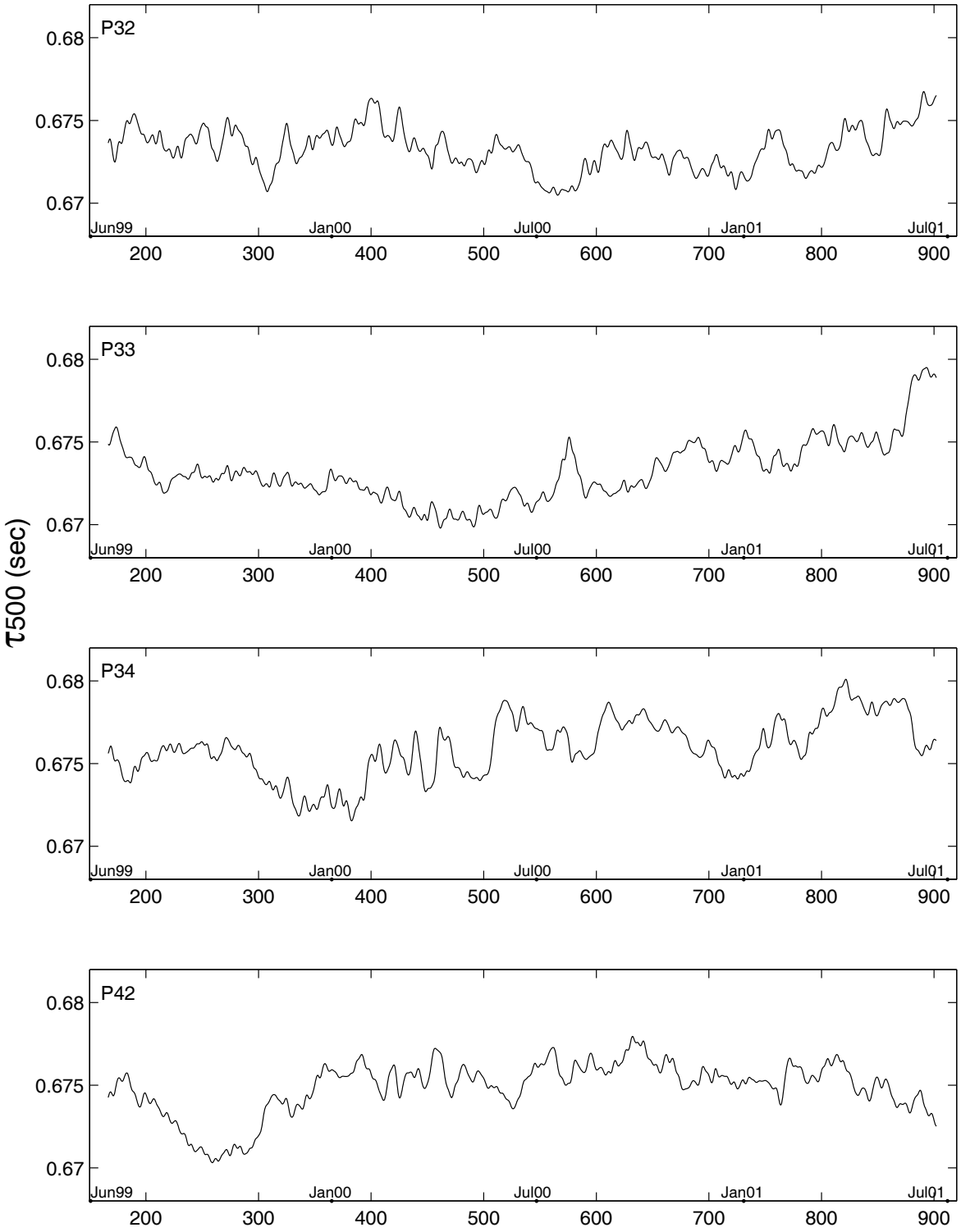

Figure 76: **P4-3–P5-1 120-hrlp** τ_{500}

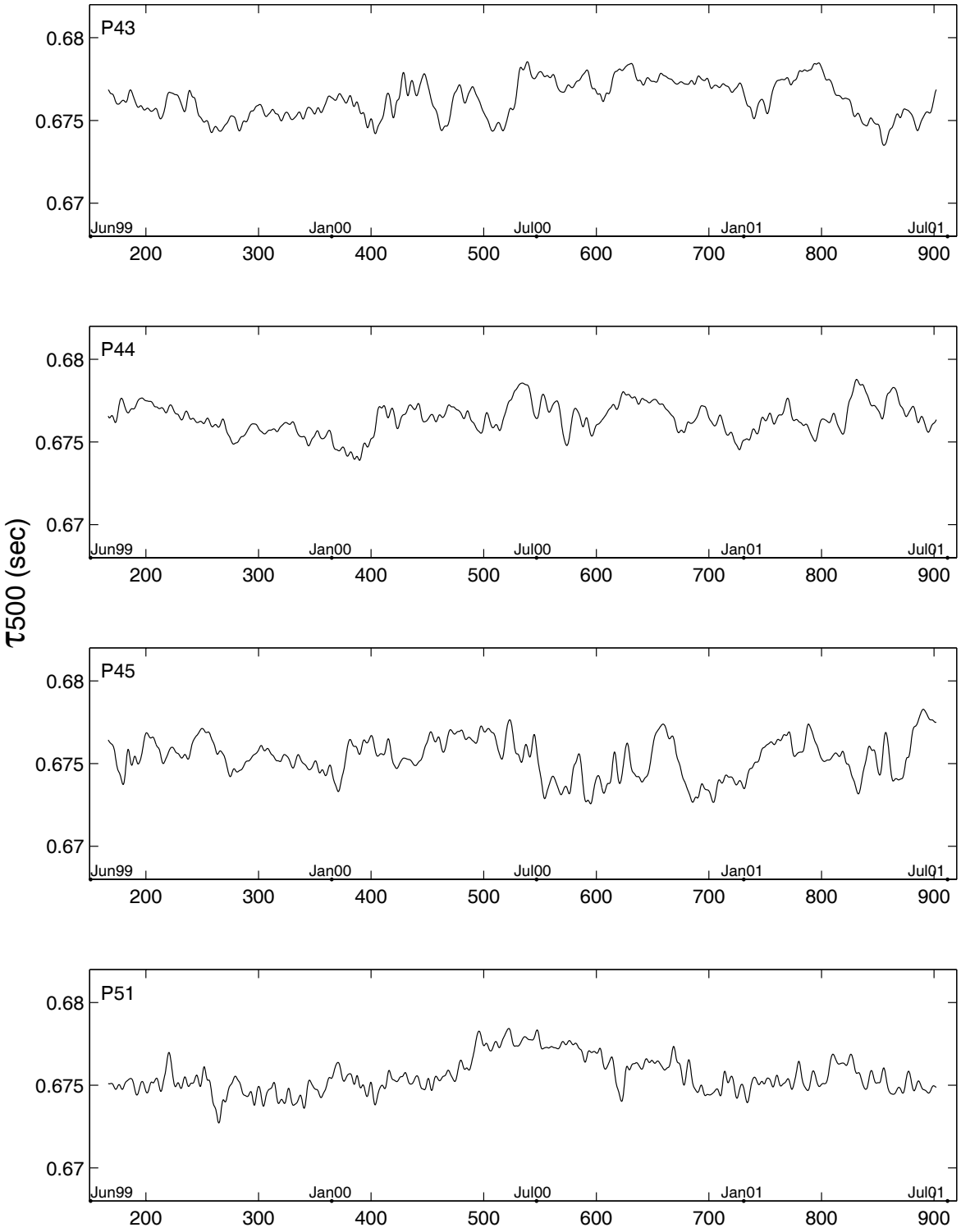

Figure 77: **P5-2–P5-5 120-hrlp** τ_{500}

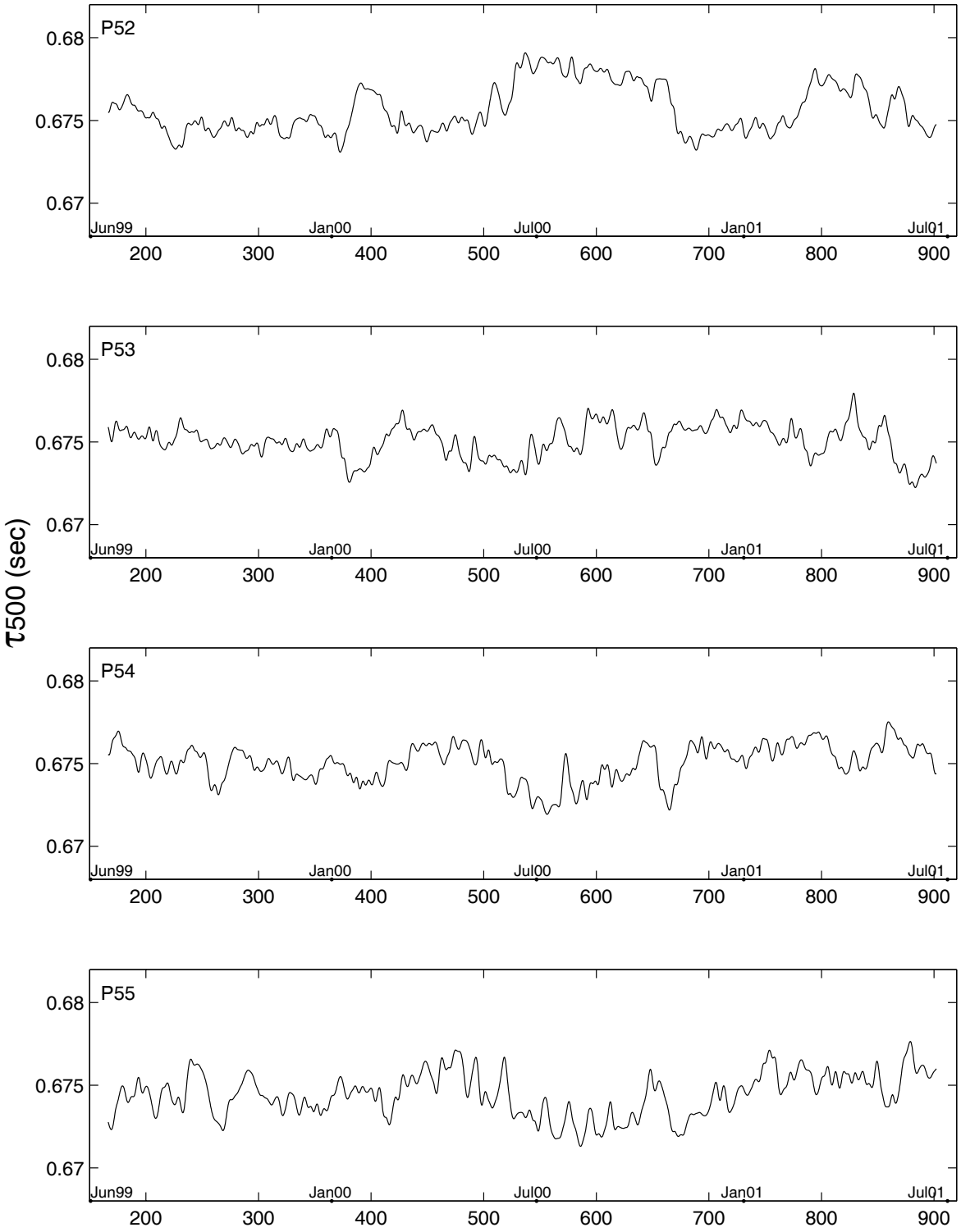

5 Temperature Records for Each Instrument

Figures 78–83 present the hourly temperature records. These records have had large data spikes (outliers) removed and replaced with linearly interpolated values. These measurements are made inside the instrument housing and therefore are not accurate measures of the instantaneous *in situ* water temperature. These records are provided on the accompanying CD-ROM.

Table 7 lists the mean, minimum, maximum, and standard deviation of the hourly temperatures measured at each site as well as the start and end time of the records.

Table 7: Statistics on the hourly temperature records shown in Figures 78–83. The mean, minimum (min), maximum (max), and standard deviations (STD) of the temperatures are reported along with the start and ending times of each data record.

Site	Start Time (UT)	End Time (UT)	Time Interval (hours)	Mean (°C)	Min (°C)	Max (°C)	STD (°C)
11	11 6 1999 07:59:43	1 July 2001 07:59:43	1.000	0.539	0.476	0.605	0.025
12	10 June 1999 20:59:24	2 July 2001 02:59:24	1.000	0.459	0.437	0.475	0.005
13	12 June 1999 05:59:30	1 July 2001 13:59:30	1.000	0.580	0.564	0.615	0.008
14	12 June 1999 09:59: 8	1 July 2001 17:59:08	1.000	0.480	0.439	0.521	0.013
15	14 June 1999 13:58:40	23 June 2001 17:58:40	1.000	0.523	0.519	0.536	0.002
16	14 June 1999 06:59:23	23 June 2001 13:54:23	1.000	0.613	0.609	0.624	0.002
21	11 June 1999 00:59:40	1 July 2001 03:59:40	1.000	0.645	0.582	0.717	0.022
22	12 June 1999 00:59:33	1 July 2001 22:59:33	1.000	0.453	0.432	0.480	0.008
23	12 June 1999 13:00: 6	23 June 2001 3:00:07	1.000	0.274	0.258	0.287	0.004
24	14 June 1999 16:59:24	23 June 2001 7:36:21	1.000	0.381	0.377	0.398	0.002
25	14 June 1999 03:59:31	23 June 2001 10:59:31	1.000	0.439	0.423	0.464	0.006
31	16 June 1999 04:58:57	29 June 2001 20:58:57	1.000	0.454	0.366	0.604	0.039
33	12 June 1999 23:59:19	29 June 2001 16:50:11	1.000	0.420	0.401	0.438	0.006
34	9 June 1999 23:59:57	30 June 2001 04:59:56	1.000	0.608	0.590	0.623	0.005
42	13 June 1999 13:59:07	25 June 2001 1:59:07	1.000	0.447	0.436	0.459	0.004
43	8 June 1999 15:59:08	28 June 2001 00:59:08	1.000	0.390	0.382	0.398	0.003
44	15 June 1999 09:59:18	27 June 2001 04:51:17	1.000	0.443	0.434	0.453	0.003
45	9 June 1999 13:59:16	25 June 2001 11:59:16	1.000	0.479	0.463	0.496	0.004
51	9 June 1999 10:00:45	25 June 2001 08:00:45	1.000	0.529	0.493	0.561	0.012
52	July June 1999 16:59:15	27 June 2001 18:49:37	1.000	0.594	0.537	0.705	0.025
53	July June 1999 10:58:32	27 June 2001 12:58:32	1.000	0.506	0.487	0.523	0.006
54	8 June 1999 23:59:20	27 June 2001 8:50:23	1.000	0.563	0.510	0.664	0.022
55	8 June 1999 08:58:34	25 June 2001 23:58:34	1.000	0.506	0.470	0.531	0.018
32	9 June 1999 06:59:32	25 June 2001 17:59:31	1.000	0.447	0.402	0.569	0.026

Figure 78: **P1-1–P1-4 Hourly Temperatures**

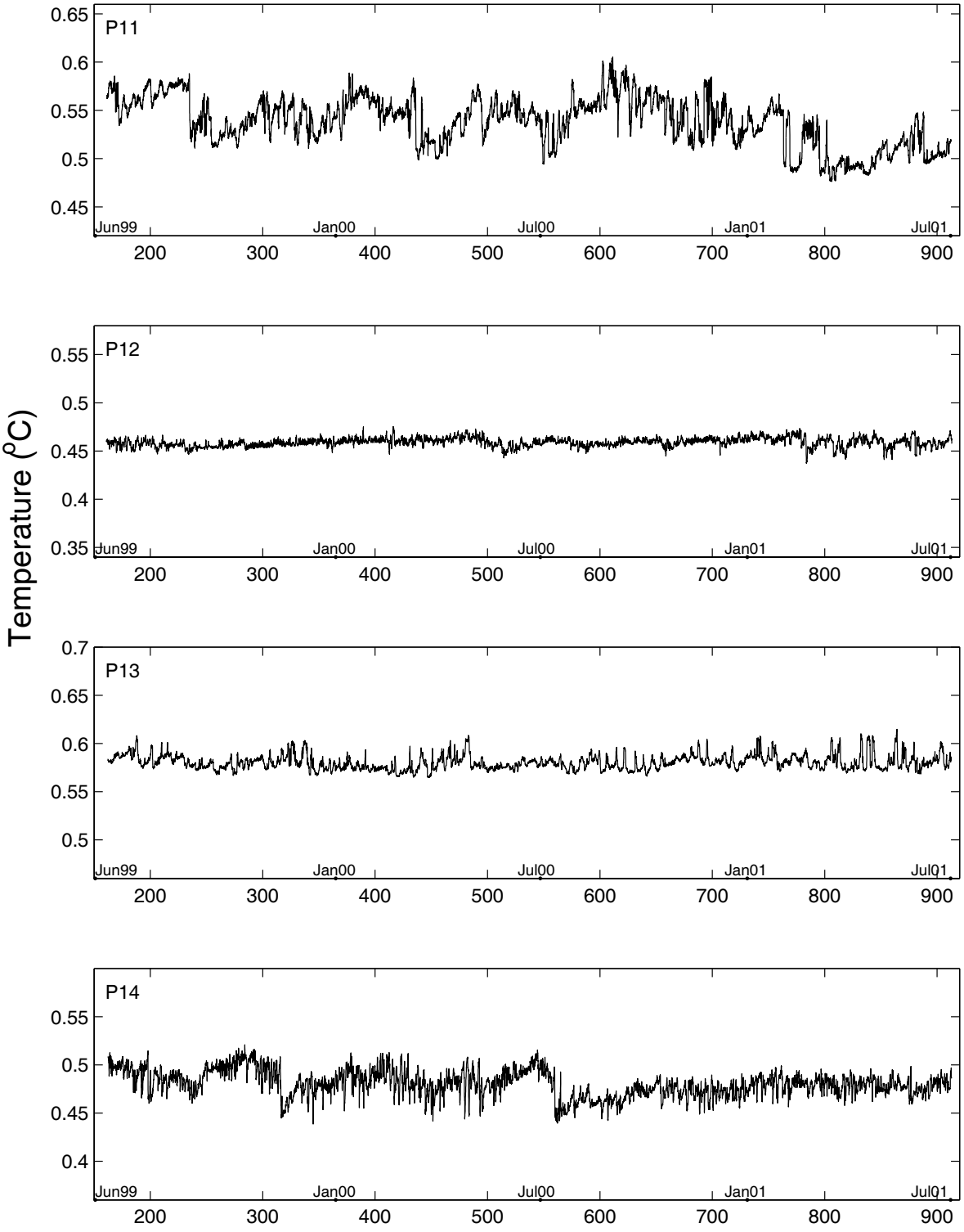

Figure 79: **P1-5–P2-2 Hourly Temperatures**

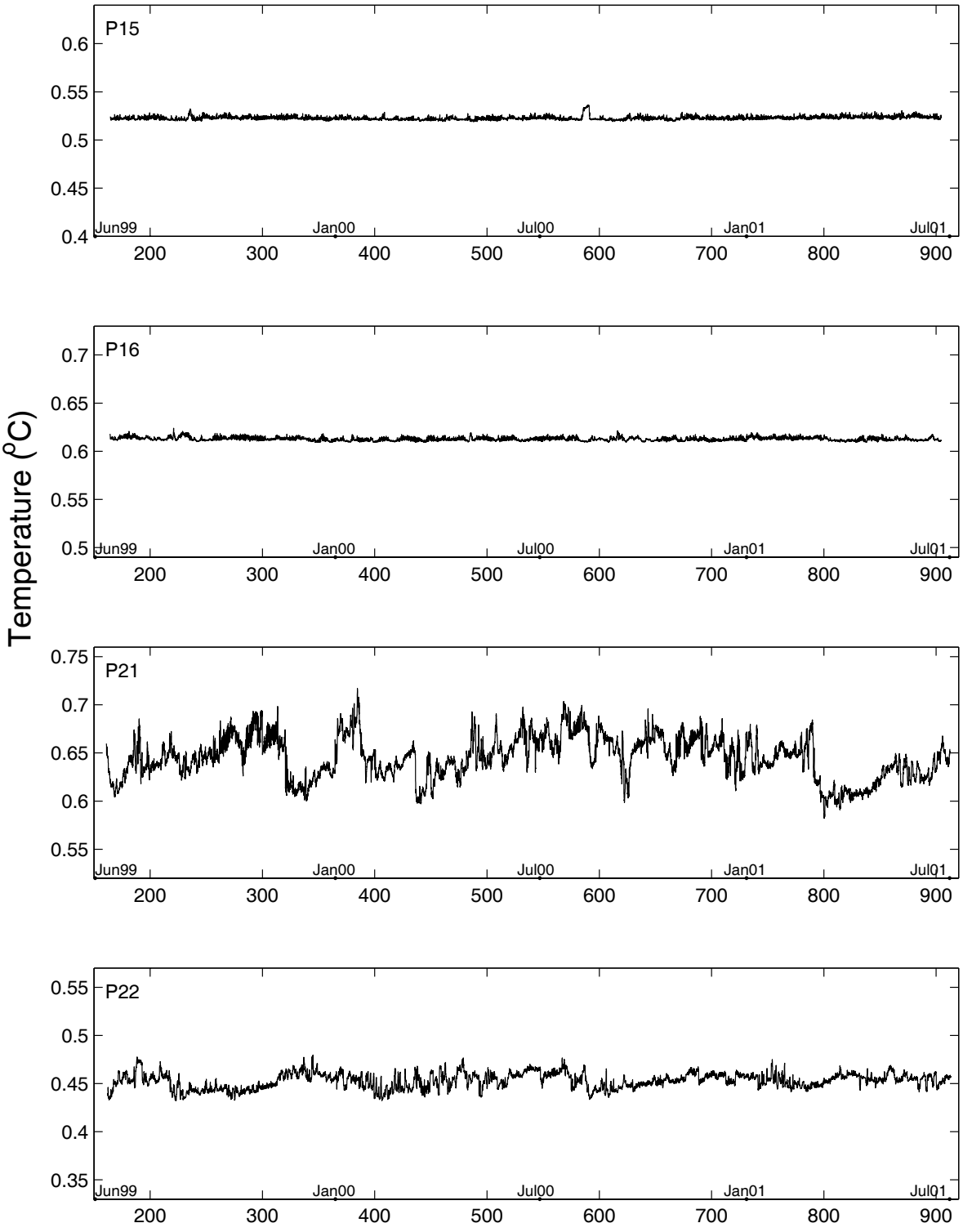

Figure 80: **P2-3–P3-1 Hourly Temperatures**

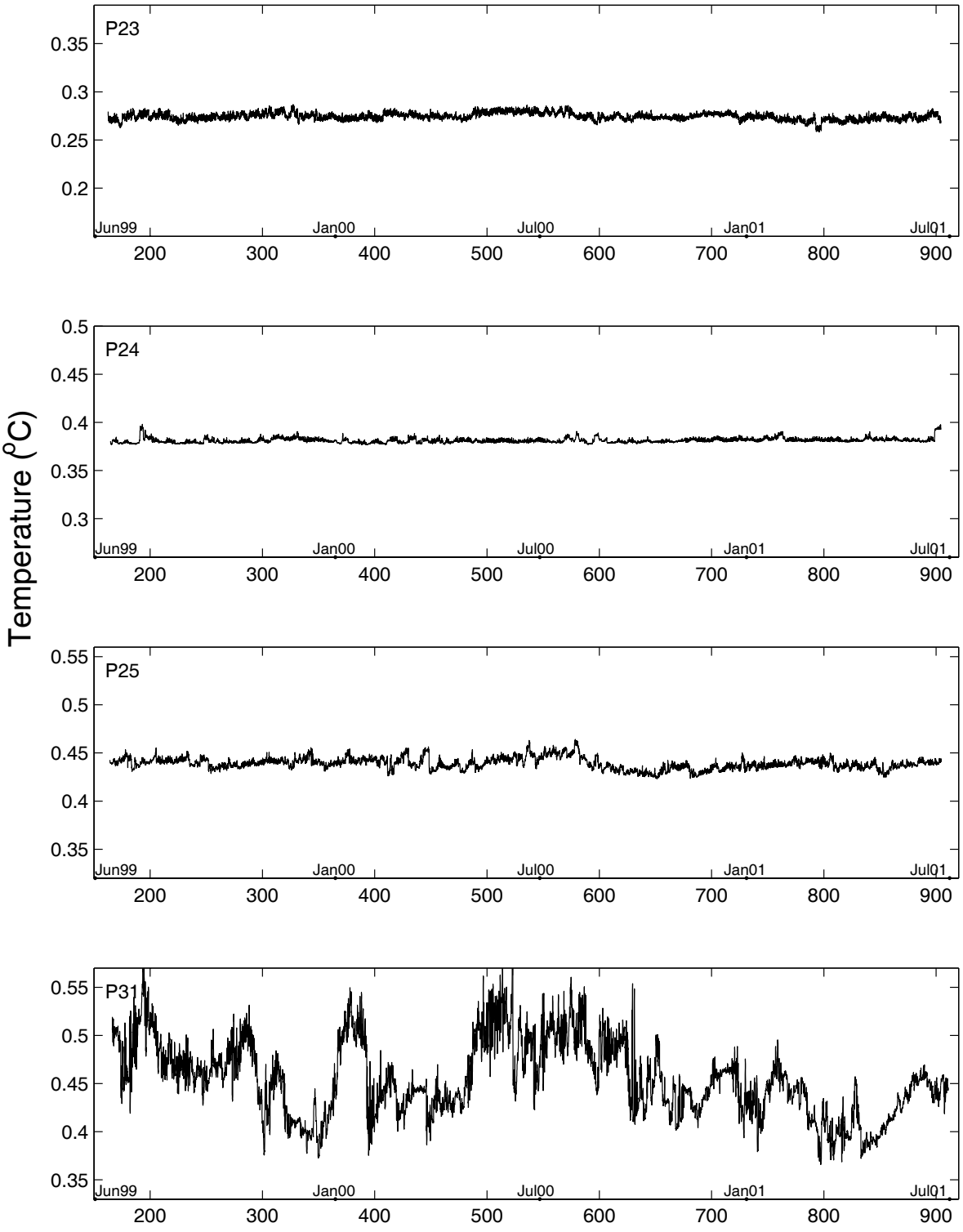

Figure 81: **P3-2–P4-2 Hourly Temperatures**

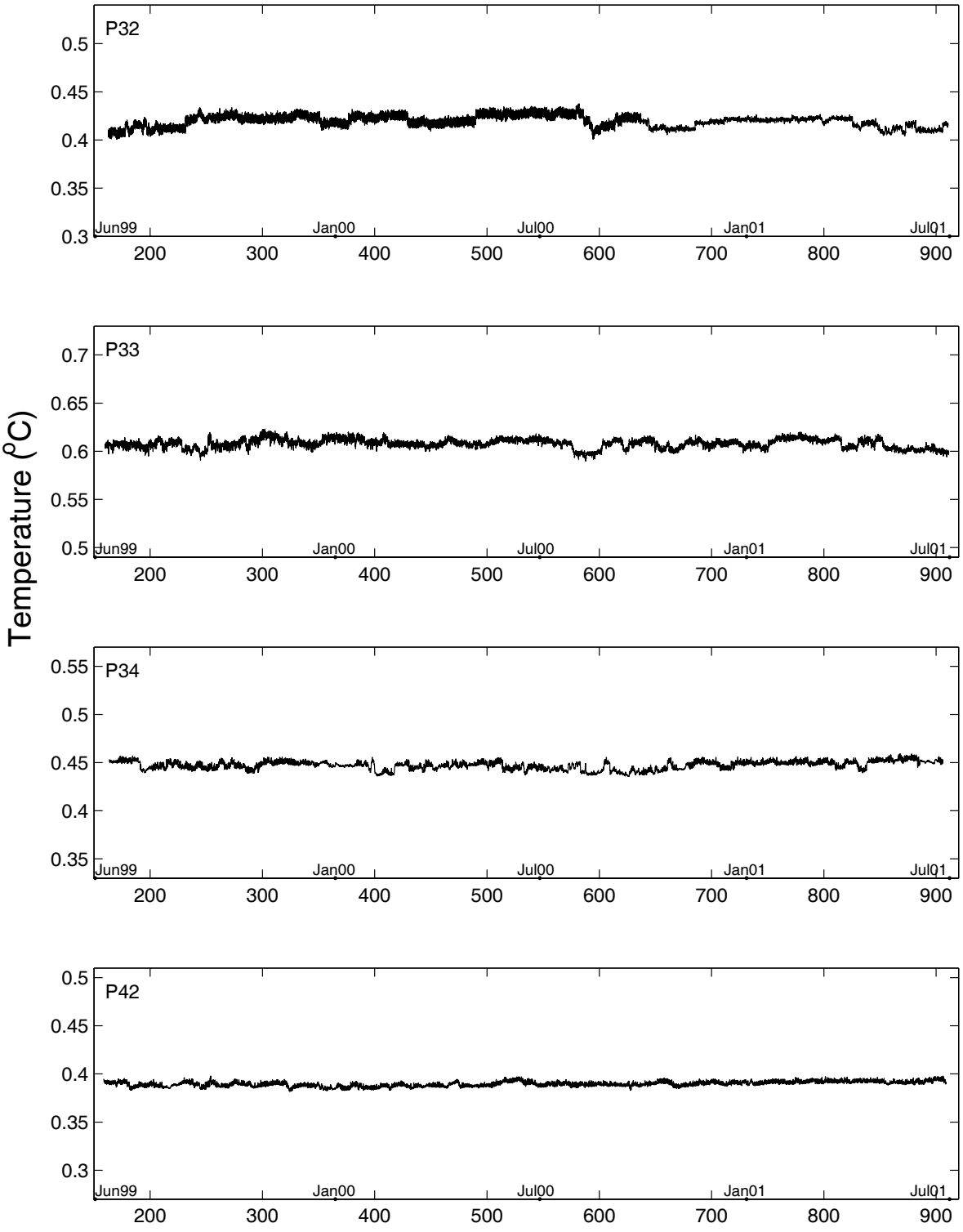

Figure 82: **P4-3–P5-1 Hourly Temperatures**

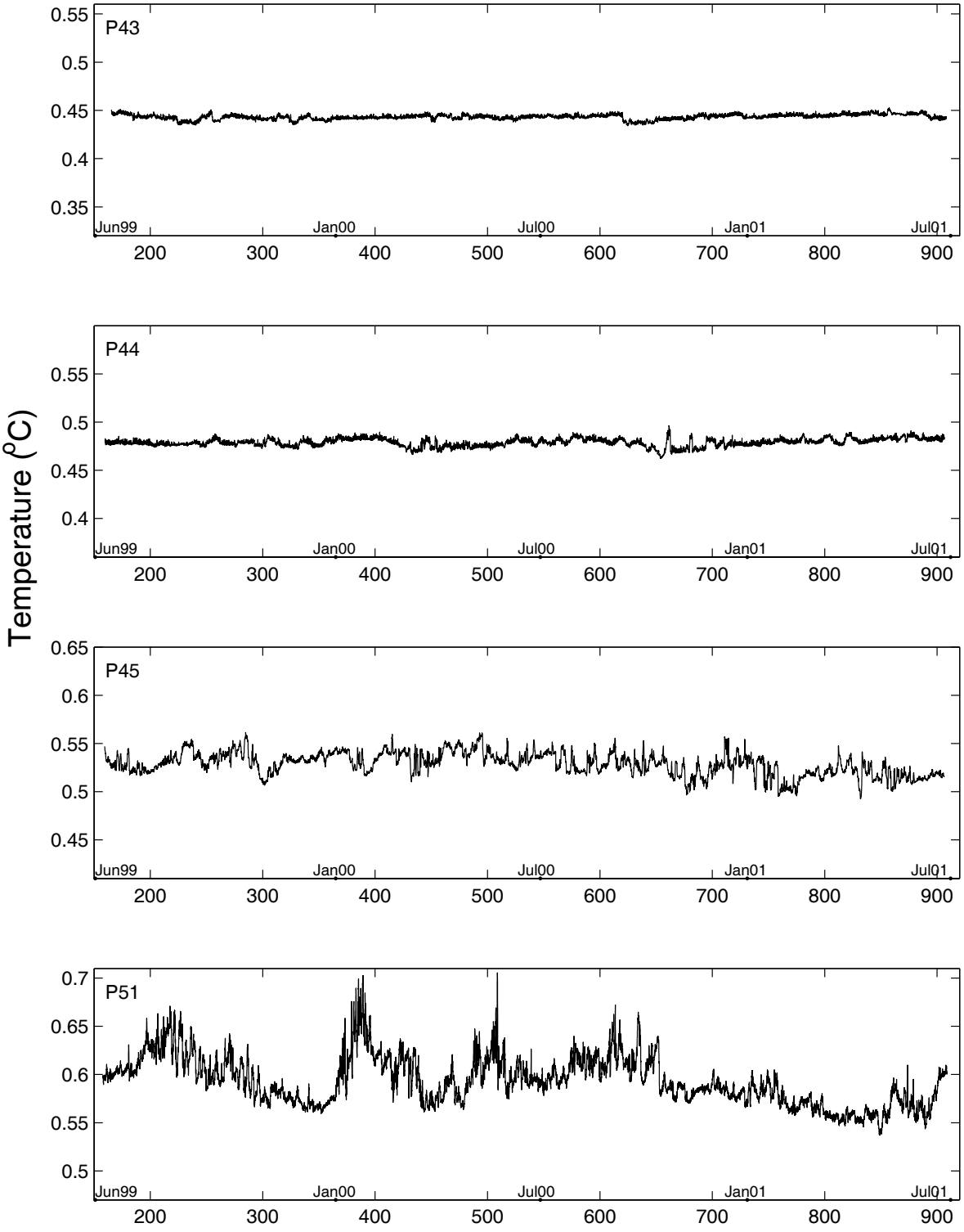

Figure 83: **P5-2–P5-5 Hourly Temperatures**

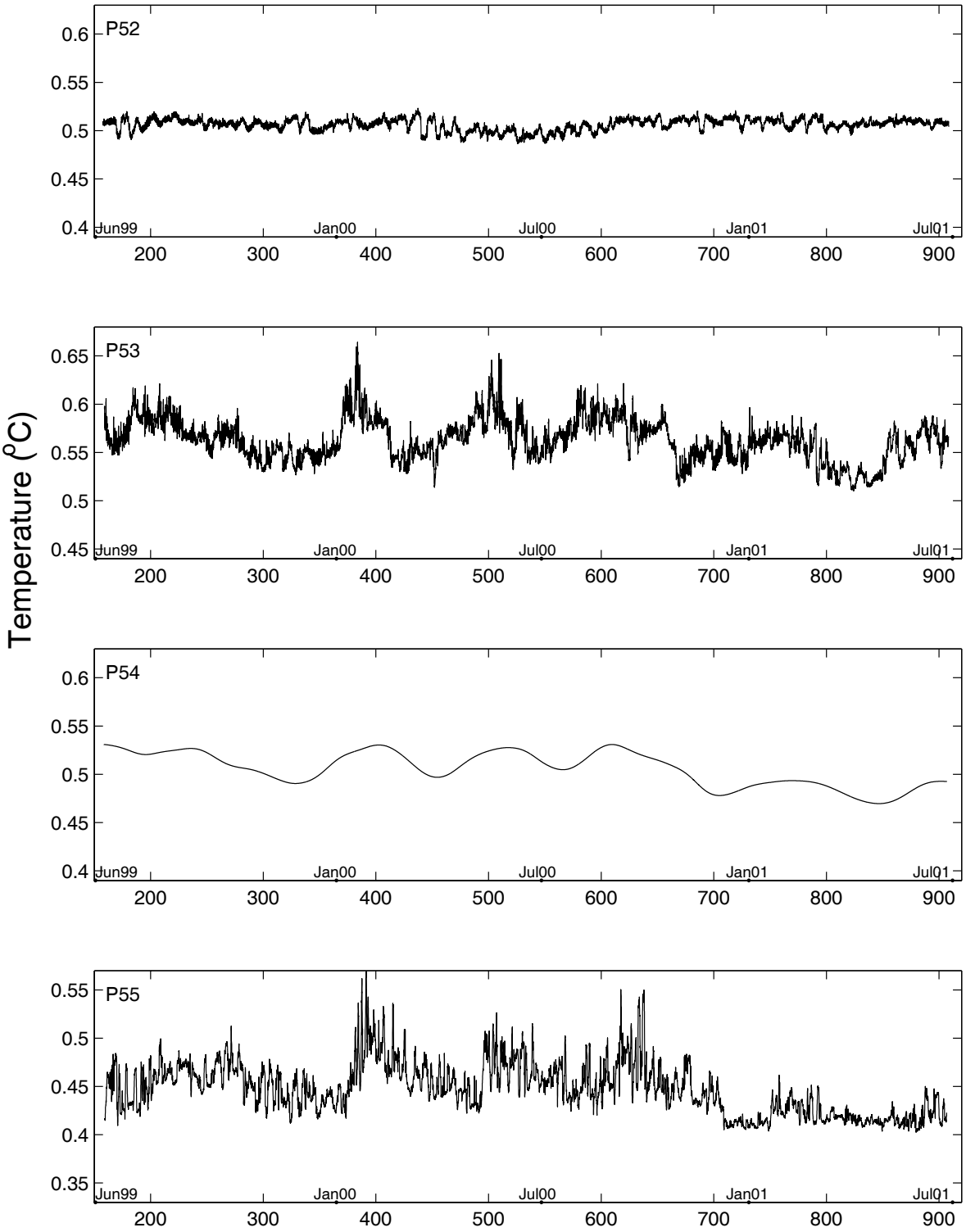

6 Acknowledgments

We gratefully acknowledge the efforts of the crews of the R/V Revelle and the R/V Melville for their efforts during the deployment and recovery cruises. The successful deployment and recovery of the inverted echo sounders is due to the instrumentation development and careful preparation done by Gerard Chaplin and Michael Mulroney. Special thanks goes to Angela Adams, a SURFO student at URI during Summer 2001, who helped with the initial data processing.

We appreciate the current meter data supplied by Dr. Moon-Sik Suk and Dr. K.-I. Chang (KORDI), and Dr. J-H Yoon (RIAM) which were used to level the bottom pressure measurements. The CTD data sets were kindly provided by Dr. Lynne Talley (SIO), Dr. Alison MacDonald (WHIO), the Korea Oceanographic Data Center, the National Fisheries and Research Development Institute (Korea), and the Japan Oceanographic Data Center.

The work of D. R. Watts and M. Wimbush was supported by the Office of Naval Research Japan/East Sea DRI through contract N00014–98–10246. The work of W. Teague was supported through the Naval Research Laboratory's "Linkages of Asian Marginal Seas' system (O601153N).

7 References

Chaplin, G. F., and D. R. Watts. 1984. Inverted ehco sounder development. *IEEE Ocean '84 Conf. Record,* Washington, DC, IEEE, 249-253.

MacDonald, A. M., T. Suga, and R. G. Curry. 2001. An isopycnally averaged North Pacific climatology. *J. Atmos. Oceanic Technol., 18,* 394–420.

Meinen, C. S. and D. R. Watts. 1998. Calibrating inverted echo sounders equipped with pressure senors. *J. Atmos. Oceanic Technol., 15,* 1339–1345.

Munk, W.H. and D.E. Cartwright. 1966. Tidal spectroscopy and prediction. *Philos. Trans. R. Soc. London, 259,* 533-581.

Park, J.H., and D. R.Watts. 2004. Response of the southwestern Japan/East Sea to the atmospheric pressure. *Deep-Sea Res.,* [accepted].

Watts, D. R., and H. Kontoyiannis. 1990. Deep-ocean bottom pressure measurement: drift removal and performance. *J. Atmos. Oceanic Technol., 7,* 296–306.

Watts, D. R., X. Qian, and K. L. Tracey. 2001. Mapping abyssal current and pressure fields under the meandering Gulf Stream. *J. Atmos. Oceanic Technol., 18,* 1052–1067.

Xu, Y., K. L. Tracey,D. R. Watts, M. Wimbush, W. Teague, *Current meter data report Ulleung Basin of Japan/East Sea June 1999 to July 2001*. University of Rhode Island. GSO Technical Report 2003-02. 118 pp.